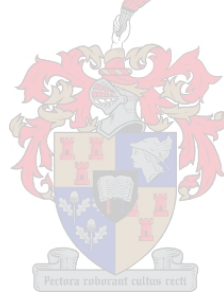


# **Agricultural field boundary delineation using earth observation methods and multi-temporal Sentinel-2 imagery**

By BARRY WATKINS

*Thesis presented in partial fulfilment of the requirements for the degree of  
Master of Science at Stellenbosch University*



Supervisor: Prof A van Niekerk

December 2019

## DECLARATION

By submitting this report electronically, I declare that the entirety of the work contained therein is my own, original work, that I am the sole author thereof (save to the extent explicitly otherwise stated), that reproduction and publication thereof by Stellenbosch University will not infringe any third party rights and that I have not previously in its entirety or in part submitted it for obtaining any qualification.

Regarding Chapters 3 and 4, the nature and scope of my contribution were as follows:

Chapter	Nature of Contribution	Extent of Contribution (%)
Chapter 3	This chapter was published as a journal article in Computers and Electronics in Agriculture and co-authored by my supervisor who helped in the conceptualisation and writing of the manuscript. I carried out the literature review, data collection and analysis components and produced the first draft of the manuscript.	BA Watkins 85% Prof A van Niekerk 15%
Chapter 4	This chapter was submitted for publishing as a journal article in Computers and Electronics in Agriculture and co-authored by my supervisor who helped in the conceptualisation and writing of the manuscript. I carried out the literature review, data collection and analysis components and produced the first draft of the manuscript.	BA Watkins 85% Prof A van Niekerk 15%

Date: December 2019

.....

Copyright © 2019 Stellenbosch University

All rights reserved

## SUMMARY

Accurate and up-to-date agricultural monitoring systems are critical for forecasting crop yield, planning resources and assessing the impact of threats to production (such as droughts or floods). The spatial extent and location of agricultural fields greatly influence these systems. Conventional methods of delineating agricultural fields, such as in situ field surveys and manual interpretation of imagery, are costly and time-consuming and are thus not suitable in an operational context. Automated earth observation techniques offer a cost-effective alternative as they can be used to execute frequent and highly detailed investigations of large areas. However, there are currently no well-established and transferable techniques to automatically delineate agricultural field boundaries. The most promising techniques found in literature include object-based image analysis (OBIA) and edge detection algorithms. This study consequently compared and evaluated multiple OBIA approaches for delineating agricultural field boundaries with multi-temporal Sentinel-2 imagery.

Two sets of experiments were carried out. The first set of experiments compared and evaluated six multi-temporal OBIA approaches with which active agricultural fields in a large irrigation scheme were delineated and identified. These approaches combined two edge enhancement algorithms (Canny and Scharr) and three image segmentation techniques (watershed, multi-threshold and multi-resolution) to create six scenarios. Results showed that the watershed segmentation scenarios outperformed the multi-threshold and multi-resolution segmentation algorithms. In addition, the Canny edge detection algorithm, in conjunction with a segmentation technique, was found to produce higher boundary accuracies than its counterpart, Scharr.

In the second set of experiments the best performing scenario from the first set of experiments, namely Canny edge detection in conjunction with watershed segmentation (CEWS), was modified slightly and applied to five regions in South Africa. The purpose of this investigation was to assess the robustness (transferability) of the methodology. A standard per-pixel supervised classification was performed to serve as a benchmark against which the CEWS approach was compared. Results showed that CEWS outperformed the supervised per-pixel classification in all experiments. CEWS' robustness in different agricultural landscapes was furthermore highlighted by its creation of closed field boundaries, independence from training data and transferability.

The quantitative experiments carried out in this study lay the foundation for the implementation of an operational workflow for delineating agricultural fields with the use of multi-temporal

Sentinel-2 imagery. The extracted field boundaries will likely aid agricultural monitoring systems in estimating crop yield and improve resource planning and food security assessments.

**KEY WORDS**

Earth observation, field boundaries, object-based image analysis, edge detection, image segmentation, multi-temporal, agricultural monitoring systems

## OPSOMMING

Akkurate en bygewerkte landboumoniteringstelsels is van kritieke belang vir die voorspelling van oesopbrengs, die beplanning van hulpbronne en die assessering van die impak van bedreigings vir produksie (soos droogtes of vloede). Die ruimtelike omvang en ligging van landboulande beïnvloed hierdie stelsels tot 'n groot mate. Konvensionele metodes om lande af te baken, soos in situ veldopnames en die visuele interpretasie van beelde, is duur en tydrowend en is dus nie geskik in 'n operasionele konteks nie. Outomatiese aardwaarnemingstegnieke bied 'n koste-effektiewe alternatief, aangesien dit gebruik kan word om gereelde en hoogs gedetailleerde ondersoeke van groot gebiede uit te voer. Daar is egter tans geen gevestigde en oordraagbare tegnieke om landbougrondgrense outomaties af te baken nie. Die mees belowende tegnieke wat in die literatuur voorkom, sluit in objek-gebaseerde-beeldanalise (OGBA) en randdeteksie-algoritmes. Hierdie studie het gevolglik verskeie OGBA-benaderings om landbougrondgrense af te baken met multi-temporale Sentinel-2 beelde, vergelyk en geëvalueer. Twee stelle eksperimente is uitgevoer.

Die eerste stel eksperimente het ses multi-temporale OGBA-benaderings waarmee aktiewe landbouvelde in 'n groot besproeiingskema afgebaken en geïdentifiseer is, vergelyk en geëvalueer. Hierdie benaderings kombineer twee randverbeteringsalgoritmes (Canny en Scharr) en drie beeldsegmenteringstegnieke (waterskeiding, multi-drempel en multi-resolusie) om ses scenario's te skep. Resultate het getoon dat die waterskeidingskenario's beter presteer as die multi-drempel- en multi-resolusie-segmenteringsalgoritmes. Daarbenewens is bevind dat die Canny-randdeteksie-algoritme, in samewerking met 'n segmenteringstegniek, hoër grensakkuraathede as sy eweknie, Scharr, produseer.

Die tweede stel eksperimente het die beste presterende scenario van die eerste stel eksperimente, naamlik die Canny-randdeteksie-algoritme in samewerking met waterskeidingsegmentasie (CRSW), op vyf streke in Suid-Afrika toegepas. Die doel van hierdie ondersoek was om die robuustheid (oordraagbaarheid) van die metodologie te evalueer. 'n Standaard per-piksel gerigte klassifikasie is uitgevoer om te dien as 'n maatstaf waarteen die voorgestelde benadering vergelyk is. Resultate het getoon dat CRSW in alle eksperimente beter as die per-piksel gerigte klassifikasie presteer het. CRSW se robuustheid in verskillende landboulandskappe is verder beklemtoon deur sy skepping van geslote veldgrense, onafhanklikheid van opleidingsdata en oordraagbaarheid.

Die kwantitatiewe eksperimente wat in hierdie studie uitgevoer is, het die basis gelê vir die implementering van 'n operasionele werkvloei vir die afbakening van landbouvelde met behulp van multi-temporale Sentinel-2-beelde. Die onttrekte veldgrense sal waarskynlik

landboumoniteringstelsels help om oesopbrengs te beraam en hulpbronbeplanning en voedselsekuriteitsevaluering te verbeter.

**SLEUTELWOORDE**

Aardwaarneming, veldgrense, objekgebaseerde-beeldanalise, randdeteksie, beeldsegmentering, multi-temporale, landbou-moniteringstelsels

## ACKNOWLEDGEMENTS

I sincerely thank:

- My family for their emotional and financial support throughout this research period;
- Prof Adriaan van Niekerk for his great insight, guidance and suggestions;
- The staff of the Department of Geography and Environmental Science for their suggestions and comments during scheduled feedback sessions;
- Helene van Niekerk ([www.linguafix.net](http://www.linguafix.net)) for the language and editing services provided;
- The Water Research Commission of South Africa for initiating and funding the project titled “Salt Accumulation and Waterlogging Monitoring System (SAWMS) Development” (contract number K5/2558//4) of which this work forms part. More information about this project is available in the 2016/2017 WRC Knowledge Review (ISBN 978-1-4312-0912-5) available at [www.wrc.org.za](http://www.wrc.org.za); and
- The NRF (grant number 106739) for funding this research. Opinions expressed and conclusions arrived at, are those of the author and are not necessarily to be attributed to the NRF.

## CONTENTS

<b>DECLARATION .....</b>	<b>ii</b>
<b>SUMMARY .....</b>	<b>iii</b>
<b>OPSOMMING .....</b>	<b>v</b>
<b>ACKNOWLEDGEMENTS .....</b>	<b>vii</b>
<b>CONTENTS .....</b>	<b>viii</b>
<b>TABLES .....</b>	<b>xii</b>
<b>FIGURES .....</b>	<b>xiii</b>
<b>ACRONYMS AND ABBREVIATIONS .....</b>	<b>xv</b>
<b>CHAPTER 1: INTRODUCTION .....</b>	<b>1</b>
<b>1.1 REMOTE SENSING IN AGRICULTURE .....</b>	<b>1</b>
<b>1.2 AGRICULTURAL FIELD BOUNDARIES .....</b>	<b>2</b>
<b>1.3 COMMON TECHNIQUES IN REMOTE SENSING FOR AGRICULTURAL     FIELD BOUNDARY DELINEATION .....</b>	<b>2</b>
<b>1.4 PROBLEM FORMULATION.....</b>	<b>4</b>
<b>1.5 AIM AND OBJECTIVES.....</b>	<b>5</b>
<b>1.6 RESEARCH METHODOLOGY.....</b>	<b>5</b>
<b>CHAPTER 2: LITERATURE REVIEW .....</b>	<b>8</b>
<b>2.1 AGRICULTURE IN SOUTH AFRICA .....</b>	<b>8</b>
<b>2.2 REMOTE SENSING FOR MONITORING AGRICULTURE.....</b>	<b>9</b>
<b>2.2.1 Characteristics of optical imagery .....</b>	<b>9</b>
<b>2.2.2 Vegetation indices.....</b>	<b>10</b>
<b>2.2.3 Image classification .....</b>	<b>11</b>
<b>2.2.3.1 Unsupervised classification.....</b>	<b>11</b>



2.2.3.2	Supervised classification .....	11
2.2.3.3	Knowledge-based classification .....	13
2.2.3.4	Classification accuracy metrics .....	14
<b>2.2.4</b>	<b>Object-based vs per-pixel image analysis.....</b>	<b>14</b>
<b>2.3</b>	<b>BOUNDARY CONCEPTS .....</b>	<b>15</b>
<b>2.3.1</b>	<b>Defining boundaries .....</b>	<b>16</b>
<b>2.3.2</b>	<b>Boundary accuracy metrics.....</b>	<b>17</b>
<b>2.4</b>	<b>REMOTE SENSING TECHNIQUES FOR AGRICULTURAL FIELD BOUNDARY DELINEATION .....</b>	<b>18</b>
<b>2.4.1</b>	<b>Point-based segmentation .....</b>	<b>18</b>
<b>2.4.2</b>	<b>Edge-based segmentation .....</b>	<b>18</b>
2.4.2.1	Sobel edge detection.....	19
2.4.2.2	Canny edge detection .....	19
2.4.2.3	Scharr edge detection .....	20
<b>2.4.3</b>	<b>Region-based segmentation .....</b>	<b>20</b>
2.4.3.1	Multi-resolution segmentation .....	21
2.4.3.2	Watershed segmentation .....	21
<b>2.4.4</b>	<b>Hybrid segmentation approaches .....</b>	<b>22</b>
<b>2.5</b>	<b>LITERATURE SUMMARY .....</b>	<b>24</b>
 <b>CHAPTER 3: A COMPARISON OF OBJECT-BASED IMAGE ANALYSIS APPROACHES FOR FIELD BOUNDARY DELINEATION USING SENTINEL-2 IMAGERY .....</b>		
<b>3.1</b>	<b>ABSTRACT .....</b>	<b>26</b>
<b>3.2</b>	<b>INTRODUCTION.....</b>	<b>26</b>
<b>3.3</b>	<b>METHODS .....</b>	<b>30</b>
<b>3.3.1</b>	<b>Study area .....</b>	<b>30</b>
<b>3.3.2</b>	<b>Image collection .....</b>	<b>31</b>

<b>3.3.3</b>	<b>Experimental overview .....</b>	<b>32</b>
3.3.3.1	Step 1: Edge detection.....	32
3.3.3.2	Step 2: Edge layer aggregation.....	34
3.3.3.3	Step 3: Image segmentation .....	34
3.3.3.4	Step 4: Uncultivated area exclusion .....	35
3.3.3.5	Step 5: Noise removal .....	36
<b>3.3.4</b>	<b>Accuracy assessment.....</b>	<b>36</b>
<b>3.4</b>	<b>RESULTS.....</b>	<b>38</b>
<b>3.5</b>	<b>DISCUSSION .....</b>	<b>41</b>
<b>3.6</b>	<b>CONCLUSION.....</b>	<b>42</b>
<b>CHAPTER 4: A MODIFIED OBIA APPROACH FOR FIELD BOUNDARY DELINEATION IN SELECTED SOUTH AFRICAN AGRICULTURAL LANDSCAPES USING MULTI-TEMPORAL SENTINEL-2 IMAGERY.....</b>		
<b>4.1</b>	<b>ABSTRACT .....</b>	<b>44</b>
<b>4.2</b>	<b>INTRODUCTION.....</b>	<b>45</b>
<b>4.3</b>	<b>METHODS .....</b>	<b>48</b>
<b>4.3.1</b>	<b>Study area .....</b>	<b>48</b>
4.3.1.1	Image collection .....	50
<b>4.3.2</b>	<b>CEWS workflow .....</b>	<b>50</b>
4.3.2.1	Original CEWS workflow .....	50
4.3.2.2	Modified CEWS workflow .....	51
<b>4.3.3</b>	<b>Supervised per-pixel classification workflow for mapping cultivated areas .</b>	<b>53</b>
<b>4.3.4</b>	<b>Accuracy assessment.....</b>	<b>53</b>
<b>4.4</b>	<b>RESULTS.....</b>	<b>55</b>
<b>4.5</b>	<b>DISCUSSION .....</b>	<b>58</b>
<b>4.6</b>	<b>CONCLUSION.....</b>	<b>61</b>

<b>CHAPTER 5: DISCUSSION AND CONCLUSIONS.....</b>	<b>63</b>
<b>5.1 REVISITING THE AIMS AND OBJECTIVES.....</b>	<b>63</b>
<b>5.2 SYNTHESIS .....</b>	<b>64</b>
<b>5.3 STUDY LIMITATIONS AND RECOMMENDATIONS FOR FUTURE RESEARCH.....</b>	<b>66</b>
<b>5.4 CONCLUSIONS.....</b>	<b>66</b>
<b>REFERENCES .....</b>	<b>68</b>

**TABLES**

Table 3-1	Sentinel-2 satellites characteristics including band names, wavelength and spatial resolution .....	32
Table 3-2	Description of the different algorithm scenarios .....	33
Table 3-3	Area- and edge-based metric results for the six experiments .....	39
Table 4-1	Summary of region characteristics for the five study sites .....	49
Table 4-2	Number of cloud-free Sentinel-2 images per study area .....	50
Table 4-3	Rule-sets per study area .....	52
Table 4-4	Area- and edge-based metric results .....	56

## FIGURES

Figure 1-1	Research design and thesis structure .....	7
Figure 2-1	Horizontal and vertical edge masks used by the Sobel edge detection algorithm.....	19
Figure 2-2	Horizontal and vertical edge masks used by the Scharr edge detection algorithm ...	20
Figure 3-1	Extent and location of the study area within South Africa.....	31
Figure 3-2	Horizontal and vertical Scharr edge masks .....	33
Figure 3-3	Conceptual illustration of ED calculations, where a) $MAE_i$ is depicting the accuracy along the boundary and b) $MAE_j$ represents the level of OS. ....	38
Figure 3-4	Illustration of how the aggregation of multiple edge layers for the Canny and Scharr edge operators reinforce persistent edges.....	40
Figure 3-5	Detailed area showing the field boundaries extracted by experiments (a) WS_C, (b) WS_S, (c) MRS_C, (d) MRS_S, (e) MTS_C and (f) MTS_S .....	40
Figure 4-1	(a) Location and extent of the five selected study sites in South Africa, (b) Patensie, (c) Swartland, (d) Grabouw, (e) Loskop, and (f) Mooketsi .....	49
Figure 4-2	Conceptual illustration of ED calculations, where (a) $MAE_i$ depicts the accuracy along the boundary and (b) $MAE_j$ represents the level of OS.....	54
Figure 4-3	Cultivated field extraction results for an area in Patensie showing an a) RGB composite of Sentinel-2 imagery acquired in June 2017, along with the b) PP and c) CEWS outputs .....	56
Figure 4-4	Cultivated field extraction results for an area in Loskop displaying an a) RGB composite of Sentinel-2 imagery acquired in January 2018, compared to the b) PP and c) CEWS outputs. ....	57
Figure 4-5	Cultivated field extraction results for an area in Mooketsi (a – c) and Swartland (d – f) displaying an a) RGB composite of Sentinel-2 imagery acquired in March 2018, as well as the related b) PP and c) CEWS outputs; and d) an RGB composite of Sentinel-2 imagery acquired during August 2017, accompanied by e) the PP and f) CEWS results. The highlighted areas show where both methods failed to identify field boundaries due to low contrast between fields.....	58

Figure 4-6 Cultivated area feature extraction results for an area in Grabouw showing a) an RGB composite of Sentinel-2 imagery acquired during September 2017, compared to the b) PP and c) CEWS outputs. The highlighted areas show where both methods struggled to accurately delineate small and irregularly shaped fields..... 58

## ACRONYMS AND ABBREVIATIONS

ACCA	Automated cropland classification algorithm
ASTER	Advanced Spaceborne Thermal Emission and Reflection Radiometer
CART	Classification and regression tree
CE	Commission error
CEWS	Canny edge detection in conjunction with watershed segmentation
DT	Decision tree
ED	Euclidean distance
EO	Earth observation
ESA	European Space Agency
EVI	Enhanced vegetation index
GEOBIA	Geographic object-based image analysis
GIS	Geographical information system
GNDVI	Green normalised vegetation index
ISODATA	Iterative self-organising data analysis technique
JNB	Jenk's natural break
K	Kappa
LS	Lambda schedule
LSD	Line segment detection
MAE	Mean absolute error
MODIS	Moderate Resolution Imaging Spectroradiometer
MRS	Multi-resolution segmentation
MTS	Multi-threshold segmentation
NDVI	Normalised difference vegetation index
NDWI	Normalised difference water index
NFA	Number of false alarms
NIR	Near-infrared
NRF	National Research Foundation
OA	Overall accuracy
OBIA	Object-based image analysis
OE	Omission error
OS	Over-segmentation
PA	Producer's accuracy

PBIA	Pixel-based image analysis
PP	Per-pixel
RA	Relative area
RAG	Region adjacency graph
RF	Random forest
RGB	Red, green, blue
RM	Ratio of missing detections
RS	Remote sensing
SAVI	Soil-adjusted vegetation index
SAWMS	Salt Accumulation and Waterlogging Monitoring System
SCRM	Size-constrained region merging
SPOT	Satellite pour l' observation de la terre
STD	Standard deviation
SVM	Support vector machine
SWIR	Short wave infrared
TOA	Top of atmosphere reflectance
TWDTW	Time-weighted dynamic time warping
UA	User's accuracy
US	Under-segmentation
VHR	Very high resolution
VI's	Vegetation indices
WRC	Water Research Commission
WS	Watershed segmentation



## **CHAPTER 1: INTRODUCTION**

In recent years, agricultural land has increased in many parts of the world (Lambin & Meyfroidt 2011). This can be attributed to the ever-increasing global population which recently exceeded seven billion people (Tollefson 2012). With this growth in population, the increased food production demand has become a major global challenge (Fritz et al. 2015). Furthermore, factors such as urban expansion and climate change have added pressure on the development of agricultural land (Inglada et al. 2015; Waldner & Defourny 2015). These negative effects on crop production can have dire impacts on food security across the world, especially in countries where food security is an existing problem. For example, Africa has the highest fertility and population growth and many countries still have food security concerns. This makes agricultural monitoring systems vital in extracting cropland areas, forecasting crop yield, and assessing the impact of threats to production such as floods, droughts, disease or human conflict (Matton et al. 2015). Agricultural monitoring systems need to be practical, sustainable and able to provide timely information to aid countries in achieving food security. Crop field extents is a fundamental dataset in most agricultural monitoring systems as it can be used to isolate crop fields from other land uses and assess factors such as crop growth, stress and potential yield estimates (Waldner & Defourny 2015).

### **1.1 REMOTE SENSING IN AGRICULTURE**

Earth observation (EO) techniques have been widely exploited in agriculture and are viable methods for long-term analysis of large areas (Villa et al. 2015). EO can provide spatially continuous and frequent observations that result in large datasets of varying spatial and temporal resolutions (Mulianga et al. 2015). These datasets can potentially be used to assess agricultural vegetation growth, maturity and harvests (Ozdogan et al. 2010). The extent and characteristics of agricultural land follows clear seasonal patterns that correlate positively to the phenology of the crops being grown (Atzberger 2013).

Data collection using remote sensing has the advantage of being less time-consuming and costly than traditional statistical surveys (Ozdogan et al. 2010; Peña et al. 2014). Traditional crop surveys typically involve the collection of in situ field data or the manual digitisation of aerial or satellite imagery. However, these processes are labour intensive and susceptible to human error (Alemu 2016). Human errors often occur due to bias of the surveyor and is influenced by their knowledge, perception and ability to delineate fields (Lucas et al. 2007). Furthermore, surveyors in the field are limited to their direct line of sight and can consequently miss the spatial variability within the

mapped fields, which is compounded in large and complex environments. Remote sensing is a viable alternative for creating cropland inventories due to its ability to capture imagery in large swaths in an automated and unbiased way. It is even more valuable in developing countries where resources are limited and data is scarce (Ozdogan et al. 2010).

## **1.2 AGRICULTURAL FIELD BOUNDARIES**

The spatial distribution, extent and location of agricultural field boundaries plays an important role in yield predictions, resource allocation and economic planning (Yan & Roy 2014). However, there are many different interpretations of “field boundaries” and they generally differ according to the interpreter (Davidse 2015). The definitions of “field” and “boundary”, according to the Oxford Dictionary, can aid in the clarification of these terms. “Field” is defined as “an area of open land, especially one with crops or pasture, typically bounded by hedges or fences”, while “boundary” is defined as a “line which marks the limits of an area; a dividing line”. In this study, “fields” relate to agricultural land-use, while “boundary” relates to whether there is a change in crop type or a natural/man-made disruption in the landscape between fields, for example a road or hedge (Rydberg & Borgefors 2001). Therefore, a farmer can have a physical field broken up into smaller parts, each with their own crop type being grown. This is important for the distinction between crop types in a multi-crop classification. However, edges between crop fields are not always easily discernible as some crops have similar spectral and structural properties at certain phases of growth (Pittman et al. 2010). This necessitates the need for multi-temporal imagery and the capturing of data throughout the growing season.

## **1.3 COMMON TECHNIQUES IN REMOTE SENSING FOR AGRICULTURAL FIELD BOUNDARY DELINEATION**

Conventional methods for field boundary delineation such as in situ field surveys and visual interpretation of satellite imagery are costly, time-consuming and susceptible to human error (Alemu 2016). Furthermore, the monitoring of crops is complicated by their dynamic nature (McNairn et al. 2002). Crop types can vary from one field to the next and from season to season. This necessitates an alternative approach, such as the use of remotely sensed data acquired by satellite sensors (Lucas et al. 2007).

One of the most important steps in defining field boundaries is the detection of the edges that make up those boundaries. An edge can be defined as a spectral discontinuity between pixel values in an image (Rydberg & Borgefors 2001). Two common techniques identified in literature to delineate agricultural field boundaries are object-based image analysis (OBIA) and edge detection

techniques (Butenuth, Straub & Heipke 2004; Davidse 2015; Rydberg & Borgefors 2001; Schultz et al. 2015).

OBIA aims to group pixels into meaningful image objects (Blaschke et al. 2000). This is differentiated from traditional per-pixel classification procedures that aim to classify individual pixels (Wuest & Zhang 2009). The major advantage of OBIA over per-pixel methods is that image objects are able to make use of their spatial neighbourhood and additional spectral information that single pixels lack, such as mean, median, minimum, maximum and variance values (Blaschke et al. 2000). Furthermore, the impact of noise is reduced as grouping pixels reduces variation and the so-called “salt-and-pepper” effect (Schultz et al. 2015).

Edge detection is a method of determining significant local change in an image (Ramadevi et al. 2010). Common edge detection algorithms make use of two-dimensional filters to determine the magnitude and strength of an edge pixel (Shrivakshan & Chandrasekar 2012). There are a number of edge detection algorithms available, which each has a different purpose. The most commonly used are the Sobel, Prewitt, Robert cross, Scharr and Canny algorithms.

The combination of edge detection and segmentation has proven to yield better results than that of a single method (Rydberg & Borgefors 2001). For example, Alemu (2016) made use of a line segment detection (LSD) algorithm to extract linear features on VHR (2 m) Worldview-2 imagery. The changes in x and y direction of each band are combined using a vector sum. A line-support region representing potential candidates for a segment was formed using a region growing technique. The Helmholtz principle, based on the number of false alarms (NFA), was calculated to assess the results. The methodology was found to omit many field boundaries, which was attributed to weak contrast between neighbouring fields. Davidse (2015) performed Lambda Schedule (FLS) segmentation on the normalised difference vegetation index (NDVI) and soil-adjusted vegetation index (SAVI). However, the method delivered poor results due to the complexity of the landscape. It was suggested that the method would likely produce better results in a more homogeneous landscape. Rydberg & Borgefors (2001) developed a hybrid approach by integrating a gradient-based edge detector with a segmentation algorithm. In this approach, all multispectral information was used by adding the magnitudes and direction of the edges for each band. The resulting edge image is combined with a segmentation method based on a simple ISODATA algorithm. This method allows for the integration of information from multiple spectral bands in the delineation of agricultural field boundaries. A high boundary accuracy (87%) was attributed to the method’s ability to exploit information from multiple bands.

## 1.4 PROBLEM FORMULATION

Conventional methods for delineating field boundaries include the manual digitisation of aerial/satellite imagery and in situ field surveys. These methods are not practical for continuous monitoring systems, as they are costly and time-consuming. EO has shown potential for crop boundary delineation by providing medium to high resolution imagery over extensive periods at relatively low cost. Currently there are no well-established and transferable models or techniques to automatically extract crop field boundaries from remotely sensed imagery. However, the most promising techniques identified in literature are based on OBIA and edge detection algorithms (Butenuth, Straub & Heipke 2004; Davidse 2015; Rydberg & Borgefors 2001). But most OBIA approaches require fine-tuning of segmentation parameters, which can be time-consuming and are often only applicable to a certain area (Duro, Franklin & Dube 2012; Schultz et al. 2015). Several edge detection algorithms have been developed, including the Sobel, Prewitt, Roberts cross, Scharr and Canny algorithms. The Canny edge detection algorithm has been shown to outperform other algorithms in many applications. However, for delineating crop field boundaries, it is still unclear which algorithm is most accurate.

The low temporal resolution of existing high spatial resolution remotely sensed data has been cited in literature as a limitation of the use of EO techniques for field boundary delineation (Gumma et al. 2014; Pittman et al. 2010) and many previous attempts have made use of only one image date (Alemu 2016; Butenuth, Straub & Heipke 2004; Rydberg & Borgefors 2001). However, agricultural land follows strong seasonal patterns that are strongly related to the phenology of the crops being grown (Atzberger 2013). Many of these phenological stages can change within very short periods, necessitating a multi-temporal approach. The increased availability of higher spatial and temporal resolution data through the Copernicus programme of the European Space Agency (ESA) opens up many opportunities for implementing and evaluating a multi-temporal approach to crop field boundary delineation. In particular, the Sentinel-2 constellation offers 10 m resolution imagery at a five-day interval, which may be ideal for agricultural field boundary delineation. To date, this data has not yet been evaluated for this purpose.

The following research questions have been set:

1. Is the spatial and temporal resolution of Sentinel-2 imagery sufficient for delineating crop field boundaries?
2. Which edge detection and segmentation algorithms are most effective for delineating field boundaries from Sentinel-2 imagery?
3. What segmentation parameters are best suited for the task of identifying field edges?

4. How can edge detection, image segmentation and classification be combined to differentiate (delineate and label) active fields from other land covers in an accurate and robust manner?

## **1.5 AIM AND OBJECTIVES**

This research aims to develop and evaluate a technique for delineating actively growing agricultural fields using multi-temporal, high resolution Sentinel-2 imagery.

The following objectives were set:

1. Review literature pertaining to multi-temporal crop type mapping and field boundary delineation;
2. Obtain suitable Sentinel-2 satellite imagery for different agricultural regions across South Africa;
3. Assess the effectiveness of multiple edge detection algorithms for delineating field boundaries in conjunction with various segmentation algorithms;
4. Determine which segmentation algorithms and parameters produce the most accurate field boundaries;
5. Develop and demonstrate a knowledge-based OBIA approach for delineating field boundaries; and
6. Evaluate the accuracy and robustness (transferability) of the developed methodology across different agricultural regions in South Africa.

## **1.6 RESEARCH METHODOLOGY**

This research was empirical and quantitative in nature. Analytical techniques such as edge detection, image segmentation and knowledge-based crop classification were employed to delineate agricultural field boundaries from multi-temporal Sentinel-2 imagery. The extracted field boundaries were quantitatively assessed using both area and edge-based metrics.

Figure 1-1 shows the research design and structure of the thesis. Chapter 1 describes the research problem along with the aim and objectives for this study. Chapter 2 provides a review of remote sensing (RS) techniques for agricultural field boundary delineation and crop mapping followed by an overview of relevant studies carried out previously.

Chapter 3 (experiment 1) evaluates several OBIA techniques for delineating agricultural field boundaries in a large irrigation scheme. The aim of the experiment is to determine which combination of edge detection and segmentation algorithms best delineates field boundaries using

multi-temporal Sentinel-2 imagery. The extracted field boundaries are quantitatively evaluated using a combination of area and edge-based metrics.

Chapter 4 (experiment 2) utilises the best approach determined in Chapter 3 (with some minor modifications) and applies it to five agricultural regions. The aim of the experiment is to determine the method's robustness in context of finding an operational solution to agricultural field boundary delineation with Sentinel-2 imagery. The extracted field boundaries were quantitatively evaluated using a combination of area and edge-based metrics.

Chapter 5 provides a summary of the research and offers some conclusions based on the findings of this research. It critically evaluates the success of the research by reflecting on the research aim and objectives, while discussing the key findings of the various experiments undertaken. Recommendations for further research are also provided.

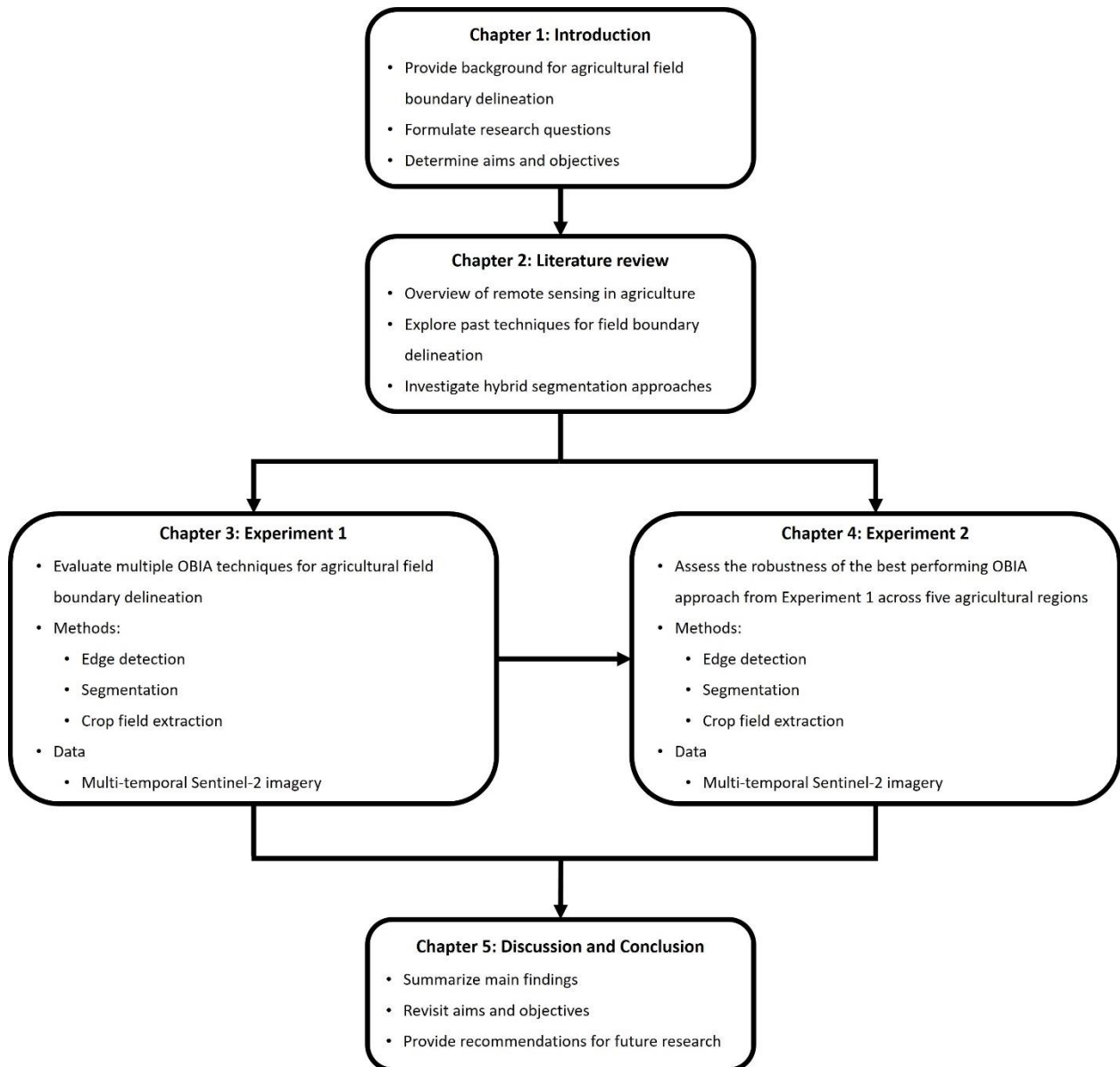


Figure 1-1 Research design and thesis structure

## **CHAPTER 2: LITERATURE REVIEW**

### **2.1 AGRICULTURE IN SOUTH AFRICA**

Food accessibility is a basic human right that is enshrined in the constitution of the Republic of South Africa (Lehohla 2012). This makes it the responsibility of the state to ensure that residents can meet their basic nutritional needs. This is in essence food security, which is said to exist when people in a society can acquire good quality and nutritious food in a socially acceptable way, for example without having to steal, scavenge or acquire emergency food supplies from outside sources (Labadarios et al. 2011). Although South Africa has been able to keep its food production within the national food requirements, large-scale inequality and poverty has led to many households being unable to enjoy food security or adequate access to food. This leaves poor households vulnerable to hunger and nutritional deficiencies.

Agricultural production is at the heart of ensuring food security but is hampered by a constantly growing population and climate change (Duveiller & Defourny 2010). Climate change poses a grave threat to South Africa's infrastructure, water sources and food security (Ziervogel et al. 2014). Climate change could modify crop production in two main ways, namely a reduction in precipitation and a modification of temperatures. Precipitation is the leading source of freshwater and impacts the soil moisture level, while temperature determines the length of the growing season and controls crop development and water requirements (Calzadilla et al. 2014). Between 1997 and 2006, South Africa became approximately 2% hotter and 6% drier, a trend that is likely to continue. It is predicted that with every 1% decrease in rainfall, there is likely to be a 1.2% and 0.5% decline in maize and wheat production respectively. The observed climate changes are, therefore expected to lead to a net decline in income for the most productive agricultural regions in South Africa (Blignaut, Ueckermann & Aronson 2009).

Traditionally, irrigation farming has been proposed as a strategy for developing the agricultural sector (Wheeler et al. 2017). Furthermore, rain-fed crop production is becoming increasingly risky due to unreliable rainfall and an increase in drought periods (Cousins & Walker 2015; Sinyolo, Mudhara & Wale 2014). However, many irrigation schemes struggle to succeed due to a lack of communication between stakeholders, a lack of investment return and a shortage of information flow (e.g. water management and market intelligence), which leads to low productivity and an eventual breakdown of the irrigation system (Van Rooyen et al. 2017). Therefore, there is an increasingly strong demand for improved methods in agricultural practices and management systems to combat the negative effects of climate change and to ensure food security for future generations. Efficient agricultural management and monitoring can provide valuable information



regarding crop yield and crop health, but such systems require timely and accurate data on the extent of agricultural land.

## **2.2 REMOTE SENSING FOR MONITORING AGRICULTURE**

RS techniques have been proven to be effective in agricultural applications and are widely exploited for their ability to provide long-term analysis of large areas (Villa et al. 2015). RS provides continuous and frequent observations, which result in large datasets with varying temporal and spatial resolutions (Mulianga et al. 2015; Valero et al. 2016). The spatial and temporal resolutions of RS imagery are key characteristics in its ability to provide sufficient information to agricultural monitoring systems.

### **2.2.1 Characteristics of optical imagery**

The spatial resolution of an image refers to the smallest object discernible on the ground surface and is commonly equivalent to the imagery's pixel size (Muller & Van Niekerk 2016). The spatial resolution of satellite imagery can vary from kilometres (low spatial resolution) to centimetres (very high spatial resolution), depending on the satellite sensor utilised. It is important to consider the pixel size in agricultural applications such as cropland mapping. For example, when the pixel size is too large, individual crop fields cannot be mapped out to their proper extent (Schultz et al. 2015). Low spatial resolution imagery, such as those acquired by MODIS, has proven to provide sufficient information to be used as a generic cropland indicator for major crop classes (Lunetta et al. 2010; Pittman et al. 2010). For example, the 250 m MODIS 16-day NDVI time series product was successfully used to separate cropland from non-cropland at a national scale in the fragmented agricultural landscape of Mali, West Africa (Vintrou et al. 2012). However, higher spatial resolution imagery is required for the separation and delineation of individual crop fields due to the finer detail provided by such imagery (Mueller, Segl & Kaufmann 2004).

The temporal resolution of remotely sensed imagery can be defined as the frequency at which images are acquired of the same region. The temporal resolution can vary from multiple revisits a day (high temporal resolution) to only a few visits a year (low temporal resolution). Agricultural land follows seasonal patterns that are strongly linked to the phenological cycles of the crops being grown in a region (Atzberger 2013). The phenology of crop fields changes every few days during the growing season, which affects the spectral and structural responses collected by the sensor at the time of observation (Ozdogan et al. 2010). In addition, the spectral response of a given crop type can vary from region to region, depending on climate, soil conditions and different farming practices such as the use of fertilizer (Valero et al. 2016). Therefore, when RS data is used to

monitor crops it is critical that precise and timely information on the phenological status and growth of cultivated vegetation is taken into account throughout a growing season (Veloso et al. 2017).

### 2.2.2 Vegetation indices

Understanding the distribution, biophysical and structural properties and temporal/spatial variations of vegetation is vital in understanding the role of these factors in large-scale global processes such as agriculture (Huete et al. 2002). Spectral vegetation indices (VIs) are popular and widely used in disciplines interested in the evaluation of plant stress, health, biomass and growth (Jackson & Huete 1991). VIs are simple spectral transformations designed to combine two or more wavelengths to enhance certain vegetation properties (Huete et al. 2002). Some of the most commonly tested VIs include: normalised difference vegetation index (NDVI), enhanced vegetation index (EVI), soil-adjusted vegetation index (SAVI), green normalised difference vegetation index (GNDVI) and normalised difference water index (NDWI).

NDVI has been used extensively in cropland mapping and has shown to provide high accuracies when used alone or in conjunction with other spectral features (Aguilar et al. 2015; Lambert, Waldner & Defourny 2015; Matton et al. 2015; Peña-Barragán et al. 2011; Wardlow, Egbert & Kastens 2007; Wu et al. 2015). NDVI compares the NIR and red bands (Wardlow, Egbert & Kastens 2007) and is defined as:

$$NDVI = \frac{NIR - RED}{NIR + RED} \quad \text{Equation 2.1}$$

Where        NIR    is the near-infrared image band; and  
              RED    is the red image band.

The main strength of NDVI lies in its ratio concept, which reduces certain forms of noise (cloud shadows, topographic variations and atmospheric attenuation) inherent in individual bands (Huete et al. 2002). This allows NDVI to provide meaningful comparisons of change in vegetation growth. Most other VIs listed above are based on the same principles as NDVI. For a comprehensive overview of other VIs, the reader is referred to Gamon & Surfus (1999); Gitelson, Gritz & Merzlyak (2003); Huete (1988); Jiang et al. (2008); and Peña-Barragán et al. (2011).

### 2.2.3 Image classification

Image classification in the context of RS is based on the principle that geographical features on the Earth's surface contain different reflectance properties and can be identified through an image classification process (Al-doski et al. 2013). One method of image classification is the visual interpretation of features by an analyst. However, manual interpretation is tedious, subjective and relies heavily on the skill of the analyst (Rozenstein & Karnieli 2011). Furthermore, this approach is not practical for image classification on a regional or global scale.

Computer-based algorithms have been developed to overcome the limitations of manual interpretation of RS imagery. Computer-based algorithms (called classifiers) vary in complexity and can perform classifications involving two or more classes of interest. Traditional computer-based methods involve per-pixel unsupervised and supervised approaches. However, object-orientated and knowledge-based approaches have recently become popular alternatives. Each of these approaches are discussed in the following subsections.

#### 2.2.3.1 Unsupervised classification

Unsupervised classification can be defined as the identification and grouping of natural structures in multidimensional space (Campbell & Wynne 2013). This approach is popular as it does not require a priori knowledge (Eva et al. 2004). However, despite the attractiveness of the automatic clustering of features, informational class labels have to be manually assigned to the final grouping of spectral clusters by an analyst. This process is challenging and prone to human subjectivity and error (Gomez, White & Wulder 2016). These problems are compounded when there are ambiguous linkages between the spectral and informational classes (Campbell & Wynne 2013). Some of the most common unsupervised classification algorithms include k-means, ISODATA, agglomerative hierarchical grouping and histogram-based clustering.

#### 2.2.3.2 Supervised classification

Supervised classification is the process of using pre-determined samples of known identity (i.e. pixels/objects already assigned to an informational class) to classify pixels/objects of unknown identity (Campbell & Wynne 2013). These samples of known identity (training samples) are created by an analyst who has knowledge of the target informational classes, providing the analyst control over the classification. This is an advantage that the unsupervised classification approach does not have. However, the selection of training data is critical as poorly defined or inappropriately selected training data can negatively affect the classification accuracy (Gomez,

White & Wulder 2016). In addition, the collection of training data can be time-consuming, expensive and is often prone to human error (Lucas et al. 2007).

Although the appropriate selection of classifier and training samples is critical, the addition of extra image features (such as transformations, textures and ancillary data) can also impact the accuracy of image classifications (Heinl et al. 2009). However, an increase in feature dimensionality can sometimes have a negative effect on classification accuracy owing to the Hughes phenomenon. This phenomenon (also referred to as the “curse of dimensionality”) states that classification accuracy will begin to decrease when the number of input features increase unless the number of training samples is also proportionally increased (Hughes 1968; Myburgh & Van Niekerk 2013). Belgiu & Drăgut (2016) list four requirements that samples need to meet in order to successfully train a classifier: (1) training and validation samples must be independent; (2) there must be an even number of samples per class; (3) training samples must accurately represent the target class; and (4) to mitigate the Hughes phenomenon, the number of training samples must be proportionate to the dimensionality of the data. A variety of supervised classification algorithms has been used in agricultural applications, including maximum likelihood (El-Magd & Tanton 2003), k-nearest neighbour (Samaniego & Schulz 2009), neural network (Shao et al. 2010), decision tree (Aguilar et al. 2015), support vector machine (Lambert, Waldner & Defourny 2016; Peña et al. 2014; Zheng et al. 2015) and random forest (Belgiu & Csillik 2018; Crnojevic et al. 2014; Inglada et al. 2015; Schultz et al. 2015; Waldner et al. 2017).

The random forest (RF) algorithm is a popular ensemble classifier. An ensemble classification algorithm uses multiple classifiers and aggregates the results (Liaw & Wiener 2002). In the case of RF, several decision trees are used in either a boosting or bagging approach for image classification or regression (Breiman 2001). Decision trees are generated using a subset of the training samples with replacement (bagging approach) (Belgiu & Drăgut 2016). A typical approach uses two thirds of the samples (*in-bag* samples) for training, with the remaining one third (*out-of bag* samples) being used in a cross validation technique to determine the algorithm’s performance (Belgiu & Drăgut 2016). RF contains two adjustable parameters, namely *mtry* and *ntree*. The *mtry* parameter determines the number of randomly sampled features used to split each node in the decision trees, while the *ntree* variable dictates the number of generated trees (Breiman 2001). The advantages of RF include computational efficiency, robustness to high dimensional data and the ability to rank feature importance for classification. A weakness of the RF algorithm is the overfitting of results when encountering noisy datasets (Liaw & Wiener 2002). However, the RF classifier has been found to be less prone to overfitting compared to many other machine learning classifiers (Belgiu & Drăgut 2016).

The RF algorithm is one of the most commonly used algorithms in remote sensing applications and has become widely accepted as an efficient tool in cropland classification (Crnojevic et al. 2014). Inglada et al. (2015) compared RF to support vector machine (SVM) for crop type mapping across 12 agricultural regions around the globe. A quantitative assessment found the RF classifier to outperform the SVM classifier in most cases. Schultz et al. (2015) used RF for crop type mapping, employing multi-temporal Landsat-8 imagery. They achieved an OA of 86%, demonstrating its effectiveness for this application. Waldner et al. (2017) showed the efficacy of the RF algorithm in generating a national scale cropland map of South Africa with an OA of 92%. Furthermore, the Gini index used by RF assists in determining feature importance for cropland mapping. Belgiu & Csillik (2018) compared RF to a time-weighted dynamic time warping (TWDTW) classification for crop type mapping. The RF algorithm was found to provide superior accuracies compared to TWDTW. However, when the number of training samples was reduced, TWDTW resulted in higher accuracies. This confirmed previous studies that showed that RF achieves lower accuracies with a reduced number of training samples (Valero et al. 2016).

#### 2.2.3.3 Knowledge-based classification

Knowledge-based (rule-based) classification systems use expert knowledge to develop a sequence of rules that can differentiate between unique geographical features in an image. The rules are often ordered in a DT style structure similar to some machine learning classifiers; however, these DTs are developed by analysts and not by algorithms. A rule-based classification (expert) system typically consists of three components, namely the knowledge base, inference engine and a database. The knowledge base stores the set of rules as if-then statements, while the inference engine stores the protocols for the application of the rules. Finally, the database stores the raw or transformed datasets. The advantage of a rule-based classification system lies in its potential to be applied to multiple dates and regions.

Lucas et al. (2007) followed a rule-based object-orientated approach to map habitat and agricultural land cover using multi-temporal Landsat-7 imagery. An overall accuracy of 85% confirmed the viability of this approach and the authors concluded that it could potentially be employed in an operational system. Thenkabail & Wu (2012) developed a rule-based automated cropland classification algorithm (ACCA) for Tajikistan by combining Landsat, MODIS and secondary data. The ACCA was applied for the year 2005 and 2010, with overall accuracies of 99% and 96% respectively. The reported results demonstrated the ability of a rule-based ACCA to accurately produce a national cropland layer over multiple years. However, it must be noted that the ACCA is only applicable in the area (country/region) for which it was developed. The need to

modify rule-sets to suit different regions and landscapes is a potential disadvantage of a rule-based expert system.

#### 2.2.3.4 Classification accuracy metrics

A commonly used method to assess the accuracy of image classification is the confusion matrix (error matrix). The rows in the confusion matrix represent instances of the actual class (reference class), whereas the columns represent instances of the predicted class or vice-versa. Four accuracy metrics, namely the overall accuracy (OA), producers accuracy (PA), users accuracy (UA) and Kappa index can be derived from the matrix (Congalton 1991). The Kappa index is a measure of agreement or accuracy and illustrates how a specific classification compares to how a random classification would have performed (Congalton 1991). In addition, the McNemar's test can be employed to determine the statistical significance of the difference between two classification results. The test performs a two-by-two cross tabulation of dichotomous data in a non-parametric procedure (McNemar 1974). The chi-square statistic is calculated using the correctly and incorrectly classified samples as input and produces a P-value as output. The procedure has been used in multiple remote sensing studies to compare classifications (Duro, Franklin & Dube 2012; Yan et al. 2006).

#### 2.2.4 Object-based vs per-pixel image analysis

Most image analysis techniques developed in the early years of RS dealt with the spectral analysis of individual pixels in an image (Addink, Van Coillie & De Jong 2012; Blaschke et al. 2014). This led to the development of well-established and effective methods for classifying remote sensing imagery (Blaschke et al. 2014). Per-pixel-based image analysis (PBIA) methods assign each individual pixel to an informational class based on its spectral properties. However, these methods do not take into account the contextual or spatial information of the neighbouring pixels (Weih & Riggan 2010). With the continued increase in spatial resolution of RS imagery, the number of pixels of the target geographical features have increased (Blaschke et al. 2014). Furthermore, due to the spectral variability within classes, the "salt-and-pepper" effect has become common in per-pixel classifications. This phenomenon has a negative effect on classification accuracy (De Jong, Hornstra & Maas 2001). These limitations, along with the increased computing power available for image analysis, have led to the awareness that PBIA techniques are not optimal under certain conditions (Addink, Van Coillie & De Jong 2012), which in turn led to the development of OBIA. The intention of OBIA is to mimic the higher order logic employed by human interpreters to group features based on their shape, size, texture and spectral characteristics (Campbell & Wynne 2013).

Image objects were traditionally created through visual interpretation; however, more recently image segmentation has been widely adopted for this purpose (Castilla, Hay & Ruiz-Gallardo 2008). With image segmentation, pixels are grouped into useable objects based on their spectral and contextual information. These objects then become the minimum mapping units in the classification step. Segmentation algorithms are commonly based on two properties of a pixel's grey level values, namely similarity and discontinuity (Addink, Van Coillie & De Jong 2012). In the similarity approach, pixels are grouped based on the homogeneity between them, with methods such as region growing and thresholding being commonly applied. In contrast, the discontinuity approach partitions an image into non-overlapping objects based on the abrupt changes in pixel values. Objects hold advantages over pixels in their capacity to obtain a significantly larger number of spectral variables (mean, median, maximum, minimum and standard deviation, etc.) and spatial features (distances, neighbourhood and topologies, etc.) (Addink, Van Coillie & De Jong 2012; Blaschke 2010). Furthermore, the availability of topological information in object-based methods allow the integration of raster and vector data, providing a more GIS-like functionality in classification (Blaschke et al. 2014). However, the creation of meaningful objects that accurately represent features of interest is challenging as the parameters and thresholds used in segmentation need to be correctly tuned (Blaschke 2010). This highlighted the need for more research into automating the segmentation step in OBIA (Castilla, Hay & Ruiz-Gallardo 2008).

Castillejo-González et al. (2009) demonstrated the superior performance of OBIA against PBI for crop type mapping with Quickbird imagery. Similar findings were made by Yan et al. (2006), where the OBIA approach outperformed PBI by 36.8%. However, contrary to most studies, Duro, Franklin & Dube (2012) reported no significant difference between OBIA and PBI for classifying agricultural landscapes using a single SPOT-5 image. A more recent study by Belgiu & Csillik (2018) compared OBIA and PBI in a multi-temporal approach for cropland mapping with Sentinel-2 imagery. The OBIA approach was found to produce more accurate results. Gilbertson, Kemp & Van Niekerk (2017) demonstrated the success with which OBIA can be used for crop classification using medium resolution Landsat-8 imagery. It was also reported that accurate segmentation is crucial for image classification, which highlights the unique ability of OBIA to deal with agricultural fields due to their relative homogeneity compared to other land cover types.

### **2.3 BOUNDARY CONCEPTS**

Three important distinctions need to be made when undertaking RS studies of agricultural landscapes, namely cropland mapping, crop type mapping and field boundary delineation.



Cropland mapping studies the dynamics of agricultural land at regional/national scales and is commonly performed using low resolution (250 m – 1 km) imagery from sensors such as MODIS (Khan et al. 2010). Although these studies provide datasets covering large areas, they can only provide generalised statistics, are prone to error and do not offer field level information. Conversely, crop type mapping identifies different crop types and makes distinctions between them. This line of research has attracted much attention in recent years and generally employs medium resolution imagery such as 30 m (15 m pansharpened) Landsat data (Gilbertson & Van Niekerk 2017). The final distinction between agricultural RS studies concerns the identification and delineation of individual field boundaries regardless of the crops being grown. Therefore, even if two adjacent fields are planted with the same crop type, a boundary will be identified and delineated between them. Field boundary datasets are vital for agricultural monitoring systems that aid in precision agriculture and resource management.

### **2.3.1 Defining boundaries**

The delineation of accurate agricultural field boundaries has become increasingly important, largely due to the role they play in key areas such as precision farming and agricultural economics (Butenuth, Straub & Heipke 2004; Yan & Roy 2014). However, there are many interpretations of “field boundaries” (Davidse 2015). Ji (1996) defines the term “field” as the basic unit used to represent a specific land-use feature, while “boundary” can be defined as the linear edge features that are characterised by abrupt changes to the grey level values in a particular direction. Williamson & Ting (2001) characterise the term “boundary” as the physical objects, imaginary line or surface that mark the limit of a parcel of land. A similar definition is used by Jing (2011), where a boundary is considered as the imaginary line denoting the borders of two adjacent portions of land. However, according to the Oxford Dictionary, the definitions of “field” and “boundary” are as follows: A “field” is “an open area of land, specifically with crops or pastures and commonly bounded by hedges or fences”. “Boundary” is defined as a “line which marks the limits of an area; a dividing line”. In an agricultural context, a “field” very specifically has an agricultural land-use, while a “boundary” relates to where a change in crop type occurs or where there is the presence of a natural/man-made disruption between adjacent fields, for example a hedge or wall (Alemu 2016; Rydberg & Borgefors 2001). An important distinction is, therefore that, even if clear disruptions are absent, adjacent crops of different types are considered separate production units. Using remote sensing techniques for separating such production units from one another can be challenging as many crops can have similar spectral and structural characteristics at certain stages of the growing season (Pittman et al. 2010).



### 2.3.2 Boundary accuracy metrics

The increased availability of high spatial resolution imagery and computing power for image analysis has led to a growing interest in OBIA (Meyer & Van Niekerk 2015), but poor segmentation can adversely affect classifications (Batz, Hoffmann & Willhauck 2008). Robust validation tools that can assess whether the results of a segmentation accurately represent the actual features of interest (such as field boundaries) or artefacts of the segmentation algorithm have been a research priority for many years (Möller, Lyburner & Volk 2007). Several measures have been proposed, but none are definitive (Clinton et al. 2010; Meyer & Van Niekerk 2015). The three most common aspects to consider in segmentation quality are over-segmentation (OS), under-segmentation (US) and object boundary delineation. Consequently, one accuracy measure is not sufficient to provide accurate validations of segmentation algorithms (Weidner 2008).

There are a variety of area-based accuracy metrics that have been proposed to calculate OS and US (Clinton et al. 2010; Weidner 2008). Möller, Lyburner & Volk (2007) proposed the relative area (RA) metric to calculate  $RA_{sub}$  and  $RA_{super}$ . Using topological relationships of containment and overlap, the over-segmentation ( $RA_{sub}$ ) and under-segmentation ( $RA_{super}$ ) could be evaluated to determine the effectiveness of a segmentation. Ortiz & Oliver (2006) developed the empirical discrepancy method and proposed a set of new performance measures. Three metrics were calculated by means of an overlapping area matrix that evaluates the degree of fragmentation for segmented objects: (1) percentage of correctly grouped pixels (CG); (2) percentage of under-segmentation (US); and (3) percentage of over-segmentation (OS). However, area-based metrics do not take into account the positional accuracy of the delineated object boundaries. Esfahani (2014) adopted a confusion matrix approach for the assessment of delineated agricultural field boundaries. Accuracy elements such as OA, UA, PA and the Kappa index were computed using a sample of 500 random points generated along the field boundaries. The approach was reported to be successful in indicating the accuracy of their methodology. However, the measure only considers the boundaries along the reference fields and does not account for over-segmentation (i.e. boundaries within and outside fields). Zhan et al. (2005) proposed a distance-based metric to assess the positional accuracy of segmented objects. The Euclidean distance is calculated between the centroids of the extracted and reference objects. The mean and standard deviation were taken as measures of segmentation quality. Delves et al. (1992) proposed an edge metric to evaluate the positional accuracy of object boundaries. The edge metric calculates the average distance error from the reference objects to the nearest extracted objects. Although this metric provides a good indication of the object boundary delineation, it does not judge the goodness of fit between objects. Meyer & Van Niekerk (2015) assessed the use of both an area and edge metric to quantify the

accuracy of a segmentation algorithm to delineate objects. They concluded that using them in conjunction can account for the various facets in segmentation accuracy, whether it is boundary delineation or area overlap.

## **2.4 REMOTE SENSING TECHNIQUES FOR AGRICULTURAL FIELD BOUNDARY DELINEATION**

With the advancement in the spatial and temporal resolution of satellite imaging systems, along with the increase in computer power, image segmentation has become a major field of interest in many applications because of its ability to reduce variability within classes. This has led to the development of numerous segmentation algorithms. The algorithms used in RS are commonly grouped into either point-based, edge-based, region-based or hybrid segmentation (Chen et al. 2015).

### **2.4.1 Point-based segmentation**

Point-based segmentation algorithms generally apply global thresholds to group pixels without consideration of the surrounding neighbourhood (Schiewe 2002). Histogram thresholding segmentation is one of the most commonly applied algorithms. It uses the shape of image histograms to differentiate between classes (Chen et al. 2015). A typical threshold segmentation procedure comprises three main steps: 1) identify histogram modes (peaks); 2) determine valleys between modes; and 3) calculate and apply the threshold that best separates the modes (Gonçalves, Gonçalves & Corte-Real 2011). Point-based techniques are quick and effective for segmenting images based on their histogram distribution (Carleer, Debeir & Wolff 2005). However, for the technique to be successful, it requires the informational classes to have evidently different spectral values. This is problematic when dealing with large remotely sensed imagery as informational classes often exhibit inter-class spectral similarity and intra-class heterogeneity, which deforms the histogram (Chen et al. 2015). Therefore, the application of point-based segmentation is commonly only applied to local object delineation or for informational classes that have very distinct spectral properties, such as water (Gonçalves, Gonçalves & Corte-Real 2011).

### **2.4.2 Edge-based segmentation**

Edge-based segmentation algorithms are designed to detect and locate sharp discontinuities within an image (Maini & Aggarwal 2009). Discontinuities can be defined as pixels that represent a local change in image intensity (edges between objects) and are consequently used as candidate pixels for object boundaries (Yang, He & Caspersen 2017). Edge detection is an important part of the segmentation procedure as it filters out unnecessary information, thus conserving the structural

properties of features (Batra et al. 2016). Edge detection commonly involves three main steps, namely:

1. filtering, to remove random variations in intensity (i.e. noise);
2. enhancement, to emphasise pixels with a significant change in local intensity (commonly performed by computing the gradient magnitude); and
3. detection, to determine the final edge points, frequently performed using a threshold value.

Image filtering (step 1) is often challenging, as there is a trade-off between reducing noise and losing edge strength. There are a variety of edge detection algorithms that have been developed, from simple algorithms such as the Sobel, Scharr and Prewitt operators, to more complex techniques such as the Canny operator (Muthukrishnan & Radha 2011; Shrivakshan & Chandrasekar 2012). These operators are described in the following subsections.

#### 2.4.2.1 Sobel edge detection

The Sobel operator uses a 3x3 pair of convolution kernels to compute the gradient magnitude in an image (Maini & Aggarwal 2009). The pixel weighting provides smoothing while also enhancing the edges in the original image (Batra et al. 2016). The edge masks are shown in Figure 2-1.

$$G_x = \begin{array}{|c|c|c|} \hline 1 & 0 & -1 \\ \hline 2 & 0 & -2 \\ \hline 1 & 0 & -1 \\ \hline \end{array} \quad G_y = \begin{array}{|c|c|c|} \hline 1 & 2 & 1 \\ \hline 0 & 0 & 0 \\ \hline -1 & -2 & -1 \\ \hline \end{array}$$

Figure 2-1 Horizontal and vertical edge masks used by the Sobel edge detection algorithm

#### 2.4.2.2 Canny edge detection

The Canny edge detector was designed with the intention of outperforming various other edge detectors (Maini & Aggarwal 2009). The method proved to be highly successful in many studies. Consequently, the algorithm is commonly used as a benchmark against which newly developed edge detection algorithms is compared (Juneja & Sandhu 2009; Maini & Aggarwal 2009; Ramadevi et al. 2010; Sharma & Mahajan 2017; Shrivakshan & Chandrasekar 2012). Canny attempts to optimise the product of signal-to-noise ratio and localisation in an image by executing the following three steps:

1. a Gaussian filter is employed to smooth the image and reduce unwanted noise;
2. the gradient magnitude and orientation is computed using the Sobel operator; and
3. non-maxima suppression is applied to the gradient magnitude, followed by a double threshold to determine the final edge pixels.

### 2.4.2.3 Scharr edge detection

The Scharr edge detection algorithm was developed as an improvement on the Sobel operator (Sharma & Mahajan 2017). An improved derivative kernel was created for better rotational invariance, thereby improving the detection of object edges and reducing noise (Kroon 2009; Scharr 2007). The improved kernel consists of the horizontal and vertical edge masks in Figure 2-2.

$$G_x = \begin{array}{|c|c|c|} \hline 3 & 0 & -3 \\ \hline 10 & 0 & -10 \\ \hline 3 & 0 & -3 \\ \hline \end{array} \quad G_y = \begin{array}{|c|c|c|} \hline 3 & 10 & 3 \\ \hline 0 & 0 & 0 \\ \hline -3 & -10 & -3 \\ \hline \end{array}$$

Figure 2-2 Horizontal and vertical edge masks used by the Scharr edge detection algorithm

These three algorithms can rapidly partition an image into edges and non-edges and are highly accurate for features with obvious edges. However, image features do not always have obvious edges/boundaries, which can lead to the creation of gaps along object borders. Furthermore, as both edges and noisy images contain high intensity content, edge detection algorithms are not very effective with noisy images (Maini & Aggarwal 2009). In addition, because most edge detectors are based on local contrasts they become particularly sensitive to noise, which often leads to the over-segmentation of real-world objects or detection of false edges (Chen et al. 2015). Although there are post-processing procedures (such as edge tracking and gap-filling) to correct some of these errors, they can be very time-consuming and add complexities to workflows (Fan et al. 2001).

### 2.4.3 Region-based segmentation

Region-based segmentation groups pixels with similar spectral or textural properties (Fan et al. 2001). A major advantage of region-based methods is the formation of closed objects, although the positional accuracy of the object boundaries are often not as accurate as those created by edge-based techniques (Zhou, Starkey & Mansinha 2004). Boundary errors often occur when the image objects stop growing before the actual feature boundary is reached (Chen et al. 2015). This is caused by feature boundaries' formation of their own regions of homogeneity, which consequently leads to the creation of sliver polygons along the boundaries and causes the resulting object border to shift inwards (towards the centre of the feature). Two popular region-based methods are the multi-resolution segmentation (MRS), as described in Baatz & Schäpe (2000), and the watershed segmentation algorithm (WS) (Roerdink & Meijster 2000).

#### 2.4.3.1 Multi-resolution segmentation

MRS is a bottom-up region merging algorithm that can be applied to both the pixel and object domains (Blaschke 2010). The algorithm was developed to merge objects in a way that would minimise the average heterogeneity between objects, while maximising the homogeneity within objects (Benz et al. 2004). It employs a mutual best-fitting approach, starting with image objects of one pixel and iteratively merging them based on user-defined homogeneity parameters. The segmentation requires a scale factor and heterogeneity criterion – the average size of objects are controlled by the scale, whereas the heterogeneity criterion comprises two properties, namely colour and shape (Li et al. 2015). While colour refers to the spectral homogeneity, the shape considers geometric properties of the objects and is further sub-divided into smoothness and compactness (Baatz & Schäpe 2000).

MRS has been applied in numerous studies for crop mapping. Vieira et al. (2012) employed it in an OBIA paradigm to map sugarcane using time series Landsat-5 imagery. The overall accuracy of 94% showed the potential of this approach. Peña et al. (2014) applied the MRS algorithm to multi-temporal ASTER data for classifying nine major summer crops in California, USA. The empirical discrepancy method (see Section 2.3.2) was used to quantify the performance of the segmentation. An accuracy of 94% was reported between the segmented and reference fields. Li et al. (2015) investigated the synergistic use of feature selection, OBIA and a decision tree classifier to map cropland using multi-temporal fused Landsat-MODIS data. The OBIA classification achieved good results with an OA of 91%. However, it was noted that errors in the segmentation of crop fields can cause uncertainties in the final classification. This highlights the importance of parameter selection in segmentation algorithms. The risks associated with inappropriate parameter selection in MRS has been echoed in many studies (Belgiu & Csillik 2018; Castillejo-González et al. 2009; Gilbertson, Kemp & Van Niekerk 2017; Peña-Barragán et al. 2011).

#### 2.4.3.2 Watershed segmentation

The WS algorithm, as described in Roerdink & Meijster (2000), is commonly applied to a gradient image. The objective of the algorithm is to extract high magnitude edges (watersheds) that divide regions of local minima (basins) (Salman 2006). Initial seed objects are created in regions of local minima. The seed objects are then expanded outwards with rising intensity levels. An object will cease to expand after coming into contact with a neighbouring object. Although many watershed algorithms have been devised, the application of WS to a gradient image is often suboptimal as the image is commonly over-segmented into a significantly large number of small objects (Bleau

& Leon 2000). Over-segmentation is largely caused by noise in gradient images. Common noise removal techniques, such as image smoothing, could potentially reduce noise, but this is often at the expense of loss in definition of actual boundary edges and is therefore not always a suitable solution (Gaetano et al. 2015). The marker-based WS method was developed as an improvement on the traditional algorithm (Gao et al. 2006). The segmentation is guided with markers drawn by the user, and all segments that border the marker will be merged, thereby reducing over-segmentation (Gaetano et al. 2015). However, the manual selection of appropriate markers requires a priori knowledge, which is often considered to be the hardest task (Bleau & Leon 2000). Sun & He (2008) performed marker-based WS on high resolution Quickbird imagery. Although the algorithm worked well in a diverse landscape, they noted the need for automated and adaptive techniques for threshold determination should the technique be applied to large areas.

A common post-segmentation technique, with a long history in image processing, is region merging (Castilla, Hay & Ruiz-Gallardo 2008). In WS, an elevation threshold can be used to merge segments (basins) if the height difference (from seed to saddle) is less than a specified threshold. While this global threshold technique is effective for dealing with the level of over- or under-segmentation, it is limited in that the same value must be used for each segment, regardless of the homogeneity of its neighbouring objects (Yang, He & Caspersen 2017). Local thresholding methods have thus been developed in an attempt to adjust the threshold per object (Chen et al. 2014; Johnson & Xie 2011). However, the implementation of local thresholding techniques can become quite complex and limits its applicability to an operational context (Yang, He & Caspersen 2017).

#### **2.4.4 Hybrid segmentation approaches**

Hybrid segmentation approaches attempt to combine the advantages of edge-based (accurate boundary edges) and region-based (closed boundary objects) segmentation techniques (Rydberg & Borgfors 2001). A variety of hybrid approaches have been developed for various applications. Rydberg & Borgfors (2001) developed a hybrid segmentation method to delineate agricultural fields using multispectral SPOT (20 m) and Landsat (30 m) single-date imagery. Edge layers, extracted from a gradient edge detector, were aggregated using a weighted vector addition, followed by an unsupervised segmentation method based on the ISODATA algorithm. The relatively high accuracy of 87% was reportedly due to the ability of the method to combine information from multiple bands. Castilla, Hay & Ruiz-Gallardo (2008) devised a hybrid method for three different types of satellite data (Landsat-7, SPOT5 and Quickbird) in three agricultural regions. WS was carried out on a filtered gradient image to create initial segments, followed by

region merging using a specified minimum size criterion. They reported good segmentation quality based on a qualitative assessment; however, the algorithm required intuitive user parameters to dictate the size of output regions. A similar split-and-merge segmentation strategy using very high resolution (2.4 m) Quickbird images was considered by Wuest & Zhang (2009). The framework comprised three steps in which (i) the image is first split into a set of initial objects; (ii) the resulting objects are merged based on a merge importance criterion; and (iii) the final objects are refined using localised border measures. The strategy was able to successfully merge objects in rough land cover classes such as vegetation, forests and urban environments. However, the authors noted that parameter selection was vital and a more dynamic method should be developed.

Li et al. (2010) employed the marker-based WS algorithm on multiple Quickbird images in suburban landscapes. Edge detection was performed using the edge detection with embedded confidence method (Meer 2001). Three commonly used edge detection steps, namely gradient estimation, non-maxima suppression and hysteresis thresholding were used; however, an independent confidence measure was employed in the gradient estimation and thresholding steps to assist the detection of weak edges and increase the positional accuracy of object boundaries. The authors reported an accuracy of 78% and observed little over-segmentation. A similar hybrid approach by Gaetano et al. (2015) applied a marker-based WS to IKONOS (1 m) panchromatic and multispectral imagery for segmenting different land cover types. This study automated the generation of markers for use in the WS algorithm. It was compared with a standard MRS segmentation and showed a higher segmentation accuracy in terms of over- and under-segmentation.

Alemu (2016) also used a hybrid approach by implementing a line segment detection (LSD) algorithm to extract linear features from high resolution (2 m) Worldview-2 imagery for crop field identification. The gradient information from all bands was aggregated by taking the vector sum of the changes in the x and y directions for all bands. A region growing technique was performed on the aggregated image to form line-support regions (potential candidates for segmentation). The validation of results used two metrics based on the distance and orientation of boundaries, namely ratio of false detection and ratio of missing detections. High accuracies were obtained; however, these could be attributed to the over detection of boundaries (false positives) as the algorithm did not distinguish between field boundaries and other edges (e.g. tree edges). Furthermore, the method had difficulty in delineating many field boundaries, which was attributed to weak contrast between fields within a heterogeneous landscape. Yang, He & Caspersen (2017) attempted to develop a hybrid region merging method using local spectral angle thresholds with Landsat-5 imagery in a large agricultural area. Initial segments were created using the watershed



transformation. A region adjacency graph (RAG) was then applied to determine neighbouring objects, which was followed by a spectral difference calculation between adjacent objects. Segments were merged if their spectral difference was below the local heterogeneity threshold specified. The method provided more accurate segmentation results than when a global threshold was applied. However, the calculation of the local threshold required manual selection of input parameters, which limits the value of the technique for operational implementations.

## **2.5 LITERATURE SUMMARY**

This chapter provided an overview of the literature relating to crop field boundary delineation. A summary was given of the three main activities in agricultural RS studies, namely (1) cropland mapping, which was identified as a method that provides an estimation of land used for agricultural purposes; (2) crop type mapping, which distinguishes between different crop types; and (3) field boundary delineation, which identifies and delineates individual fields regardless of the crop type being grown within or adjacent to a cultivated field. Accurate and up-to-date agricultural field boundaries are critical in agricultural monitoring systems as agricultural statistics are commonly calculated per-field. These monitoring systems are used for the implementation of precision agriculture, food security evaluations and resource planning.

According to literature, a hybrid segmentation approach works best for delineating agricultural field boundaries as it combines the advantages of edge- and region-based methods. However, as with edge- and region-based methods, the automation of segmentation parameters is still a difficult task and needs further investigation. Although the tuning of segmentation parameters can be difficult, the advantages of OBIA over per-pixel analysis are compelling. This includes the reduction in noise (e.g. “salt-and-pepper effect”), generation of closed field boundaries, and a general improvement in cropland classification accuracies. Regarding segmentation accuracy: a wide range of evaluation techniques have been proposed, but it has been noted that no single measure can fully assess a segmentation output in terms of over-segmentation, under-segmentation and boundary accuracy. Therefore, different measures have to be considered to get a true sense of segmentation output quality. It is clear from the literature that different crop types can have similar spectral and structural properties at certain stages of growth. Determining the edges of fields using single-date imagery can thus become challenging. Therefore, it is essential to use imagery from multiple dates in a growing season to detect the spatial transition (edges) between crops of different types as well as crops of the same type.

The next chapter (Chapter 3) evaluates several combinations of edge detection and segmentation techniques for delineating crop field boundaries in a large irrigation scheme. The main purpose of



the chapter is to determine which combinations of techniques produce the most accurate field boundaries when multi-temporal Sentinel-2 imagery is used as the data source. This leads directly to Chapter 4, which describes the implementation of the best combination of techniques (identified in Chapter 3) across five different agricultural landscapes to determine the robustness and flexibility of the proposed technique. Chapters 3 and 4 are structured as research articles (at the time of writing, Chapter 3 has been published and Chapter 4 has been submitted for review). Consequently, some degree of overlap (duplication) between these two chapters can be expected. Chapter 5 provides a synthesis of the research. Some conclusions are also drawn and recommendations for operational implementation are made.

## **CHAPTER 3: A COMPARISON OF OBJECT-BASED IMAGE ANALYSIS APPROACHES FOR FIELD BOUNDARY DELINEATION USING SENTINEL-2 IMAGERY \***

### **3.1 ABSTRACT**

In this study we evaluated several Earth observation methodologies for automatically delineating crop field boundaries from multi-temporal Sentinel-2 imagery. The methodology makes use of edge detection that is applied to multiple images acquired during a growing season and image segmentation to delimit agricultural fields, orchards and vineyards. Two edge detection operators (Canny and Scharr) and three image segmentation algorithms (watershed, multi-threshold and multi-resolution) were combined and evaluated, resulting in six experiments (scenarios). A rule-based (knowledge-based) classification was applied to the extracted image objects to discard uncultivated areas. Reference field boundaries, manually digitised from very high (10 cm) resolution aerial imagery, were used for quantitative accuracy assessments and qualitative comparisons. The quantitative accuracy assessment consisted of both area- and edge-based metrics. The results showed that the watershed segmentation, combined with Canny edge detection, produced the most accurate field boundaries with an OA of 92.9% and combined MAE of 24.5 m. The Scharr algorithm produced thicker edges, causing positional errors along the boundaries. The multi-resolution and multi-threshold segmentation algorithms produced boundary inaccuracies ranging from 1 to 3 pixels, largely due to the creation of thick boundary objects, which caused offsets of the extracted borders on both sides of the reference boundaries. The combination of Canny edge detection (performed on multiple Sentinel-2 images acquired during the growing season) and watershed segmentation is thus recommended for operational field boundary delineation.

### **3.2 INTRODUCTION**

The spatial extent and location of agricultural fields is critical for the implementation of precision agriculture, crop yield estimations, food security assessments and resource planning (Alemu 2016; Johnson 2013; Yan & Roy 2014). Agricultural statistics are commonly calculated per-field, and results are negatively affected by inaccurate or outdated field boundaries (Rydberg & Borgefors 2001; Turker & Kok 2013). Classifying crops using a per-field (object-based) approach is known

---

\* This chapter was published in *Computers and Electronics in Agriculture* and consequently conforms to the structure of the prescribed journal.

to produce better results than a per-pixel method (Blaschke et al. 2014; Peña et al. 2014; Schultz et al. 2015). However despite the advantages of such object-based methods, robust techniques to automatically delineate agricultural field boundaries remain elusive (Belgiu & Csillik 2018).

A number of remote sensing approaches for determining cropland extent have been explored. Many of these approaches are applied at regional or global scale, using low to medium resolution satellite imagery (Lunetta et al. 2010; Wardlow, Egbert & Kastens 2007). Pittman et al. (2010) showed the benefits of using multi-temporal MODIS (250 m spatial resolution) imagery for generating a global cropland probability layer. Roumenina et al. (2015) assessed the crop mapping performance of multi-temporal PROBA-V (100 m spatial resolution) against PROBA-V (300 m spatial resolution) imagery in a test site in Bulgaria. Their findings demonstrated an increase in crop mapping accuracy (by 5.8% to 14.8%) when the higher (100 m) spatial resolution imagery was used. Gilbertson, Kemp & Van Niekerk (2017) showed that pansharpening Landsat-8 imagery from 30 m to 15 m spatial resolution improved crop type classification accuracies by up to 15%, but noted that the use of multi-temporal imagery is critical for achieving good results. From these studies it would seem that both high spatial and high temporal resolution imagery is required for accurate field boundary delineation (Alemu 2016; Mueller, Segl & Kaufmann 2004).

The Copernicus programme is an Earth observation initiative that will provide unprecedented levels of observational capabilities, mainly through the operations of recently launched satellites (called Sentinels). The Sentinel-2 satellite constellation provides a significant increase in observational capacity compared to other satellites such as Landsat, thanks to its large number (13) of spectral bands, high (10 m – 60 m) spatial resolutions and short (five-day) revisit times (Lebourgeois et al. 2017). This data allows for more timely estimates of crop area extents, crop types and crop conditions, which are all major indicators of a region's agricultural activity (Bontemps et al. 2015). Although the resolution of Sentinel-2 images is not as high as many commercial very high resolution (VHR) satellites (e.g. WorldView 2 – 4), its short revisit periods, wide spectral range (including narrow red edge bands) and free access hold much potential for operational (automated) field boundary delineation.

Field boundary delineation using remotely sensed imagery can generally be categorised into edge-based and region-based techniques (Rydberg & Borgfors 1999; Turker & Kok 2013; Wuest & Zhang 2009). Edge-based methods focus on detecting the edges (discontinuities between pixel values) in images that are used as candidate pixels for region boundaries. There are a range of edge detectors; from simple algorithms such as the Sobel or Scharr operators, to more complex techniques such as the Canny operator (Shrivakshan & Chandrasekar 2012). These algorithms

rapidly partition images into edges and non-edges. However, boundaries between objects are not always well defined, which can lead to gaps in the boundaries. Furthermore, most edge detectors are sensitive to noise as they often exploit local contrasts, which may lead to errors such as false edges (Chen et al. 2015). These errors require post-processing procedures such as gap-filling, edge tracking and smoothing in order to create well defined boundaries (Fan et al. 2001). Rydberg & Borgefors (1999) presented a multispectral edge detection method to delineate agricultural fields using single-date Landsat (30 m) imagery. A gradient edge detector was used to generate the edge magnitude and direction. Weighted addition, based on the edge direction, was applied to enhance edges and reduce noise. The resulting edge image was thinned using edge direction and magnitude, followed by hysteresis thresholding to produce the field boundaries. A qualitative assessment showed accurate field boundary delineation, but the method did not produce closed boundaries. Turker & Kok (2013) devised a method for detecting sub-boundaries by employing Canny edge detection on single-date SPOT4 (20 m) and SPOT5 (10 m) multispectral imagery covering an agricultural area in Turkey. Line segments were created from edge chains, followed by the elimination of spurious line segments through a geometrical simplification process. Lastly, perceptual grouping of the line segments was performed using Gestalt laws. The study reported matching percentages between the reference data and extracted segments of 82.6% and 76.2% for the SPOT5 and SPOT4 images respectively.

In contrast to edge-based methods that exploit variations in the image, region-based methods group pixels into objects based on some homogeneity criterion (Alemu 2016; Mueller, Segl & Kaufmann 2004). Multi-resolution segmentation (MRS), as detailed in Baatz & Schäpe (2000), is a popular region-based segmentation algorithm used for field boundary delineation. MRS begins with a set of seed pixels that are iteratively merged according to some heterogeneity/homogeneity criterion (Schultz et al. 2015). Belgiu & Csillik (2018) performed MRS on multi-temporal Sentinel-2 imagery for cropland mapping. Segmentation of crop fields proved difficult as fields with high internal variation were found to be over-segmented, while small adjacent fields were under-segmented. Watershed segmentation (WS), another popular region-based segmentation algorithm, is applied to a single gradient image with the objective of finding regions of high intensity (watersheds) that divide regions of local minima (basins) (Salman 2006). Butenuth, Straub & Heipke (2004) employed the WS algorithm to delineate agricultural fields from aerial imagery. GIS knowledge of existing field boundaries were used to support the segmentation. The results displayed the potential of the technique to delineate agricultural fields. Multi-threshold segmentation (MTS) is another simple and effective segmentation algorithm that can quickly partition an image based on the image histogram (Carleer, Debeir & Wolff 2005). A disadvantage

of region-based algorithms is that errors often occur along field boundaries when objects stop growing before the actual boundary is reached (Chen et al. 2015). Field boundaries consequently form a separate region of homogeneity, which can lead to the creation of sliver polygons along field edges. In effect, this causes the extracted field boundary to shift inwards (towards the centre of the field).

A hybrid approach, that integrates both edge-based and region-based methods has been proposed to exploit the advantages of each (Rydberg & Borgefors 2001). For instance, Mueller, Segl & Kaufmann (2004) demonstrated the value of object-based image analysis (OBIA) for extracting agricultural fields from very high resolution single-date panchromatic imagery. Edge detection was performed at different spatial resolutions (4.5 m, 5.8 m and 1 m) to detect pertinent edges. This was followed by an edge-guided smoothing and region growing segmentation to produce field boundaries. Similarly, Rydberg & Borgefors (2001) segmented single-date high resolution (20 m SPOT4 and 30 m Landsat-7) multispectral images to delineate agricultural field boundaries. A gradient edge detector was utilised to extract edge images from each band, which were then aggregated using weighted vector addition. The resulting edge image was combined with a segmentation algorithm based on an ISODATA algorithm. The high (87%) overall accuracy (OA) achieved was attributed to the method's ability to exploit edges from several bands. Li et al. (2010) also followed a hybrid approach by employing the WS algorithm on multiple Quickbird images. Edge detection with an embedded confidence measure was first performed to amplify weak edges. This was followed by a marker-based watershed algorithm to delineate the object boundaries. The procedure was reported to provide satisfactory results with little over-segmentation and a boundary accuracy of approximately 78%. In another hybrid approach, Alemu (2016) made use of a line segment detection algorithm to extract linear features on very high resolution (2 m) Worldview-2 imagery. Changes in the x and y directions of each band were combined using a vector sum. A line-support region representing potential candidates for a segment was formed using a region growing technique. Two metrics based on the distance and orientation of boundaries, namely ratio of missing detections (RM) and ratio of false detections (RFD), were used to validate the results. The results obtained for RM and RFD were 0.78 and 0.73 respectively (where values closer to one represent higher accuracies). However, the accuracy measures did not distinguish between field boundary edges and other edges (e.g. edges formed by tree shadows), thus leading to the false detection of edges and overestimation of RM and RFD values. Upon visual inspection of the results, the developed methodology tended to omit many field boundaries, which was attributed to the heterogeneous landscape and weak contrast between neighbouring fields.

One common limitation of the field boundary delineation methods mentioned above is the use of single-date imagery. Finding the edge of a field is challenging when different crop types have similar spectral and structural properties at certain stages of their phenological growth cycle (Esfahani 2014; Pittman et al. 2010). This is compounded when a single crop is grown on adjacent fields. Therefore, it is necessary to use multiple images throughout the growing season to accurately detect spatial transitions (edges) between different crop types as well as crops of the same type (Inglada et al. 2015). Sentinel-2 imagery (Drusch et al. 2012), available at 10 m spatial resolution and at unprecedentedly short intervals (five-day revisit time), has opened up new possibilities for operational (automated) crop field boundary delineation using Earth observation methods.

The primary aim of this study is to compare and evaluate several OBIA techniques for automatically delineating agricultural field boundaries from multi-temporal Sentinel-2 imagery. Two edge detection and three image segmentation algorithms are configured in different combinations to construct six experiments. The results of the experiments are compared and assessed against reference field boundaries in Vaalharts, the largest irrigation scheme of South Africa. The results of the experiments are interpreted in the context of finding an operational methodology for identifying agricultural field boundaries in complex and dynamic irrigation schemes.

### **3.3 METHODS**

#### **3.3.1 Study area**

The Vaalharts irrigation scheme (Figure 3-1) is located at the border of the Northern Cape, North West and Free State provinces of South Africa, near the towns of Warrenton and Hartswater. The area is approximately 369.5 square kilometres in size and has a semi-arid climate with cold, dry winters and long warm summers (Maisela 2007). The annual rainfall is approximately 450 mm, with around 89% of precipitation falling during summer (October–April), peaking from January to April (Maisela 2007). The main crops grown in the area are maize, barley, groundnuts, pecan nuts and lucerne. Wheat, barley and lucerne are grown during the dry winter months.

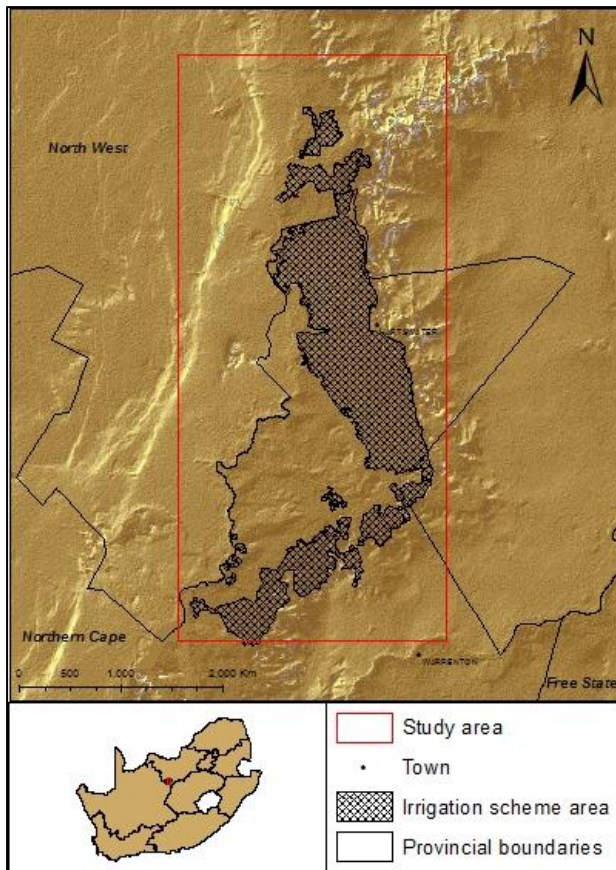


Figure 3-1 Extent and location of the study area within South Africa

### 3.3.2 Image collection

In this study, focus was placed on the summer growing season when the diversity of crops is at its greatest. Seven cloud-free Sentinel-2 images were acquired for the months of November 2016 to April 2017. The Sentinel-2 satellite constellation offers spatial resolutions of 10 m, 20 m and 60 m across 12 bands with a revisit time of five days (Table 3-1). The Sentinel-2 imagery was acquired in Level-1C format, which is radiometrically and geometrically corrected to top of atmosphere (TOA) reflectance.



Table 3-1 Sentinel-2 satellites characteristics including band names, wavelength and spatial resolution

Sentinel-2 bands	Central wavelength ( $\mu\text{m}$ )	Resolution (m)
Band 1 – Coastal aerosol	0.443	60
Band 2 – Blue	0.490	10
Band 3 – Green	0.560	10
Band 4 – Red	0.665	10
Band 5 – Vegetation red edge	0.705	20
Band 6 – Vegetation red edge	0.740	20
Band 7 – Vegetation red edge	0.783	20
Band 8 – Near-infrared (NIR)	0.842	10
Band 8A – Vegetation red edge	0.865	20
Band 9 – Water vapour	0.945	60
Band 10 – SWIR – cirrus	1.375	60
Band 11 – SWIR	1.610	20
Band 12 – SWIR	2.190	20

### 3.3.3 Experimental overview

The OBIA experiments evaluated in this study consisted of five main processing steps:

1. Edge detection, performed on all individual images;
2. Aggregation of edge layers generated in Step 1;
3. Image segmentation, carried out on the aggregated edge image produced in Step 2;
4. Discarding of uncultivated image objects; and
5. Removal of noise.

The following subsections expand on each of these steps.

#### 3.3.3.1 Step 1: Edge detection

Two edge detection algorithms were considered in Step 1, namely the Scharr and Canny operators (Table 3-2). An edge in an image can be defined as a sharp change or discontinuity in the grey level values (Christe, Vignesh & Kandaswamy 2011; Ramadevi et al. 2010; Rydberg & Borgefors 2001; Shrivakshan & Chandrasekar 2012). Edge detection is a very common operation performed in image analysis, and many algorithms have been developed for detecting and enhancing edges (Christe, Vignesh & Kandaswamy 2011). Examples include Sobel, Prewitt, Robert, Scharr and Canny. The edge detection algorithm generates an edge layer, which can be described as a grey



level image representing object edges. High grey level values indicate a sharp discontinuity with the adjacent pixels. The Canny and Scharr operators were used in this study due to their superior performance in comparison to other edge detection algorithms (Batra et al. 2016; Muthukrishnan & Radha 2011; Sharma & Mahajan 2017).

Table 3-2 Description of the different algorithm scenarios

Scenario	Edge detection algorithm	Segmentation method
MTS_C	Canny	MTS
MTS_S	Scharr	MTS
MRS_C	Canny	MRS
MRS_S	Scharr	MRS
WS_C	Canny	WS
WS_S	Scharr	WS

#### *Canny edge detection*

The Canny edge detector is generally considered to provide better results than other edge detectors and is often used as a benchmark against which other edge operators are compared (Canny 1986). The Canny operator involves a multistage process that can be summarized as follows: the image is first smoothed with a Gaussian filter, followed by gradient computation, non-maxima suppression and hysteresis thresholding (Juneja & Sandhu 2009). The Trimble eCognition Developer (version 9) implementation of the Canny algorithm was used in this study.

#### *Scharr edge detection*

The Scharr operator was developed to alleviate the rotational invariance inherent in operators such as Sobel and Prewitt (Kroon 2009; Scharr 2007). This is achieved by using differently weighted horizontal and vertical edge masks, as shown in Figure 3-2. These edge masks help to suppress noise that is inherent in the Sobel operator (Christe, Vignesh & Kandaswamy 2011).

$$G_x = \begin{bmatrix} 3 & 0 & -3 \\ 10 & 0 & -10 \\ 3 & 0 & -3 \end{bmatrix} \quad G_y = \begin{bmatrix} 3 & 10 & 3 \\ 0 & 0 & 0 \\ -3 & -10 & -3 \end{bmatrix}$$

Figure 3-2 Horizontal and vertical Scharr edge masks

The Scharr edge detection algorithm was implemented in Python using the Scikit image library (version 0.13.1). The algorithm requires no input parameters, apart from the input image.

The Canny and Scharr algorithms were applied on all seven cloud-free Sentinel-2 images collected from November 2016 to April 2017. The red, blue, green and NIR bands were used as input to the edge detection algorithms due to their relatively high (10 m) spatial resolution. This resulted in four 10 m resolution edge layers per image per operator.

### 3.3.3.2 Step 2: Edge layer aggregation

Step 2 of the workflow involved the aggregation of the 28 (4 bands x 7 acquisition dates) multi-temporal edge layers generated by each edge operator. A simple equal weight summation of the edge layers was used to combine the images into one composite, multi-temporal edge image per operator.

### 3.3.3.3 Step 3: Image segmentation

In the image segmentation step (Step 3), the aggregated edge images (one for Canny and one for the Scharr operator) were used as input to three selected image segmentation algorithms, namely MRS, WS and MTS. The MRS and WS algorithms were chosen due to their frequent use in agricultural applications (Butenuth, Straub & Heipke 2004; Conrad et al. 2010; Lebourgeois et al. 2017; Li et al. 2010; Peña et al. 2014; Schultz et al. 2015). The MTS algorithm was selected as it is an effective technique to rapidly segment images based on the distribution of the input image's histogram (Carleer, Debeir & Wolff 2005).

#### *Watershed segmentation*

WS is a region-based algorithm that is applied to a single gradient image (Li et al. 2010). The objective of the algorithm is to find the high gradient magnitudes (watersheds) that divide regions of local minima (basins) (Salman 2006). The algorithm uses local minima as seed points and expands objects outward with rising intensity levels. Objects cease to expand after they reach the borders of another object. The WS algorithm is prone to over-segmentation and often produces a large number of small objects, thereby making it necessary to perform some form of region merging during or after the execution (Bleau & Leon 2000).

The WS algorithm, as implemented in Trimble eCognition Developer 9, has four parameters for region merging, namely area, height, depth and volume. The height parameter is used to control when adjacent objects should be merged (i.e. when an object's maximum pixel value is below the specified height threshold). Given that the ultimate aim is to develop an automated system for field boundary delineation, Jenks' (Jenks 1967) natural breaks (JNB) algorithm, as implemented in ArcMap (version 10.4.1), was used to automatically find a suitable threshold. The JNB algorithm minimises intra-class variance while maximising inter-class variance. The algorithm was used to

sequentially group the pixel values into two, three, four and five classes to find the most suitable thresholds. Through experimentation it was determined that grouping pixels into three classes and using the threshold separating the first and second class produced the best merging threshold for the WS algorithm. The final threshold values were 0.1214 and 0.0812 for the Canny and Scharr edge layers respectively.

#### *Multi-resolution segmentation*

MRS, as implemented in Trimble eCognition Developer 9, is a region-based procedure that maximises the homogeneity within objects while minimising the average heterogeneity between objects (Baatz & Schäpe 2000). The MRS procedure follows a mutual best-fitting approach by starting with image objects of one pixel and repeatedly merging them based on a user-defined homogeneity criterion. MRS parameters were chosen using a trial and error approach where individual parameters were systematically increased and the resulting segmentations evaluated against reference field boundaries (see Section 3.3.4). The parameters that produced the most meaningful (slightly over-segmented) segmentation results were 60 (scale), 0.8 (compactness) and 0.5 (shape).

#### *Multi-threshold segmentation*

MTS classifies an image into subsets based on pre-defined threshold values (Trimble 2016). For example, a single threshold will group the image pixels into two classes. The first class contains pixels with values below the defined threshold, while the second class contains pixels with values above the threshold. MTS was used in this study to group pixels into two classes, namely edge and not-edge. The edge pixels were then discarded, leaving only homogenous areas (objects) such as fields. The threshold values for the Canny and Scharr edge layers were identical to the WS thresholds (0.1214 and 0.0812 respectively).

#### 3.3.3.4 Step 4: Uncultivated area exclusion

Expert rules were used in Step 4 to automatically discard uncultivated areas from further consideration. The rule-set was designed to be reproducible and fully automatic. Normalised difference vegetation index (NDVI) time series have been shown to correlate strongly with the phenology of crops during the growing season (Huete 1988; Maselli & Rembold 2001; Zheng et al. 2015). Four NDVI-based features, namely maximum, minimum, range and standard deviation were consequently extracted per-pixel from the seven Sentinel-2 images considered. These features were used as input to a classification and regression tree (CART) algorithm to generate a decision tree for separating (classifying) cultivated and uncultivated objects. Manually selected

sample points were used to train the CART algorithm. The resulting rule-set was implemented in Trimble eCognition Developer (version 9) software and used in all experiments. An additional threshold-based rule was added to the MRS workflow to remove sliver polygons (i.e. high magnitude edges) along the field boundaries that were erroneously classified by the decision tree as crop fields. The rule makes use of the Scharr and Canny edge layers to identify and discard objects (segments) with high edge values. The threshold values for the Scharr (0.0812) and Canny (0.1214) edge layers that were determined using the JNB algorithm and applied to the WS and MTS implementations were used for this purpose.

#### 3.3.3.5 Step 5: Noise removal

Although OBIA approaches are not prone to the so-called “salt-and-pepper” effect of per-pixel classifications, noisy imagery can cause the formation of small (< 40 pixels) objects during segmentation. In this study, some small objects related to infrastructure (e.g. pivot irrigation) or small areas affected by soil conditions (e.g. salt accumulation and waterlogging) were present in some of the fields. A simple rule to identify and discard small objects that were completely surrounded by cultivated areas was used in the final step (Step 4) of the workflow to remove such anomalies.

### 3.3.4 Accuracy assessment

A reference field boundary dataset, consisting of 400 fields, was manually digitised from very high resolution (10 cm) aerial imagery acquired in February and March 2016. Given that the aerial imagery was captured a year prior to the Sentinel-2 imagery used in the experiments, the digitised field boundaries were overlaid onto red, green and blue composites of the Sentinel-2 images acquired in the 2016-2017 growing season to remove inconsistent reference boundaries (i.e. boundaries that changed between March 2016 and the 2016-2017 growing season were discarded from the reference field boundary dataset).

Despite the popularity of image segmentation algorithms, effective and efficient methods to evaluate the ability of a segmentation algorithm to accurately delineate boundaries of the objects of interest remain elusive (Clinton et al. 2010; Meyer & Van Niekerk 2015). Over-segmentation (OS), under-segmentation (US) and boundary offset are the most common causes of poor or inappropriate image segmentations, and no single accuracy measure can sufficiently quantify all of these errors in combination (Weidner 2008). OS and US is commonly measured using topological (area) relationships, while boundary offsets are calculated using geometrical (edge) metrics (Zhan et al. 2005). Several area-based metrics have been proposed to calculate OS and US

(Clinton et al. 2010; Möller, Lymburner & Volk 2007; Weidner 2008), but these measures do not take the accuracy of delineated boundaries into account. A common edge metric, such as proposed by Delves et al. (1992), calculates the average distance error between reference and extracted object boundaries and has proven to be successful in determining the accuracy of segmented boundaries (Meyer & Van Niekerk 2015). A similar edge metric, namely the mean absolute error (MAE) distance metric, was implemented in this study.

MAE considers the Euclidean distance (ED) between the centres of two cells representing the reference and extracted boundary respectively (Figure 3-3). Two different instances of MAE were calculated to evaluate how closely the extracted field boundaries matched those in the reference database.  $MAE_i$  measures the distance from each reference boundary cell to the nearest extracted boundary cell, which provides an indication of how close in geographical space the extracted boundaries are to the actual boundary. Conversely,  $MAE_j$  measures the distance from each extracted boundary cell to the nearest reference boundary cells and is an indicator of boundaries within a field (caused by OS). The formulae to calculate both instances of MAE are defined as:

$$MAE_i = \frac{\sum ED_i}{N} \quad \text{Equation 3.1}$$

where  $ED_i$  refers to the ED measured from the centre of the reference cell to the centre of the extracted cell, while  $N$  is the total number of boundary cells in the reference dataset.

$$MAE_j = \frac{\sum ED_j}{N} \quad \text{Equation 3.2}$$

where  $ED_j$  refers to the ED measured from the centre of the extracted cell to the centre of the reference cell.  $MAE_i$  and  $MAE_j$  were summed to get a sense of overall agreement between the reference boundaries and those that were extracted, with low values indicating a high agreement.

$$MAE = MAE_i + MAE_j \quad \text{Equation 3.3}$$

The blue arrows in Figure 3-3b illustrate the increased distance calculated from the extracted field boundaries to the reference boundaries when OS occurs.

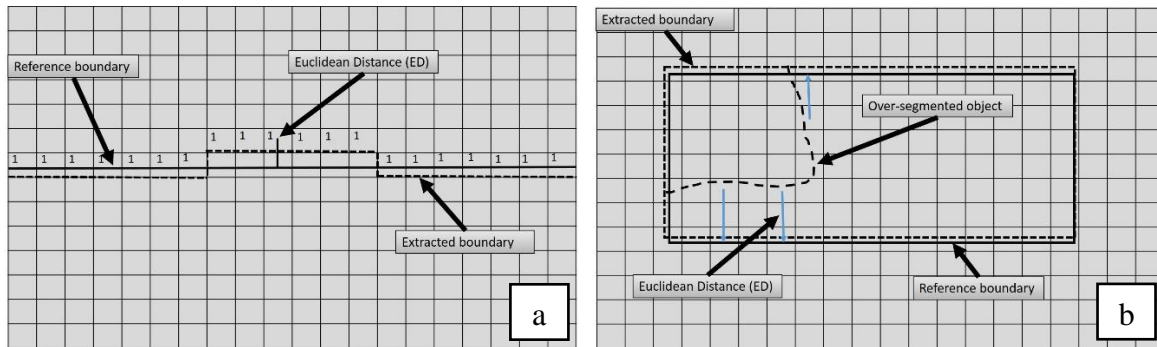


Figure 3-3 Conceptual illustration of ED calculations, where a)  $MAE_i$  is depicting the accuracy along the boundary and b)  $MAE_j$  represents the level of OS.

A confusion matrix was used to calculate several area-based metrics. The matrix consisted of 10 000 samples, with 5000 “boundary” samples selected randomly within 10 m of the reference boundaries and another 5000 “not-boundary” samples randomly selected more than 10 m away from the reference boundaries. The accuracy metrics obtained from the confusion matrix included the overall accuracy (OA), Kappa index (K), commission error (CE) and omission error (OE). The OE provides an indication of extracted boundaries accuracy along the reference field boundaries, where a high error suggests that the segmentation did not delineate the field boundaries well. CE gives an indication of false boundaries within a field, often caused by OS within the fields. Additionally, the McNemar’s test was used to test for statistical significance, with p-values of 0.05 (or lower) taken as being significant.

### 3.4 RESULTS

The results in Table 3-3 show that the combination of WS and the Canny edge detection algorithm (experiment WS\_C) produce the best OA (92.9%). This OA is, however, not significantly higher than the OA (92.7%) when the Scharr algorithm was combined with WS (i.e. experiment WS\_S). In contrast, the OAs of these two experiments (WS\_C and WS\_S) are significantly higher ( $p = 0.0001$ ) than the third best combination of algorithms, namely experiment MRS\_C (80.5%). The lowest OA (70.3%) for any experiment was recorded for the MRS and Scharr combinations (MRS\_S). Although the OA of MTS\_S (71.9%) is only 1.6% higher than MRS\_S, the McNemar’s test show a significant difference ( $p = 0.0001$ ) between these two results. When the OEs are considered, the two WS experiments (WS\_C and WS\_S) performed on par with one another, with OEs ranging from 10.1% to 12.8%. In contrast, the OEs for the MTS and MRS experiments are significantly higher than the WS-based techniques and range from 35.6% to 54.9%. This clearly demonstrates that the WS-based techniques identify field boundaries much more accurately than the experiments involving MRS and MTS. Regarding CE, the WS\_S experiment produced the lowest error (1.8%), and the highest CE was recorded by MTS\_C (8.5%). The consistent superior

performance of the WS-based experiments is underscored by the significantly ( $p < 0.0001$ ) higher mean OA of 92.8%, compared to the mean OAs of 73.4% and 75.4% of the MTS and MRS respectively.

Table 3-3 Area- and edge-based metric results for the six experiments

Experiment name	Area-based metrics				Edge-based metrics				
	OA %	OE %	CE %	K	Mean OA %	MAE <sub>i</sub> (m)	MAE <sub>j</sub> (m)	Combined MAE	Mean combined MAE
MTS_C	74.8	41.9	8.5	0.5	73.4	15.2	28.3	33.5	35.5
MTS_S	71.9	51.9	4.3	0.44		17.9	19.5	37.4	
MRS_C	80.5	35.6	3.5	0.61	75.4	15.1	19.2	34.3	40.1
MRS_S	70.3	54.9	4.4	0.41		22.9	22.9	45.8	
WS_C	92.9	10.1	4.1	0.86	92.8	7.6	16.9	24.5	26.1
WS_S	92.7	12.8	1.8	0.9		16.5	11.3	27.8	

In contrast to the area-based metrics that show the WS\_S and WS\_C experiments to be on par with each other, the edge-based metrics reveal that the field boundaries of the WS\_C experiments match the reference boundaries more closely than those of the WS\_S experiment. Specifically, the MAE<sub>i</sub> of the WS\_C experiment is 7.6 m, which is significantly ( $p = 0.0028$ ) lower than any of the other techniques evaluated, including WS\_S. The MAE<sub>i</sub> of 7.6 m is remarkable as it means that the technique generated boundaries that are, on average, less than one pixel (10 m) displaced from the reference boundaries. This low MAE<sub>i</sub>, however, came at the cost of a slightly elevated (16.9 m) MAE<sub>j</sub> compared to the 11.3 m MAE<sub>j</sub> of the WS\_S experiment, which suggests that the level of OS is higher in WS\_C compared to WS\_S. Nevertheless, when the combined MAE of these two methods are compared, it seems that WS\_C was substantially more accurate. Similarly, based on the edge metrics, the WS\_C approach significantly outperformed the other edge and segmentation algorithm combinations.

Figure 3-4 demonstrates the compositing of edge images. The edge layer for each individual date is the aggregation of four edge layers, generated from the red, green, blue and NIR bands. This example qualitatively illustrates how multi-temporal compositing of edge layers captures and accentuates persistent field boundaries. Some field boundaries that are faint (have low intensities) on specific dates become more pronounced as images of different dates are combined. One can also see that the Scharr algorithm tends to be more sensitive to variations (noise) within fields, which might have contributed to the WS\_C experiment's superior accuracies.



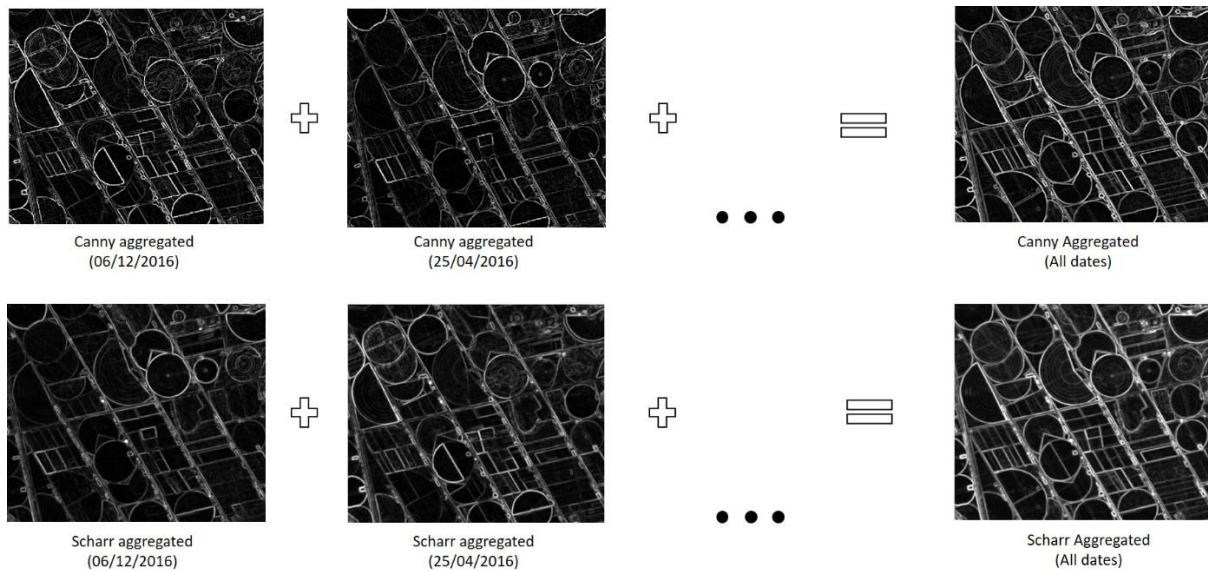


Figure 3-4 Illustration of how the aggregation of multiple edge layers for the Canny and Scharr edge operators reinforce persistent edges

Figure 3-5 visualises the outputs of the six experiments in a small test site. Gaps between adjacent fields are clearly noticeable in the MTS and MRS approaches (Figure 3-5c–f). These gaps represent edge objects that were removed in Step 4. Effectively, these edge objects offset the resulting boundaries by approximately one to three pixels towards the centre of the fields. This had a substantial effect on both the area and edge-based measures in Table 3-3.

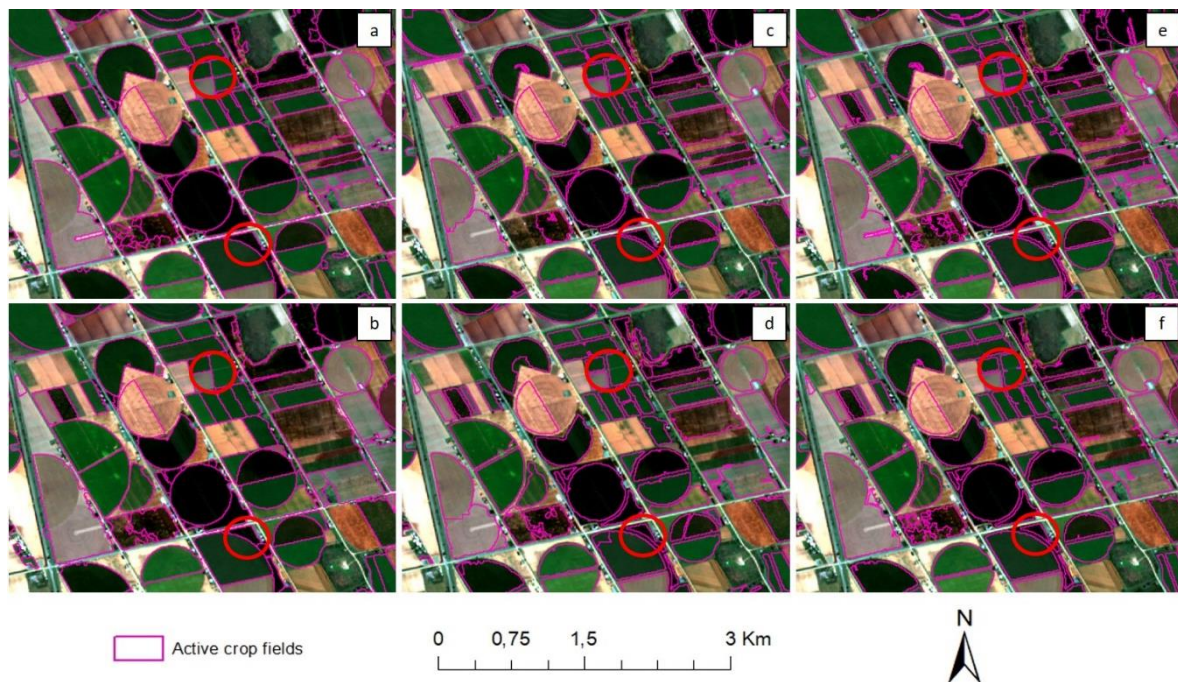


Figure 3-5 Detailed area showing the field boundaries extracted by experiments (a) WS\_C, (b) WS\_S, (c) MRS\_C, (d) MRS\_S, (e) MTS\_C and (f) MTS\_S



### 3.5 DISCUSSION

Both the area- and edge-based metrics show that the WS workflows significantly outperform those involving MRS and MTS. Although no other studies have directly compared the WS, MRS and MTS algorithms for field boundary delineation, Gaetano et al. (2015) found that a marker-based WS algorithm generated more accurate image objects than MRS using a 1 m resolution IKONOS image as input. However, this disagrees with Kavzoglu & Tonbul (2017) who found that MRS outperformed WS when using a 2 m resolution Worldview-2 image. A likely explanation for the improved performance of WS in our study is the multi-temporal approach used. Employing multi-temporal imagery reinforces object edges (in this case field boundaries), while potentially reducing the noise within a field as noise is unlikely to be present in the same location over multiple dates (as illustrated in Figure 3-4). In addition, the WS method created sharper boundaries along the high magnitude edges, which resulted in more defined object borders. This is a conceptual difference between WS and the other segmentation techniques evaluated. WS attempts to create boundaries where the values are highest (i.e. at points of discontinuity), while MRS groups values together based on their homogeneity. High values (edges) are consequently often grouped together, which results in objects being formed along the boundaries of image features, in our case crop fields. The edge objects formed along the boundary cause the field edges to be shifted towards the centre, resulting in an offset between the reference and segmented field boundaries. This is evident in the lower accuracies obtained by the MRS and MTS workflows. It is likely that the MRS and MTS approaches can be improved by implementing additional rules (e.g. object thinning or centre line extraction), but this will substantially increase the complexity of the workflow, which will likely reduce its robustness. Given the excellent performance and suitability of WS for the task at hand, an attempt to add rules to improve the MRS and MTS results seemed pointless (especially within the context of finding a technique that can be operationalised). However, it is acknowledged that the MRS and MTS may perform better with such rules.

The results obtained from the area- and edge-based metrics show that the WS\_C experiment provides far more accurate and consistent results than the WS\_S experiment, thus illustrating the superior performance of the Canny edge detection algorithm. This is consistent with findings of Juneja & Sandhu (2009) and Maini & Aggarwal (2009) who also found that the Canny edge detector produces better overall results. A likely explanation is the improved signal-to-noise ratio established by the non-maxima suppression method used by the Canny operator (Shrivakshan & Chandrasekar 2012). The non-maxima suppression results in magnitude edges with a width of one pixel, which allows WS to more accurately delineate the boundaries. In contrast, the Scharr algorithm does not use non-maxima suppression and thus creates thicker edges, which can cause

uncertainties and reduce the WS's ability to find sharp boundaries (i.e. the boundaries become erratic). The slightly higher OS observed for the Canny edge detector (Table 3-3) agrees with Batra et al. (2016), who showed that the improved capability of the Canny algorithm to detect weak edges can cause the generation of false edges within fields, which in turn leads to too many objects being created during segmentation.

Our results show that multi-temporal Sentinel-2 imagery holds much potential for delineating field boundaries. The 10 m spatial resolution of the Sentinel-2 images seems sufficient in most cases, although not ideal for small and narrow fields. Similar observations were made by Lebourgeois et al. (2017) who used Landsat-8 and SPOT-5 imagery to simulate Sentinel-2 time series imagery for mapping smallholder fields. They found that the spatial resolution of Sentinel-2 is potentially too low to map some of the smaller and irregularly shaped fields. Although the spectral resolution of Sentinel-2 imagery is higher than those of many other EO satellites (e.g. Landsat-8, SPOT-6/7, RapidEye), only four of the bands are at 10 m resolutions. The other bands, such as red edge and SWIR bands, will likely improve discrimination between agricultural land covers, but owing to their relatively low (20–60 m) spatial resolutions, they have little value for field boundary delineations (Valero et al. 2016). Despite these shortcomings, the boundaries produced in this study were generally highly accurate. This is mainly attributed to the use of a time series of images in the edge detection process, as illustrated in Figure 3-4. Although the increased temporal frequency of Sentinel-2 imagery has significant advantages, the selection of cloud-free imagery is critical. A limitation of this study was the manual selection of cloud-free imagery. However, image compositing techniques such as rule-based compositing and linear temporal resampling have been proposed as possible solutions for creating cloudless and artefact-free imagery (Inglada et al. 2015; Lück & Van Niekerk 2016).

A wide range of annual crops are grown in Vaalharts and as such it was an ideal testing site. However, it is unclear whether the recommended WS\_C method will perform equally well in other agricultural areas and under different conditions. For instance, the phenology of perennial crops (e.g. vineyards and fruit trees) grown in the Mediterranean climate of the Western Cape Province are very different to the annuals grown in Vaalharts. More work is therefore needed to investigate the transferability and robustness of the methods evaluated in this study. Given their demonstrated superiority, future efforts should focus on the WS-based methods.

### **3.6 CONCLUSION**

This study compared and evaluated six multi-temporal OBIA approaches for identifying and delineating active crop field boundaries. The approach combined two edge enhancement (Canny

and Scharr) and three image segmentation (WS, MRS and MTS) techniques. The key findings and conclusions of the study are:

1. Canny edge detection provides finer field boundary edges compared to the Scharr algorithm and is consequently better suited for enhancing field boundaries.
2. WS is more suitable than MRS and MTS for delineating agricultural field boundaries when edge layers are used as input to the algorithms.
3. The relatively low spatial resolution of Sentinel-2 imagery limits the delineation of small, narrow or irregularly shaped fields, but was sufficient for the majority of fields in the study area.
4. Due to the dynamic nature of field crops (especially annuals), a multi-temporal approach to field boundary delineation is essential.
5. More work is needed to evaluate the Canny edge detection and WS segmentation approach in other agricultural environments.

Given the results obtained in this study, the Canny edge detection algorithm, in conjunction with WS, is effective in a multi-temporal approach to delineate active crop fields. The WS experiments show good potential for use in an operational workflow, although future research should focus on applying it on a regional or national scale. Nevertheless, the high accuracy suggests that the WS workflow can provide valuable information about the extent and location of agricultural field boundaries. These boundaries can be subsequently used in agricultural monitoring systems to aid the implementation of precision agriculture, crop yield estimations, food security assessments and resource planning.

## **CHAPTER 4: A MODIFIED OBIA APPROACH FOR FIELD BOUNDARY DELINEATION IN SELECTED SOUTH AFRICAN AGRICULTURAL LANDSCAPES USING MULTI-TEMPORAL SENTINEL-2 IMAGERY\***

### **4.1 ABSTRACT**

Knowledge of the extent and location of cultivated fields are critical for agricultural monitoring, food security planning and commodity trading. The increased observational capacity of remotely sensed data, such as Sentinel-2 imagery, constitutes a major advantage over in situ methods, particularly for agricultural applications that require frequent updates. However, the development of fully automated cultivated field delineation methods remains a challenge. In this study an existing object-based image analysis (OBIA) methodology, called Canny edge detection in conjunction with watershed segmentation (CEWS), was modified to automatically identify and delineate agricultural fields from multi-temporal Sentinel-2 imagery in five diverse agricultural landscapes. The robustness of the technique was evaluated by comparing its outputs to those of standard per-pixel, supervised classifications. Reference field boundaries were manually digitised and used for quantitative accuracy assessments. Area and edge metrics were used to evaluate the accuracy of the extracted boundaries. Results show that, on average, CEWS produced significantly higher field boundary accuracies than the supervised per-pixel approach in terms of both mean absolute error (MAE) (~31 m lower) and overall accuracy (~13.8% higher). The closed field boundaries produced by CEWS, as well as its capability to operate without any a priori knowledge, was found to be its main strengths for integration into operational workflows. However, in complex landscapes (e.g. Swartland and Mooketsi) it was found that some fields had weak boundaries due to the homogeneity between adjacent fields, making edge detection problematic. The incorporation of higher resolution imagery into the edge detection process is proposed, particularly in agricultural areas with very small and irregularly shaped fields. Despite these challenges, it was concluded that the multi-temporal CEWS approach will perform well in most agricultural areas and is suitable for operational implementation.

**Keywords:** Sentinel-2 imagery, Edge detection, Watershed segmentation, Object-based image analysis, Agricultural field boundary delineation

---

\* This chapter is structured as an article and has been submitted to Computers and Electronics in Agriculture for publication.

## 4.2 INTRODUCTION

With the global population exceeding seven billion, food production has become a global concern (Fritz, See, McCallum, et al. 2015; Tollefson 2012). Factors such as urban expansion and climate change are placing enormous pressure on agricultural land (Inglada et al. 2015). Conversely, agriculture is cited as one of the driving forces of climate change, contributing 30 – 35% to global greenhouse gas emissions. This poses a significant global challenge: to maintain food security while reducing the carbon footprint of agricultural activities (Karamura et al. 2013). Effective and responsive decisions on agricultural matters are needed to address these challenges simultaneously. It calls for the development of timely and accurate agricultural monitoring systems that can provide up-to-date insights into crop conditions, generate accurate estimations of crop yields and inform decision-making relating to hazards such as floods, droughts and civilian conflicts (Matton et al. 2015).

The extent and location of agricultural fields are fundamental data requirements of agricultural monitoring systems. Remote sensing (RS) techniques can provide datasets that cover extensive areas at high spatial and temporal resolution and are thus well suited for collecting agricultural data (Valero et al. 2016). However, remotely sensed imagery with high temporal resolution is critical as the seasonal patterns of agricultural fields are strongly related to the phenology of crops being grown (Atzberger 2013). Changes in the phenological stages of crops, which can happen within short periods, lead to changes in the spectral and structural properties of the crops. It has been shown that RS data acquired at short temporal intervals have the ability to capture crop properties throughout the growing season (Ozdogan et al. 2010; Pittman et al. 2010).

A number of techniques using low to high spatial resolution imagery have been developed to identify cultivated field extent (Matton et al. 2015). Low (250 m) resolution imagery provided by sensors such as MODIS have proved to be appropriate for quantifying cultivated extents (acreage) over very large areas (Lunetta et al. 2010; Pittman et al. 2010; Roumenina et al. 2015). However, such imagery is unsuitable for agricultural monitoring in heterogeneous landscapes where fields are smaller than the pixel size (Duveiller & Defourny 2010). Conversely, very high resolution (VHR) imagery provides finer detail and allows for more accurate delineation of individual cultivated fields but is often only available at low temporal frequency and can be expensive to acquire (Mueller, Segl & Kaufmann 2004). The recently launched Sentinel-2 satellite constellation can provide both relatively high spatial and temporal resolution imagery at no cost, thus offering a potential alternative to VHR imagery. Compared to Landsat-type sensors, the observational capacity of the Sentinel-2 satellite system offers significant improvements with its high number of

spectral bands (13), five-day revisit time, 10 m – 60 m spatial resolutions and wide swath of 290 km. This allows for more timely estimates of crop extent, crop condition and crop type, which are fundamental indicators of a region's agricultural activities (Bontemps et al. 2015). From this perspective, the development of operational field boundary delineation methods that can be implemented for large areas and are transferable from one agricultural region to the next have become a priority (Matton et al. 2015).

A number of RS techniques to identify and delineate cultivated fields have been explored. The most commonly used technique is supervised classification (Peña et al. 2014). Supervised classification algorithms such as support vector machine (SVM) and random forest (RF) use in situ data, or a priori knowledge, to differentiate between crop type and land cover classes (Matton et al. 2015). However, the collection of in situ data is often expensive, time-consuming and prone to human error (Lucas et al. 2007). Furthermore, expert interaction is a prerequisite for successful implementation and consistent and accurate results (Thenkabail & Wu 2012). An alternative is the knowledge-based approach, which uses expert knowledge to develop a sequence of rules for differentiating between classes. The main advantage of the knowledge-based approach is that the same model can potentially be used for multiple dates and regions. This makes it very attractive for operational systems as it can be fully automated. However, the creation of rules that are robust (i.e. will work in a variety of conditions) has been cited as the main limitation of a knowledge-based approach (Belgiu & Csillik 2018).

Another differentiating aspect of cultivated field mapping methods relates to the spatial unit (minimum mapping unit) used in the classification step (Matton et al. 2015). Per-pixel classification assigns a class label to individual pixels based on their spectral signatures. However, this method does not take contextual information (surrounding the pixel of interest) into account, which tends to produce noisy maps (the so-called salt-and-pepper effect) (Blaschke et al. 2000; Schultz et al. 2015). In contrast to per-pixel techniques, OBIA groups pixels based on a homogeneity criterion (Blaschke 2010). Each object represents a homogenous region, and in the case of cultivated field mapping, individual fields are the objects of interest. In contrast to per-pixel classifications, entire objects are handled as minimum mapping units and are assigned labels according to a classification scheme (Lebourgeois et al. 2017). OBIA techniques often produce higher accuracies than per-pixel approaches (Belgiu & Csillik 2018; Duro, Franklin & Dube 2012), but the implementation of transferable OBIA techniques for individual field boundary delineation remains a research gap (Yan & Roy 2016).

Few examples of RS studies in which field boundaries were extracted exist. Those that are available have typically been carried out in small, localised areas or make use of visual interpretation to manually digitise field boundaries (Yan & Roy 2016). A number of semi-automated techniques have been investigated, often involving either edge- or region-based methods (Ramadevi et al. 2010; Rydberg & Borgefors 1999; Turker & Kok 2013; Wuest & Zhang 2009). Edge-based methods (or edge detection) focus on detecting object boundaries in an image. These boundaries are found by measuring the differences in grey level values between pixels (Kaganami & Beiji 2009). Conversely, region-based methods group pixels together based on their grey level similarity (Li et al. 2010). Typical errors produced by edge-based techniques (e.g. gaps between edges) and region-based techniques (e.g. boundary errors) have limited their successful implementation for operational purposes (Chen et al. 2015; Fan et al. 2001). Hybrid methods that combine these techniques and exploit the strengths of each have consequently been proposed (Alemu 2016; Butenuth, Straub & Heipke 2004; Li et al. 2010; Mueller, Segl & Kaufmann 2004; Rydberg & Borgefors 2001). For instance, Li et al. (2010) proposed a hybrid approach to segment single-date Quickbird imagery in both an urban and agricultural landscape. Edge detection was performed to improve the positional accuracy of object borders and to emphasise weak edges. This was followed by a marker-based watershed algorithm to delineate the targeted object boundaries. A satisfactory boundary accuracy (78%) was achieved and the method reportedly performed well in reducing over-segmentation and retaining weak boundaries. In another hybrid approach, Chen et al. (2015) adopted a three-step strategy. First, the image was over-segmented into small objects. Second, the objects were merged in a global mutual best-fitting strategy using edge penalty and constrained spectral variance difference as merging criteria. The final step removed noise by merging very small objects with their nearest neighbour. The hybrid technique was quantitatively compared to a method based on the multi-resolution segmentation (MRS) algorithm using three measures, namely the rate of under-, over- and well-segmented objects. The hybrid method achieved a much higher rate of well-segmented objects (2.04/2.5) compared to MRS (1.07/2.5), highlighting its advantage over the traditional region-based approach. However, reliance on the manual selection of segmentation parameters was noted as a significant weakness of both approaches.

One limitation of the hybrid segmentation methods overviewed above is the use of single-date imagery. Delineating agricultural fields from such imagery can be challenging, as different crops can have similar spectral and structural characteristics during certain stages of the growing season (Esfahani 2014). This is compounded when identical crops are planted on adjacent fields. Therefore, the acquisition of multi-temporal imagery throughout the growing season is necessary



for consistent and accurate field boundary delineation. Watkins & Van Niekerk (2019) showed the advantage of using a multi-temporal OBIA approach for field boundary delineation. Edge detection was performed on multiple Sentinel-2 images in the Vaalharts irrigation scheme, South Africa. The multi-temporal edge layers were aggregated to enhance field edges while reducing within-field heterogeneity. Three segmentation algorithms, namely watershed, multi-resolution and multi-threshold, were compared for segmenting the aggregated edge layer. Canny edge detection in conjunction with watershed segmentation (CEWS) was identified as the best method for mapping field boundaries (92.9%). The 10 m spatial resolution of the Sentinel-2 imagery was found to be too low for delineating small and irregular fields, but it produced satisfactory results in most cases. A major limitation of their study was that the evaluations were carried out in a single, relatively small area. No attempt was made to evaluate the robustness and transferability of the technique to other areas and in diverse agricultural systems (e.g. irrigated vs rain-fed).

This article evaluates the robustness of the CEWS approach to identify and delineate agricultural fields using multi-temporal Sentinel-2 imagery. The methodology is evaluated in five study sites representing different climatic regions and agricultural practices, as well as a range of crop types. The paper also presents a number of proposed modifications to the CEWS technique to make it more transferable and robust. A per-pixel supervised classification was performed as a benchmark against which the CEWS approach was compared. The results are interpreted in the context of finding an operational solution for the identification and delineation of individual agricultural fields in complex and dynamic agricultural landscapes.

## **4.3 METHODS**

### **4.3.1 Study area**

Five study sites in South Africa, each with different environmental and agricultural conditions, were selected (Figure 4-1). Two of the study areas (Swartland and Grabouw) have a Mediterranean climate (i.e. winter rainfall), two (Loskop and Mooketsi) receive rainfall predominantly during the summer and the fifth area (Patensie) receives rainfall throughout the year. These sites constitute a large variety of crops ranging from annuals (e.g. wheat, canola and tobacco) to perennial crops (e.g. vineyards and fruit trees). Irrigated and rain-fed crops were also represented, thus providing a large variation with which to test the robustness of the proposed methodology. Table 4-1 summarizes the chosen study areas.



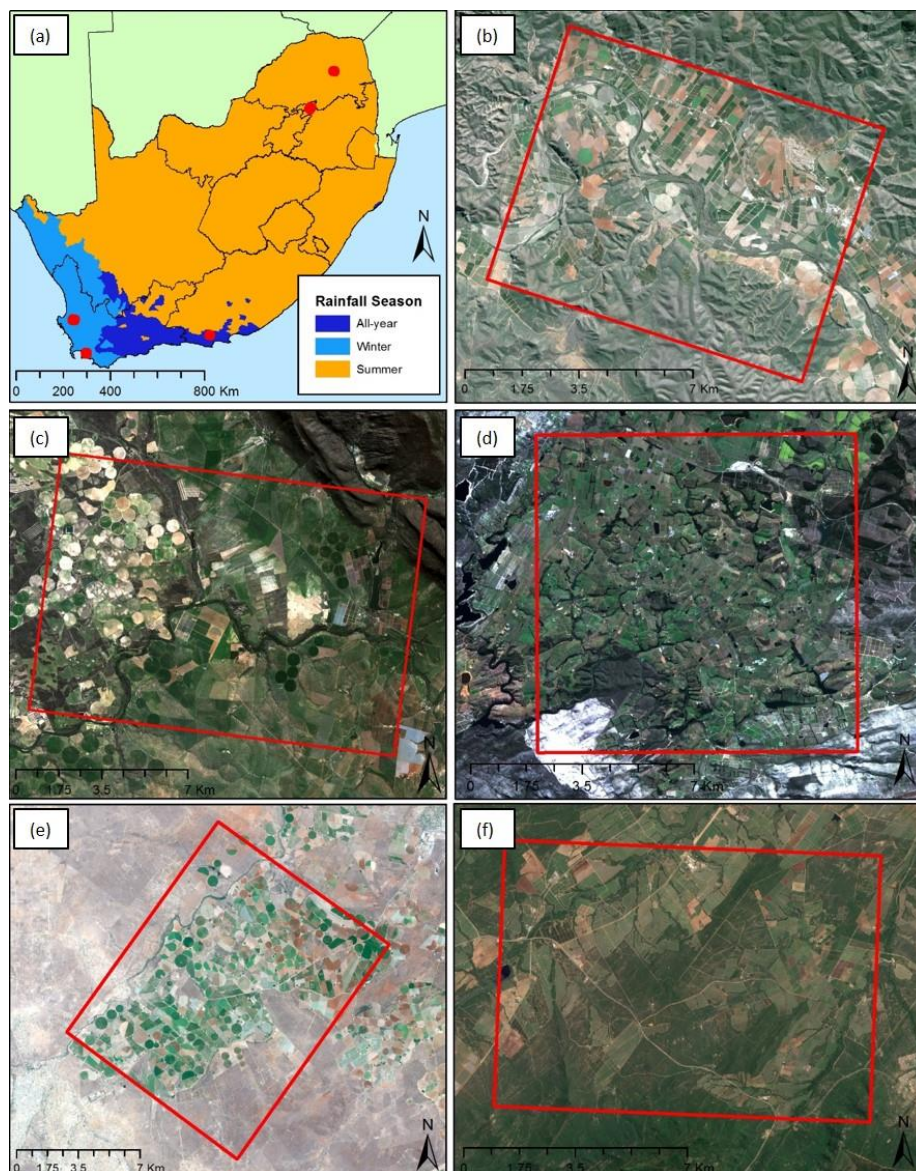


Figure 4-1 (a) Location and extent of the five selected study sites in South Africa, (b) Patensie, (c) Swartland, (d) Grabouw, (e) Loskop, and (f) Mooketsi

Table 4-1 Summary of region characteristics for the five study sites

Study site	Size	Rainfall regime	Mean annual rainfall	Common crops
Swartland	150 km <sup>2</sup>	Winter	550 mm	Grapes, wheat and canola
Grabouw	100 km <sup>2</sup>		950 mm	Horticulture and viticulture
Loskop	180 km <sup>2</sup>	Summer	680 mm	Citrus, wheat, cotton, tobacco and groundnuts
Mooketsi	100 km <sup>2</sup>		650 mm	Horticulture and wheat
Patensie	80 km <sup>2</sup>	All-year round	487 mm	Citrus, tobacco and vegetables

#### 4.3.1.1 Image collection

Multiple cloud-free Sentinel-2 images were acquired from April 2017 to April 2018. The imagery was acquired in Level-1C format, which is geometrically corrected and radiometrically calibrated to top of atmosphere (TOA) reflectance. Table 4-2 lists the number of cloud-free images used per study site.

Table 4-2 Number of cloud-free Sentinel-2 images per study area

Study area	Number of image dates
Swartland	58
Patensie	24
Grabouw	20
Loskop	31
Mooketsi	19

#### 4.3.2 CEWS workflow

##### 4.3.2.1 Original CEWS workflow

The original CEWS workflow, developed by Watkins & Van Niekerk (2019), comprised five main processing steps:

1. Edge detection, executed on all individual images;
2. Aggregation of edge layers obtained in Step 1;
3. Image segmentation, performed on the aggregated edge layer created in Step 2;
4. Cultivated field extraction; and
5. Noise removal.

However, Watkins & Van Niekerk (2019) indicated that certain elements of this workflow might not be effective for application in multiple areas. For example, the watershed segmentation parameter was calculated using the Jenks natural breaks algorithm, which had to be manually adjusted. It is thus unlikely that the same parameter will work in all regions. This was confirmed when the original CEWS method was applied to the five selected sites. It was also noted that the rules used to differentiate crops from other land covers need to be adjusted to account for crop variations caused by environmental conditions. For instance, annual crops grown in the Loskop study site (summer rainfall regime) have different spectral signatures and temporal characteristics compared to the perennial crops (e.g. fruit trees and vineyards) grown in the Grabouw study site

(winter rainfall regime). It was thus clear that the CEWS method would require modification for it to be transferable.

#### 4.3.2.2 Modified CEWS workflow

Modifications were made to the original CEWS workflow to overcome some of the limitations described in the previous section. The objective of the modifications was to improve the transferability of the workflow so that it can be applied to diverse agricultural landscapes. The following subsections overview the alterations performed.

##### *Step 1: Edge detection*

Step 1 of the CEWS workflow required no major modifications, except that the Canny algorithm was implemented in Python using the Scikit image Library (version 0.13.1). The red, blue, green and NIR bands were retained as input to the edge detection algorithm due to their higher (10 m) spatial resolution, which resulted in four edge images per Sentinel-2 image capture date (Table 4-2).

##### *Step 2: Edge layer aggregation*

The modified CEWS uses the mean value per-pixel to aggregate the multi-temporal edge layers, which results in a single composite image per study area. The Z-score algorithm, followed by a linear scaling (from 0 to 1), was employed to standardize the composite edge layer and aid in the automation of the WS parameter selection (see next section).

##### *Step 3: Image segmentation*

CEWS makes use of the WS algorithm, as implemented in Trimble eCognition Developer 9, to segment the aggregated edge layer. As input, WS requires a height parameter for region merging. This parameter is used to compensate for the over-segmentation inherent in the WS algorithm and controls when adjacent objects can be merged (i.e. if an objects' maximum pixel value is below the specified height threshold). To make CEWS more robust, the Jenk's algorithm was substituted with a local thresholding procedure, as applied in the Scikit image Python package, to automatically find the most appropriate height threshold. The procedure applies a Gaussian filter to the aggregated edge image (in an 11 x 11-pixel window) and calculates the weighted mean per-pixel, resulting in a generalised edge image. The height value is found by taking the standard deviation of the generalised image. Using this threshold in WS results in a set of image objects (segments) with boundaries coinciding with spectral transitions (edges).

#### *Step 4: Cultivated field extraction*

The original CEWS method employed a single rule-set to differentiate between actively cultivated fields and other land covers (non-cultivated). This was substituted by a rule-set per rainfall regime. The rule-sets were designed to be fully automated and reproducible, and replaces the commonly used supervised classification approach that requires a priori data. Based on the work by Huete (1988), Maselli & Rembold (2001), and Zheng et al. (2015), four normalised difference vegetation index (NDVI)-based features, namely maximum (max), minimum (min), range (ran) and standard deviation (std) were derived from the Sentinel-2 images acquired per area. These features were used as input for a classification and regression tree (CART) algorithm, as implemented in Salford Predictive Modeler software, to generate a decision tree, from which the values that best separate (classify) actively cultivated fields from other land uses could be determined. To train the CART algorithm, randomly sampled points (1 250) were generated and manually labelled (using visual interpretation) as either cultivated or non-cultivated fields.

Table 4-3 lists the rules per rainfall region. Image objects that did not satisfy the conditions of the rules were excluded from further consideration.

Table 4-3 Rule-sets per study area

Rule set	Winter rainfall		All-year rainfall	Summer rainfall	
	Swartland	Grabouw	Patensie	Loskop	Mooketsi
#1	min NDVI > 0.51 & std NDVI > 0.05		max NDVI > 0.63	max NDVI > 0.48 & min NDVI <= 0.17	
#2	-		-	max NDVI > 0.53 & min NDVI > 0.17 & std NDVI <= 0.12	

The all-year round and winter rainfall regions required one or two rules, while the summer rainfall region required five. A commonality among the regions is the use of the max NDVI feature. The summer rainfall region rule-set made use of three features, namely max, std and min NDVI.

#### *Step 5: OBIA noise removal*

Although the salt-and-pepper effect is not common in OBIA approaches, small irrelevant objects can occur. These can be the result of infrastructure (e.g. pivot irrigation) or small areas affected by salt accumulation or waterlogging. Therefore, a simple rule to identify and discard small objects that are completely surrounded by cultivated areas, was employed in the final step (Step 5). The rule was identical to that of the original CEWS method.

### 4.3.3 Supervised per-pixel classification workflow for mapping cultivated areas

A semi-automated supervised per-pixel (PP) classification was performed to serve as a benchmark for the autonomous knowledge-based results. The RF algorithm was chosen for this purpose, as it has been shown to provide good accuracies for crop type differentiations (Belgiu & Csillik 2018; Forkuor et al. 2017). Scikit-learn's RF package version 0.18.2 was used for the implementation. All features used by CEWS were used as input for the RF algorithm and trained with the identical sets of training samples used in the CART analysis (see Step 4 of the CEWS workflow). A majority filter (3 x 3 pixels) was used as a post classification step to remove some of the salt-and-pepper effect inherent in PP approaches (Quynh Trang et al. 2016). The subsequent raster classifications (cultivated vs. non-cultivated) were converted to a vector format. The resulting polygons thus represented contiguous areas covered by actively growing crops.

### 4.3.4 Accuracy assessment

Despite the popularity of image segmentation algorithms, methods to evaluate the effectiveness of a segmentation output remain elusive (Clinton et al. 2010; Meyer & Van Niekerk 2015). Ideally, an image segmentation output should result in object delineations (boundaries) that match those of the targeted real-world features (e.g. agricultural fields). The most common causes of poor image segmentations are over-segmentation (OS), under-segmentation (US) and boundary offsets. OS occurs when the segmented objects are smaller than the target features, whereas US causes objects to be larger. Boundary offsets occur when there is a consistent spatial shift in the extracted boundaries.

No single accuracy measure can adequately assess the combined three types of segmentation errors (Weidner 2008). While OS and US are commonly calculated using topological (area) relationships, boundary offsets are measured using geometrical (edge) metrics (Zhan et al. 2005). A number of area-based metrics have been proposed to calculate US and OS (Clinton et al. 2010; Möller, Lymburner & Volk 2007; Weidner 2008); however, these metrics do not evaluate the accuracy of the delineated object boundaries. Delves et al. (1992) proposed an edge metric that calculates the average distance error between reference boundaries and the extracted boundaries. This method has been shown to be successful in assessing the accuracy of segmented object boundaries (Meyer & Van Niekerk 2015). A similar metric, namely the MAE distance metric, was applied in this study.

MAE calculates the Euclidean distance (ED) between the centres of two cells representing the extracted and reference boundary respectively (Figure 4-2). To assess the accuracy of the extracted boundaries, two measures of MAE were calculated.  $MAE_i$  measures the distance from the centre



of a reference boundary cell to the centre of the nearest extracted boundary cell, thereby providing an indication of how closely the extracted boundaries represent the reference boundaries in geographical space. Conversely,  $MAE_j$  measures the distance from each extracted boundary cell to the nearest reference boundary cell, thus providing an indication of boundaries within a field (i.e. providing an indication of OS). Both instances of MAE were calculated by the following formulae:

$$MAE_i = \frac{\sum ED_i}{N} \quad \text{Equation 4.1}$$

where  $ED_i$  represents the ED measured from the centre of the reference cell to the centre of the extracted cell, while  $N$  is the total number of boundary cells in the reference dataset.

$$MAE_j = \frac{\sum ED_j}{N} \quad \text{Equation 4.2}$$

where  $ED_j$  refers to the ED measured from the centre of the extracted cell to the centre of the reference cell.  $MAE_i$  and  $MAE_j$  were summed to get a sense of overall agreement between the extracted and reference boundaries, where low values indicate high agreement.

$$MAE = MAE_i + MAE_j \quad \text{Equation 4.3}$$

The blue arrows in Figure 4-2b illustrate the increased distance calculated from the extracted field boundaries to the reference boundaries when OS occurs.

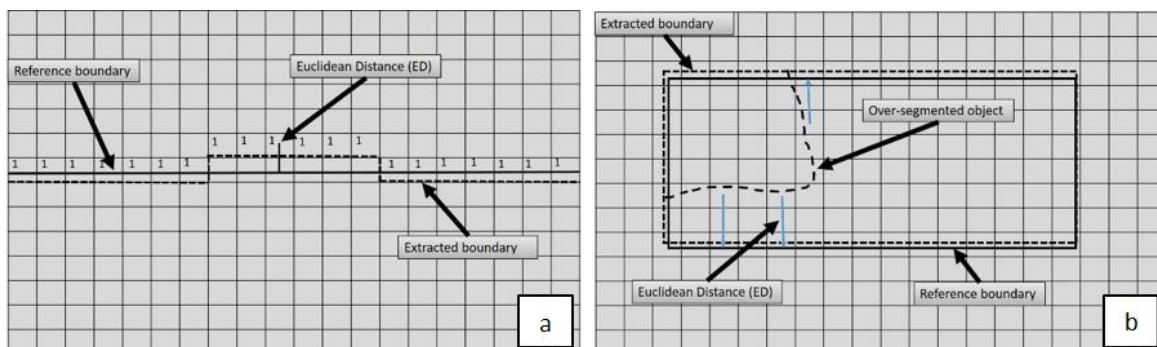


Figure 4-2 Conceptual illustration of ED calculations, where (a)  $MAE_i$  depicts the accuracy along the boundary and (b)  $MAE_j$  represents the level of OS

Reference field boundary datasets consisting of 100 active fields per study site were manually digitised using a combination of Sentinel-2 (10 m) imagery acquired from April 2017 to April 2018 and very high resolution (50 cm to 30 cm) satellite imagery from the ArcMap (version 10.4) base layer.

A confusion matrix approach was devised to calculate several area-based metrics. The matrix consisted of 10 000 samples, with 5 000 “boundary” samples selected randomly along the reference boundaries and another 5 000 “not-boundary” samples randomly selected more than

10 m away from the reference boundaries. The overall accuracy (OA), Kappa index (K), commission error (CE) and omission error (OE) were calculated from the confusion matrix. The OE quantifies the accuracy of the extracted boundaries along the reference boundaries, where a high value suggests that the extracted field boundaries were not delineated well. CE indicates false boundaries within a field, often due to OS. The McNemar's test was employed as an additional measure to test for significance of differences among accuracy measures, with p-values of 0.05 (or lower) regarded as significant.

#### **4.4 RESULTS**

The results in Table 4-4 show that the two highest OAs (82.9% and 83.6%) of the CEWS methodology are recorded in the Patensie and Grabouw regions (Experiments 5 and 2). The lowest OA (61.3%) was obtained when the PP approach was applied in Mooketsi (Experiment 3). In addition, the PP approach also produced the second lowest OA (69%) in Swartland (Experiment 1). When OEs are considered, the CEWS scenarios recorded errors ranging from 27.1% to 38%. In contrast, the OEs for the PP scenarios are significantly ( $p < 0.0001$ ) higher and range from 44.3% to 54%. Regarding CE, the CEWS scenarios in Experiments 4 and 5 (Loskop and Patensie) produced the lowest errors (1.3% and 1.4% respectively), and the highest CE (31.2%) was recorded by the PP scenario in Mooketsi (Experiment 3). CEWS recorded a significantly ( $p < 0.0001$ ) higher mean OA (82.0%) than the OA (69%) of the PP approach. In addition, the lower standard deviation produced by the OBIA method for OA (1.4%) suggests a higher consistency. Similarly, the mean and standard deviation for the OE and CE of CEWS were lower (with the exception of the standard deviation for the OE).

Table 4-4 Area- and edge-based metric results

Rainfall regime	Region	Experiment	Method	Area-based metrics				Edge-based metrics		
				OA (%)	OE (%)	CE (%)	K	MAEi (m)	MAEj (m)	Combined MAE
Winter	Swartland	Experiment 1	CEWS	82.0	31.4	2.5	0.7	22.1	19.5	41.6
			PP	69.0	54.0	7.5	0.4	35.3	79.7	115
	Grabouw	Experiment 2	CEWS	83.6	27.1	8.2	0.7	6.9	7.8	14.7
			PP	72.0	44.3	9.0	0.4	14.2	15.3	29.5
Summer	Mooketsi	Experiment 3	CEWS	79.7	38.0	2.9	0.6	10.0	16.3	26.3
			PP	61.3	47.2	31.2	0.3	14.0	52.1	66.1
	Loskop	Experiment 4	CEWS	81.8	35.0	1.3	0.6	7.8	14.1	21.9
			PP	72.9	49.1	5.2	0.5	14.9	16.4	31.3
All-year round	Patensie	Experiment 5	CEWS	82.9	32.8	1.4	0.7	9.2	11.4	20.6
			PP	69.9	45.0	16.5	0.4	13.0	27.8	40.8
		Mean	CEWS	82.0	32.9	3.3	0.7	11.2	13.9	25.0
		Standard deviation		1.4	3.6	2.5	0.05	5.6	4.0	9.1
		Mean	PP	69.0	47.9	13.9	0.4	18.3	38.3	56.5
		Standard deviation		4.1	3.5	9.5	0.06	8.5	24.6	32.0

Figure 4-3 visually compares the CEWS and PP results in a detailed area in Patensie (Experiment 5). In this area, CEWS was 13% more accurate than the PP method. In addition, CEWS has the benefit of producing closed individual field boundaries while reducing the salt-and-pepper effect common in PP classification outputs. The red circles in Figure 4-3b highlight some examples of this salt-and-pepper effect, whereas the red circles in Figure 4-3c illustrate the closed field boundaries created by CEWS.

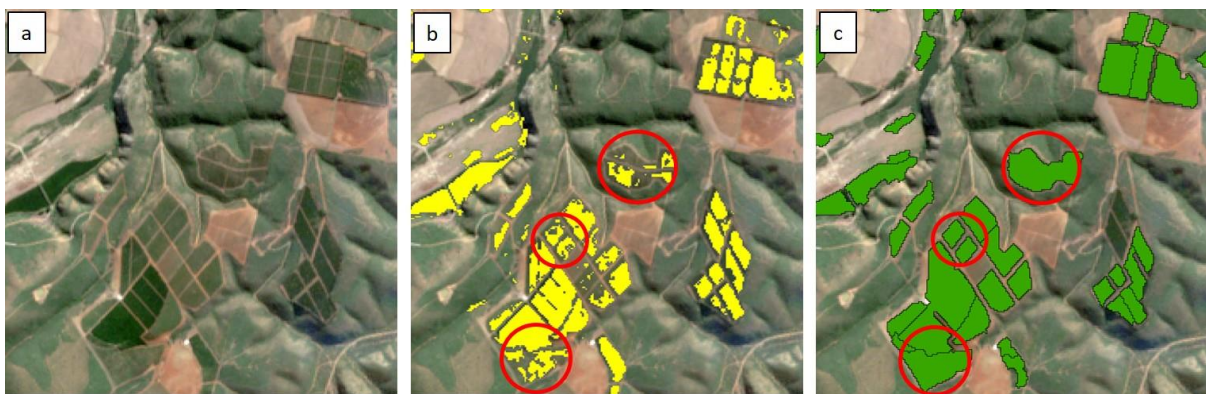


Figure 4-3 Cultivated field extraction results for an area in Patensie showing a) RGB composite of Sentinel-2 imagery acquired in June 2017, along with the b) PP and c) CEWS outputs



The edge-based metrics reveal that the field boundaries created by CEWS match the reference fields more closely than those produced by the PP method. The MAE<sub>i</sub> for the CEWS scenarios show a low mean of 11.2 m (with the exception of Experiment 1, which recorded an MAE<sub>i</sub> of 22.1 m). Generally, the MAE<sub>i</sub> of the PP experiments are substantially higher, with a mean of 18.3 m. The 11.2 m mean MAE<sub>i</sub> of CEWS is notable as it means that the technique produced field boundaries that are, on average, approximately one pixel (10 m) displaced from the reference boundaries. However, this low MAE<sub>i</sub> comes at the cost of a slightly higher MAE<sub>j</sub>, which suggests some level of OS. A similar observation is made for the PP scenarios. When the combined MAE is considered, it is clear that the CEWS boundaries are substantially more accurate than those generated by the PP approach.

Figure 4-4 demonstrates the qualitative advantage of the automated CEWS approach. The red circles in Figure 4-4b and Figure 4-4c outline where the PP approach was unable to delineate individual fields (they are regarded as one field). In contrast, CEWS produces clear divisions between the fields.

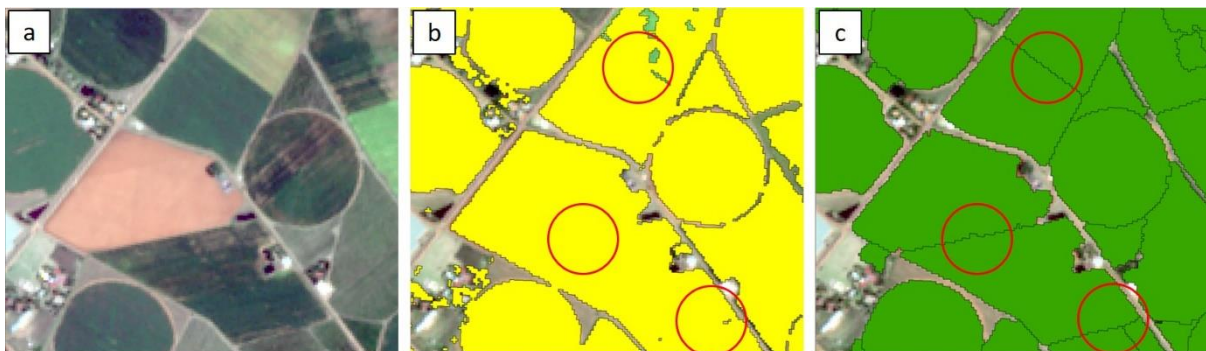


Figure 4-4 Cultivated field extraction results for an area in Loskop displaying an a) RGB composite of Sentinel-2 imagery acquired in January 2018, compared to the b) PP and c) CEWS outputs.

Figure 4-5 illustrates a limitation of both the CEWS and PP approaches. The techniques fail in areas with a high degree of homogeneity between adjacent fields (typical in areas such as Swartland and Mooketsi). The red circles in Figure 4-5 indicate where the CEWS and PP experiments were unable to delineate the individual adjacent fields. However, the larger areas making up those individual fields were successfully identified and delineated. The agriculture in these regions comprise largely annual rain-fed crops (e.g. wheat, canola, medics). The blue circles indicate individual fields that were not successfully identified and delineated by CEWS. This contributed to the slightly larger combined MAE values obtained in Swartland (41.6 m) and Mooketsi (26.3 m) compared to Grabouw (14.7 m), Patensie (20.6 m) and Loskop (21.9 m).

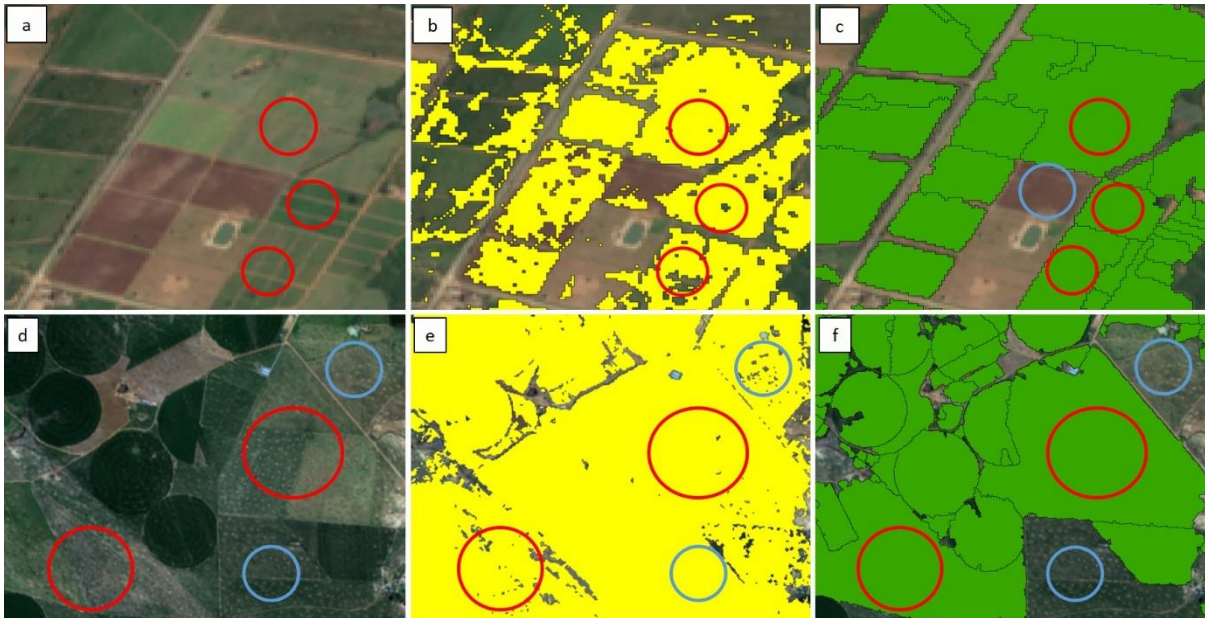


Figure 4-5 Cultivated field extraction results for an area in Mooketsi (a – c) and Swartland (d – f) displaying an a) RGB composite of Sentinel-2 imagery acquired in March 2018, as well as the related b) PP and c) CEWS outputs; and d) an RGB composite of Sentinel-2 imagery acquired during August 2017, accompanied by e) the PP and f) CEWS results. The highlighted areas show where both methods failed to identify field boundaries due to low contrast between fields.

Figure 4-6 illustrates the inability of the Sentinel-2 (10 m) imagery to effectively delineate small and irregular fields in a detailed area of Grabouw (red circles). However, the high mean OA (83.6%) and low mean combined MAE (14.7 m) of the CEWS workflow suggests that it works well for most of the fields included in the reference set.

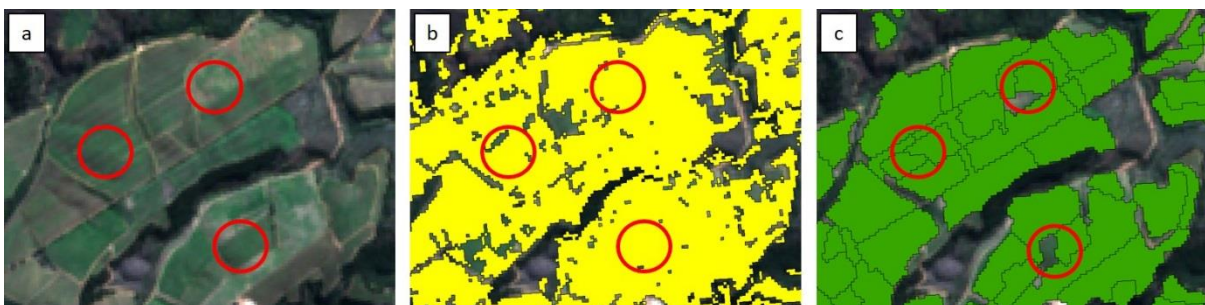


Figure 4-6 Cultivated area feature extraction results for an area in Grabouw showing a) an RGB composite of Sentinel-2 imagery acquired during September 2017, compared to the b) PP and c) CEWS outputs. The highlighted areas show where both methods struggled to accurately delineate small and irregularly shaped fields.

## 4.5 DISCUSSION

Agricultural monitoring systems are becoming increasingly important in addressing challenges relating to climate change and food security. Accurate and up-to-date field boundary information is vital for developing efficient and effective agricultural monitoring systems, and the development of operational field boundary delineation methods have become a priority. An OBIA field

boundary delineation procedure, originally developed by Watkins & Van Niekerk (2019), was modified in this study to make it more universally applicable. Firstly, the selection of the WS height parameter, which was originally manually selected from the output of the Jenks natural breaks algorithm, was substituted for an automated process using a thresholding method available in the Scikit image python package. Secondly, five study sites located throughout South Africa were selected to represent various environmental and agricultural regions. The sites were grouped into three different rainfall regimes and a knowledge-based rule-set was developed for each regime to eliminate non-cultivated areas from further consideration.

Results show that the modified CEWS approach produces superior results when compared to the conventional PP supervised classifications. CEWS produced objects with reduced within-field heterogeneity (salt-and-pepper effect) (Figure 4-3b). This finding is in agreement with Belgiu & Csillik (2018) who compared PP and OBIA techniques to classify various crop types using multi-temporal Sentinel-2 imagery. They found that the OBIA techniques outperformed the PP approaches in three study sites. Another advantage of an OBIA approach is that individual cultivated fields are delineated with closed boundaries (Figure 4-3c). Closed field boundaries provide a significant advantage and allow agricultural statistics to be calculated per-field, which is highly beneficial in agricultural monitoring systems.

The low standard deviations of the CEWS outputs suggest consistency across different agricultural landscapes. However, some patterns in accuracy were observed. Lower accuracies were noted in areas made up of largely annual rain-fed crops. Waldner et al. (2017) found that annual precipitation and field density were important factors in cropland identification. These factors were also the likely drivers of the lower accuracies (Table 4-4) recorded in Swartland and Mooketsi, as both sites have relatively low annual precipitation (Table 4-1). The fields in both sites are also generally irregular in shape and the same crops are often grown in adjacent fields, with minimal separating features (e.g. roads or hedges) that can be utilised by the segmentation algorithm. Therefore, some fields were not effectively delineated or identified (Figure 4-5). In contrast, higher accuracies were recorded in areas containing predominantly irrigated or perennial crops. For instance, both Loskop and Grabouw have high levels of annual precipitation and more defined boundaries (e.g. roads or hedges) and were thus more easily identified and delineated.

A major advantage of CEWS is that the requirement for training data (of supervised classification) was circumvented by implementing a knowledge-based (rule-set) technique for excluding non-cultivated areas. The collection of training samples relies on human interpretation, making the process time-consuming, expensive and difficult to apply on a large-scale (Thenkabail & Wu

2012). In addition, samples will likely have to be collected for each season due to the dynamic nature of crops (e.g. crop rotations), thus making a supervised approach impractical in the context of operational systems. CART's selection of the maximum NDVI feature for the decision trees of all three of the rainfall regimes suggests that it is a robust multi-temporal variable for discriminating agricultural fields from other land covers across varying climatic regions. This agrees with Waldner et al. (2017), who found that maximum NDVI was the most important variable in developing a national cropland map for South Africa. In contrast, Lambert, Waldner & Defourny (2016) found that minimum NDVI was more important for cultivated field identification. Our findings support those of Jia et al. (2014) who also noted the benefits of using multi-temporal NDVI features (maximum, minimum and standard deviation) for land cover differentiation (including cultivated fields). They also found that higher temporal resolution imagery improved the efficiency of the NDVI features.

Our results show that multi-temporal Sentinel-2 imagery can be used to identify and delineate agricultural field boundaries using an OBIA approach. The relatively high temporal frequency (five days) of the imagery allowed for a large number of observations spanning an entire year (e.g. 58 observation dates for the Swartland site). This relatively high temporal frequency increases the chance of cloud-free observations during the growing season. However, the manual selection of cloud-free imagery (as undertaken in this study) should be avoided and an automated technique, such as image compositing, should rather be used for operational implementations. Regarding the spatial resolution of the Sentinel-2 imagery used, the 10 m resolution was sufficient in most cases, but was less effective in areas containing small and irregularly shaped fields (such as those in the Grabouw and Mooketsi study sites). A potential advantage of Sentinel-2 imagery, compared to other EO satellites (e.g. Landsat-8, SPOT-6/7 and RapidEye) is the higher spectral resolution (number of available bands). However, while the red edge and SWIR bands could potentially aid in the better discrimination between agricultural land covers (e.g. crop type classification), their use for agricultural field boundary delineation is of less value as their spatial resolutions are significantly lower (20 – 60 m) (Valero et al. 2016). This observation is in agreement with Immitzer, Vuolo & Atzberger (2016) who mapped crop and tree species in Central Europe using single-date Sentinel-2 imagery. They noted a potential limitation of the spatial resolution of Sentinel-2 imagery (particularly the 20 m bands) to map highly fragmented landscapes. A potential solution would be to incorporate VHR imagery (e.g. SPOT 6/7, WorldView 2/3) into the edge detection phase to enhance the field boundaries more finely. This could prove to be advantageous for areas with high homogeneity between fields (e.g. Swartland). It is likely that a single VHR



image might be sufficient for identifying permanent field divisions (e.g. hedges or narrow roads), but more work is needed to investigate such an approach.

The five sites selected in this study covered a range of agricultural landscapes with varying environmental conditions. Although the evaluated automated OBIA methodology showed great promise for agricultural field boundary delineation under diverse conditions, it is still unclear whether the developed methodology will perform consistently well when applied to a larger (e.g. national) scale. It is recommended that the modified CEWS is implemented in an operational workflow and evaluated at national or at least regional (provincial) levels.

#### **4.6 CONCLUSION**

This study evaluated the robustness of a modified OBIA method, called CEWS, to identify and delineate agricultural fields in five agricultural landscapes. The original CEWS method was only implemented in a single, relatively small area with similar conditions, therefore an evaluation and subsequent modification was required to test its efficacy in different agricultural and environmental conditions. The CEWS technique was modified in this study and was implemented to delineate agricultural field boundaries in five very diverse agricultural landscapes. A supervised per-pixel classification was performed to serve as a benchmark for comparison purposes. The key findings of the study are:

1. Compared to the supervised per-pixel approach, the knowledge-based CEWS method provided statistically significant and superior results when delineating agricultural fields;
2. The spatial resolution (10 m) of Sentinel-2 imagery is well suited to field boundary delineation in most cases; however, it is less effective in regions containing small and irregular fields;
3. The high temporal resolution (five-day interval) of Sentinel-2 imagery can adequately represent crop phenology throughout the growing season (at least in the selected sites representing South African conditions); and
4. The robustness and transferability of the region-specific rule-sets for excluding uncultivated areas are very encouraging and suggest that an automated knowledge-based approach is feasible for incorporation into an operational multi-temporal OBIA workflow to delineate agricultural fields.

Given the results obtained in this study, the modified CEWS methodology shows great potential for automatically delineating agricultural field boundaries at regional scales. CEWS is recommended for integration into an operational workflow. It is suggested that further research is

conducted in which the workflow is applied to a larger scale (i.e. regional or national). The resulting field boundaries can subsequently be integrated into agricultural monitoring systems and aid in the implementation of precision agriculture, crop yield estimates and resource planning.

## **CHAPTER 5: DISCUSSION AND CONCLUSIONS**

This chapter summarises and evaluates the results of this research. The aim and objectives are revisited in the first section, followed by an evaluation of the findings from Chapters 3 and 4. Limitations and recommendations for further research are also discussed, while the final section draws conclusions from this study.

### **5.1 REVISITING THE AIMS AND OBJECTIVES**

This research aimed to evaluate Earth observation methods for automatically delineating agricultural field boundaries using multi-temporal Sentinel-2 imagery. Effective agricultural monitoring systems are vital as they provide key information regarding crop yield estimations, food security assessments and resource planning. Therefore, this research was completed in the context of finding an operational solution for field boundary delineation, with the ultimate goal of supporting agricultural monitoring.

Several studies have evaluated remote sensing methods for field boundary delineation; however, a number of gaps in the research were identified in Chapter 1. For instance, edge detection algorithms have been shown to be effective at enhancing the borders of image features, but little is known about which algorithm is best suited for crop field boundary delineation. Furthermore, existing research on the integration of multi-temporal edge layers is very limited. In segmentation algorithms, multi-resolution segmentation (MRS) and watershed segmentation (WS) have both been successfully implemented in OBIA, but a direct comparison has not yet been made for field boundary delineation.

The literature review (Objective 1) exposed a range of remote sensing approaches for field boundary delineation. Existing knowledge suggests that a multi-temporal approach is needed to achieve consistent and accurate results. Furthermore, previous studies showed that hybrid segmentation approaches more accurately delineate field boundaries than a single edge- or region-based method. The literature review assisted in formulating the research questions and in conceptualising the experiments carried out in this study.

The launch of the Sentinel-2 satellite constellation has opened up new opportunities for crop field boundary delineation using remote sensing methods. Thus, Sentinel-2 imagery was acquired for six agricultural regions in South Africa (Objective 2). The Vaalharts irrigation scheme was selected for the initial experiments (Chapter 3), with a focus on the summer growing season (November 2016 to April 2017). In Chapter 4, five study sites were selected and grouped into three



regions based on their rainfall regimes, namely winter, summer and all-year round precipitation. Imagery for each study site was acquired from April 2017 to April 2018.

Objective 3 related to the first set of experiments and was devised to compare two edge detection algorithms (Canny and Scharr) for delineating agricultural fields, in conjunction with various segmentation algorithms. Results from Chapter 3 showed that the Canny edge detection algorithm produced boundaries that were consistently more accurate than those that were generated with the Scharr algorithm.

A comparison of three common segmentation algorithms was performed in Chapter 3 to satisfy Objective 4. The MRS, WS and MTS algorithms were applied to composite Canny and Scharr edge layers, resulting in six experiments. Overall, the WS algorithm provided the most consistent and accurate field boundaries, with a highest OA of 92.9% (using the Canny layer as input) and combined MAE of 24.5 m. It was concluded that the WS algorithm is best suited for accurately delineating field boundaries. Subsequently, the MRS and MTS algorithms were not considered further.

In Chapter 4, the knowledge-based OBIA methodology developed in Chapter 3 was compared to a standard supervised per-pixel classification (Objective 5). Although the methods (per-pixel vs OBIA and supervised- vs knowledge-based) differ, the favourable results obtained by the proposed CEWS approach illustrate its potential for automated crop field boundary extraction. Furthermore, the closed field boundaries obtained using CEWS provide a significant advantage and are more useful for agricultural monitoring. In addition, the proposed knowledge-based approach does not rely on manually selected training samples and is thus better suited for integration into an operational workflow.

To evaluate the transferability of the proposed methodology (Objective 6), the CEWS was implemented across three climatic regions with varying agricultural landscapes. Due to the likelihood that a single rule-set would not accurately extract crop fields on a national scale, a unique rule-set was developed per rainfall regime region to account for similar growing seasons and environmental conditions. The relatively high and consistent results obtained demonstrate that the proposed approach will be robust enough to be successfully applied over a range of agricultural regions.

## **5.2 SYNTHESIS**

The experiments performed in this research showed that the WS workflows significantly outperformed those of MRS and MTS. This is attributed to WS' creation of sharper borders along

high magnitude edges, which result in higher accuracies along object boundaries. Furthermore, the MRS and MTS experiments create boundary objects (due to boundary edges forming their own homogenous regions), which offset the resulting boundaries and shift them towards the centre of fields. Consequently, a greater distance is created between the reference field boundaries and the extracted field boundaries. Although it is possible for the MRS and MTS procedures to be improved through additional rules (e.g. object thinning or centre line extraction), it would substantially increase the complexity of the workflow, thus making it less suitable for implementation into an operational methodology.

The area- and edge-based metrics showed that the Canny experiments provided far more consistent and accurate field boundaries, thus illustrating the superior performance of the Canny edge detection algorithm at enhancing field edges. This is due to the non-maxima suppression performed in the Canny algorithm, which results in magnitude edges with a width of one pixel. Subsequently, this enables WS to more accurately delineate field boundaries.

The temporal and spatial resolution of Sentinel-2 imagery showed much potential for field boundary delineation. Although the 10 m spatial resolution was less effective for delineating small and irregular fields, the boundaries generated in this study were generally of high enough accuracy for most applications. This was also in part due to the aggregation of time series edge layers throughout the growing season, which helped to reduce some of the within-field noise and enhance field boundary edges.

Findings from Chapter 4 illustrated that a knowledge-based CEWS approach produces superior field boundaries compared to a conventional per-pixel supervised classification approach. In addition, the CEWS approach has the advantage of creating closed field boundaries and lower within-field heterogeneity (i.e. salt-and-pepper effect). The often time-consuming and subjective task of manually fine-tuning segmentation parameters was circumvented by developing an automated process, which adds significant practical value to the implementation of an operational workflow.

Despite applying a median filter to the per-pixel classification outputs, the salt-and-pepper effect was still prevalent in some areas. Furthermore, the manual collection of training samples to train the supervised classification algorithms is time-consuming, expensive and prone to human error. This is compounded by the likelihood that samples will have to be collected each season due to the dynamic nature of crops, thus making it impractical for implementation in an operational workflow, especially at regional scales.

An assessment of the rule-sets used in the proposed automated procedure revealed the importance of using maximum NDVI (NDVI\_max) for extracting actively cultivated fields. Furthermore, the consistent results obtained from applying the rule-sets within the respective rainfall regions illustrate the potential of using environmental conditions (variables) to aid knowledge-based crop field extractions.

Findings from both Chapter 3 and Chapter 4 illustrate the potential of using Sentinel-2 imagery for identifying and delineating cultivated fields. The high temporal frequency (five-day revisit time) allows for the acquisition of a large number of images, which substantially increases the chances of obtaining observations that are not contaminated by clouds. Furthermore, as noted above, the 10 m spatial resolution produced satisfactory results in most cases, but was too low to delineate small and irregular fields.

### **5.3 STUDY LIMITATIONS AND RECOMMENDATIONS FOR FUTURE RESEARCH**

Although the WS workflow was successfully implemented and evaluated in five different agricultural landscapes (Chapter 4), they represented relatively small localised areas. It is recommended that the WS workflow is applied to larger areas (e.g. at regional or national scales) to more thoroughly evaluate its performance.

This study found that the spatial resolution (10 m) of Sentinel-2 imagery was too low to generate consistent and accurate boundaries for small and narrow fields. More research is needed to investigate the combination of higher spatial resolution imagery (such as WorldView-2/3) with Sentinel-2 imagery to overcome this limitation.

The high temporal frequency (five-day revisit time) of the Sentinel-2 constellation allowed for the collection of a large number of cloud-free images. However, these images were manually chosen, which is a time-consuming process and is not viable in the context of an operational methodology. Therefore, it is recommended that image compositing techniques (Lück & Van Niekerk 2016) are investigated and implemented in future studies.

### **5.4 CONCLUSIONS**

The spatial extent and location of agricultural field boundaries play an important role in agricultural monitoring systems. A timely and accurate delineation of agricultural fields is needed for operational workflows. This study evaluated several multi-temporal OBIA approaches, combining edge enhancement and segmentation techniques, to identify and delineate the boundaries of actively growing crops using Sentinel-2 imagery.

The combination of edge detection and image segmentation seems to be the most viable approach to automatic field boundary delineation. The Canny edge detection algorithm, in conjunction with a watershed segmentation procedure, is suggested. In addition, knowledge-based crop field extraction can be integrated into an operational workflow.

The techniques developed in this study laid the foundation for the development of an operational workflow to delineate agricultural field boundaries. Once operationalised, the resulting boundaries can be integrated into agricultural monitoring systems to aid resource planning, crop yield estimations and food security assessments.

## REFERENCES

- Addink EA, Van Coillie FMB & De Jong SM 2012. Introduction to the GEOBIA 2010 special issue: From pixels to geographic objects in remote sensing image analysis. *International Journal of Applied Earth Observation and Geoinformation* 15, 1: 1-6.
- Aguilar M, Vallario A, Aguilar F, Lorca A & Parente C 2015. Object-based greenhouse horticultural crop identification from multi-temporal satellite imagery: a case study in Almeria, Spain. *Remote Sensing* [online], 7, 6: 7378-7401. Available from: <http://www.mdpi.com/2072-4292/7/6/7378/>
- Al-doski J, Mansor SB, Zulhaidi H & Shafri M 2013. Image classification in remote sensing. *Journal of Environment and Earth Science* 3, 10: 141-148.
- Alemu MM 2016. Automated farm field delineation and crop row detection from satellite images. University of Twente. [online]. Available from: [http://www.itc.nl/library/papers\\_2016/msc/gfm/alemu.pdf](http://www.itc.nl/library/papers_2016/msc/gfm/alemu.pdf)
- Atzberger C 2013. Advances in remote sensing of agriculture: Context description, existing operational monitoring systems and major information needs. *Remote Sensing*, 5, 2: 949-981.
- Baatz M, Hoffmann C & Willhauck G 2008. Progressing from object-based to object-oriented image analysis. In *Object-Based Image Analysis* [online], 29-42. Available from: [http://link.springer.com/10.1007/978-3-540-77058-9\\_2](http://link.springer.com/10.1007/978-3-540-77058-9_2)
- Baatz M & Schäpe A 2000. Multiresolution segmentation: an optimization approach for high quality multi-scale image segmentation. *Angewandte Geographische Informationsverarbeitung XII. Beiträge zum AGIT-Symposium Salzburg 2000, Karlsruhe, Herbert Wichmann Verlag* [online], 12-23. Available from: <http://scholar.google.com/scholar?hl=en&btnG=Search&q=intitle:Multiresolution+Segmentation+:+an+optimization+approach+for+high+quality+multi-scale+image+segmentation#1>
- Batra B, Singh S, Sharma J & Arora SM 2016. Computational analysis of edge detection operators. *International Journal of Applied Research*, 2, 11: 257-262.
- Belgiu M & Csillik O 2018. Sentinel-2 cropland mapping using pixel-based and object-based time-weighted dynamic time warping analysis. *Remote Sensing of Environment* 204, November 2017: 509-523.

- Belgiu M & Drăgut L 2016. Random forest in remote sensing: A review of applications and future directions. *ISPRS Journal of Photogrammetry and Remote Sensing*, 114: 24-31.
- Benz UC, Hofmann P, Willhauck G, Lingenfelder I & Heynen M 2004. Multi-resolution, object-oriented fuzzy analysis of remote sensing data for GIS-ready information. *ISPRS Journal of Photogrammetry and Remote Sensing* 58, 3-4: 239-258.
- Blaschke T 2010. Object based image analysis for remote sensing. *ISPRS Journal of Photogrammetry and Remote Sensing* [online], 65, 1: 2-16. Available from: <http://dx.doi.org/10.1016/j.isprsjprs.2009.06.004>
- Blaschke T, Hay GJ, Kelly M, Lang S, Hofmann P, Addink E, Queiroz Feitosa R, Van der Meer F, Van der Werff H, Van Coillie F & Tiede D 2014. Geographic object-based image analysis - towards a new paradigm. *ISPRS Journal of Photogrammetry and Remote Sensing* [online], 87: 180-191. Available from: <http://dx.doi.org/10.1016/j.isprsjprs.2013.09.014>
- Blaschke T, Lang S, Lorup E, Strobl J & Zeil P 2000. Object-oriented image processing in an integrated GIS/remote sensing environment and perspectives for environmental applications. *Environmental Information for Planning, Politics and the Public*, 1995: 555-570.
- Bleau A & Leon LJ 2000. Watershed-based segmentation and region merging. *Computer Vision and Image Understanding* [online], 77: 317-370. Available from: <http://www.sciencedirect.com/science/article/pii/S1077314299908226>
- Blignaut J, Ueckermann L & Aronson J 2009. Agriculture production's sensitivity to changes in climate in South Africa. *South African Journal of Science* [online], 105, February: 61-68. Available from: [www.sajs.co.za](http://www.sajs.co.za)
- Bontemps S, Arias M, Cara C, Dedieu G, Guzzonato E, Hagolle O, Inglada J, Matton N, Morin D, Popescu R, Rabaute T, Savinaud M, Sepulcre G, Valero S, Ahmad I, Bégué A, Wu B, De Aballeyra D, Diarra A, Dupuy S, French A, Akhtar I ul H, Kussul N, Lebourgeois V, Page M Le, Newby T, Savin I, Verón SR, Koetz B & Defourny P 2015. Building a data set over 12 globally distributed sites to support the development of agriculture monitoring applications with Sentinel-2. *Remote Sensing* 7, 12: 16062-16090.
- Breiman L 2001. Random forests. *Machine Learning* 45, 1: 5-32.
- Butenuth M, Straub B & Heipke C 2004. Automatic extraction of field boundaries from aerial imagery. *KDNet Symposium on Knowledge-Based Services for the Public Sector*, 14-25.

- Calzadilla A, Zhu T, Rehdanz K, Tol RSJ & Ringler C 2014. Climate change and agriculture: Impacts and adaptation options in South Africa. *Water Resources and Economics* [online], 5: 24-48. Available from: <http://dx.doi.org/10.1016/j.wre.2014.03.001>
- Campbell JB & Wynne RH 2013. Image classification. In *Introduction to Remote Sensing 5th Edition*, 369-415.
- Canny J 1986. A computational approach to edge detection. *IEEE Transactions on Pattern Analysis and Machine Intelligence* PAMI-8, 6: 679-698.
- Carleer AP, Debeir O & Wolff E 2005. Assessment of very high spatial resolution satellite image segmentations. *Photogrammetric Engineering and Remote Sensing* [online], 71, 11: 1285-1294. Available from: [http://www.armurs.ulb.ac.be/images/8/86/PERS\\_Carleer\\_05.pdf](http://www.armurs.ulb.ac.be/images/8/86/PERS_Carleer_05.pdf)
- Castilla G, Hay GG & Ruiz-Gallardo JR 2008. Size-constrained region merging (SCRM). *Photogrammetric Engineering & Remote Sensing* [online], 74, 4: 409-419. Available from: <http://openurl.ingenta.com/content/xref?genre=article&issn=0099-1112&volume=74&issue=4&spage=409>
- Castillejo-González IL, López-Granados F, García-Ferrer A, Peña-Barragán JM, Jurado-Expósito M, De la Orden MS & González-Audicana M 2009. Object- and pixel-based analysis for mapping crops and their agro-environmental associated measures using QuickBird imagery. *Computers and Electronics in Agriculture* 68, 2: 207-215.
- Chen B, Qiu F, Wu B & Du H 2015. Image segmentation based on constrained spectral variance difference and edge penalty. *Remote Sensing* 7, 5: 5980-6004.
- Chen J, Deng M, Mei X, Chen T, Shao Q & Hong L 2014. Optimal segmentation of a high-resolution remote-sensing image guided by area and boundary. *International Journal of Remote Sensing* [online], 35, 19: 6914-6939. Available from: <http://dx.doi.org/10.1080/01431161.2014.960617>
- Christe MSA, Vignesh M & Kandaswamy A 2011. An efficient FPGA implementation of MRI image filtering and tumour characterization using Xilinx system generator. *International Journal of VLSI design & Communication Systems (VLSICS)* 2, 4: 95-109.
- Clinton N, Holt A, Scarborough J, Yan L & Gong P 2010. Accuracy assessment measures for object-based image segmentation goodness. *Photogrammetric Engineering and Remote Sensing* 76, 3: 289-299.



- Congalton RG 1991. A review of assessing the accuracy of classifications of remotely sensed data. *Remote Sensing of Environment* 37, 1: 35-46.
- Conrad C, Fritsch S, Zeidler J, Rücker G & Dech S 2010. Per-field irrigated crop classification in arid Central Asia using SPOT and ASTER data. *Remote Sensing* 2, 4: 1035-1056.
- Cousins B & Walker C 2015. 'Through a glass, darkly': Towards agrarian reform in South Africa. In *Land Divided, Land Restored. Land Reform in South Africa for the 21st Century* [online], 1-25. Available from:  
[http://www.kzndard.gov.za/images/Documents/RURAL\\_DEVELOPMENT/KZN\\_DARD\\_Coalition/PLENERY\\_1/Prof.-Ben-Cousins-PLAAS---Through-a-glass-darkly\\_Towards-Agrarian-Reform-in-South-Africa.pdf](http://www.kzndard.gov.za/images/Documents/RURAL_DEVELOPMENT/KZN_DARD_Coalition/PLENERY_1/Prof.-Ben-Cousins-PLAAS---Through-a-glass-darkly_Towards-Agrarian-Reform-in-South-Africa.pdf)
- Crnojevic V, Lugonja P, Brkljac B & Brunet B 2014. Classification of small agricultural fields using combined Landsat-8 and RapidEye imagery: case study of northern Serbia. *Journal of Applied Remote Sensing* [online], 8, 1: 083512. Available from:  
<http://remotesensing.spiedigitallibrary.org/article.aspx?doi=10.1117/1.JRS.8.083512>
- Davidse J 2015. Semi-automatic detection of field boundaries from high-resolution satellite imagery. Wageningen University.
- De Jong SM, Hornstra T & Maas HG 2001. An integrated spatial and spectral approach to the classification of Mediterranean land cover types: The SSC method. *ITC Journal* 3, 2: 176-183.
- Delves L, Wilkinson R, Oliver C & White R 1992. Comparing the performance of SAR image segmentation algorithms. *International Journal of Remote Sensing* 13, 11: 2121-2149.
- Drusch M, Del Bello U, Carlier S, Colin O, Fernandez V, Gascon F, Hoersch B, Isola C, Laberinti P, Martimort P, Meygret A, Spoto F, Sy O, Marchese F & Bargellini P 2012. Sentinel-2: ESA's Optical High-Resolution Mission for GMES Operational Services. *Remote Sensing of Environment* 120: 25-36.
- Duro DC, Franklin SE & Dube MG 2012. A comparison of pixel-based and object-based image analysis with selected machine learning algorithms for the classification of agricultural landscapes using SPOT-5 HRG imagery. *Remote Sensing of Environment* [online], 118: 259-272. Available from: <http://dx.doi.org/10.1016/j.rse.2011.11.020>
- Duveiller G & Defourny P 2010. A conceptual framework to define the spatial resolution requirements for agricultural monitoring using remote sensing. *Remote Sensing of Environment*, 114, 11: 2637-2650.

- El-Magd IA & Tanton TW 2003. Improvements in land use mapping for irrigated agriculture from satellite sensor data using a multi-stage maximum likelihood classification. *International Journal of Remote Sensing* 24, 21: 4197-4206.
- Esfahani ALIG 2014. Delineation of agricultural field boundaries using random sets. University of Twente.
- Eva HD, Belward AS, De Miranda EE, Di Bella CM, Gond V, Huber O, Jones S, Sgrenzaroli M & Fritz S 2004. A land cover map of South America. *Global Change Biology* 10, 5: 731-744.
- Fan J, Yau DKY, Elmagarmid AK & Aref WG 2001. Automatic image segmentation by integrating color-edge extraction and seeded region growing. *IEEE Transactions on Image Processing* 10, 10: 1454-1466.
- Forkuor G, Conrad C, Thiel M, Zoungrana BJB & Tondoh JE 2017. Multiscale remote sensing to map the spatial distribution and extent of cropland in the sudanian savanna of West Africa. *Remote Sensing* 9, 8: 1-24.
- Fritz S, See L, Mccallum I, You L, Bun A, Moltchanova E, Duerauer M, Albrecht F, Schill C, Perger C, Havlik P, Mosnier A, Thornton P, Wood-Sichra U, Herrero M, Becker-Reshef I, Justice C, Hansen M, Gong P, Abdel Aziz S, Cipriani A, Cumani R, Cecchi G, Conchedda G, Ferreira S, Gomez A, Haffani M, Kayitakire F, Malanding J, Mueller R, Newby T, Nonguierma A, Olusegun A, Ortner S, Rajak DR, Rocha J, Schepaschenko D, Schepaschenko M, Terekhov A, Tiangwa A, Vancutsem C, Vintrou E, Wenbin W, Van der Velde M, Dunwoody A, Kraxner F & Obersteiner M 2015. Mapping global cropland and field size. *Global Change Biology* 21, 5: 1980-1992.
- Gaetano R, Masi G, Poggi G, Verdoliva L & Scarpa G 2015. Marker-controlled watershed-based segmentation of multiresolution remote sensing images. *IEEE Transactions on Geoscience and Remote Sensing* 53, 6: 2987-3004.
- Gamon JA & Surfus JS 1999. Assessing leaf pigment content and activity with a reflectometer. *New Phytologist*. 143: 105-117. Cambridge: Cambridge University Press.
- Gao L, Yang S, Xia J, Liang J & Qin Y 2006. A new marker-based watershed algorithm. *IEEE*: 6-9.
- Gilbertson J, Kemp J & Van Niekerk A 2017. Effect of pan-sharpening multi-temporal Landsat 8 imagery for crop type differentiation using different classification techniques. *Computers and Electronics in Agriculture*, 134: 151-159.

- Gilbertson J & Van Niekerk A 2017. Value of dimensionality reduction for crop differentiation with multi-temporal imagery and machine learning. *Computers and Electronics in Agriculture*, 142: 50-58.
- Gitelson AA, Gritz Y & Merzlyak MN 2003. Relationships between leaf chlorophyll content and spectral reflectance and algorithms for non-destructive chlorophyll assessment in higher plant leaves. *Journal of plant physiology* 160, October: 271-282.
- Gomez C, White JC & Wulder MA 2016. Optical remotely sensed time series data for land cover classification: A review. *ISPRS Journal of Photogrammetry and Remote Sensing* 116: 55-72.
- Gonçalves H, Gonçalves JA & Corte-Real L 2011. HAIRIS: a method for automatic image registration through histogram-based image segmentation. *IEEE transactions on image processing: A publication of the IEEE Signal Processing Society* 20, 3: 776-789.
- Gumma M, Pyla K, Thenkabail P, Reddi V, Naresh G, Mohammed I & Rafi I 2014. Crop dominance mapping with IRS-P6 and MODIS 250-m Time Series Data. *Agriculture*, 4, 2: 113-131.
- Heinl M, Walde J, Tappeiner G & Tappeiner U 2009. Classifiers vs. input variables – The drivers in image classification for land cover mapping. *International Journal of Applied Earth Observation and Geoinformation* 11, 6: 423-430.
- Huete A, Didan K, Miura H, Rodriguez EP, Gao X & Ferreira LF 2002. Overview of the radiometric and biophysical performance of the MODIS vegetation indices. *Remote Sensing of Environment*, 83: 195-213.
- Huete AR 1988. A soil-adjusted vegetation index (SAVI). *Remote Sensing of Environment* 25, 3: 295-309.
- Hughes GF 1968. On the Mean Accuracy of Statistical Pattern Recognizers. *IEEE Transactions on Information Theory* 14, 1: 55-63.
- Immitzer M, Vuolo F & Atzberger C 2016. First experience with Sentinel-2 data for crop and tree species classifications in central Europe. *Remote Sensing* 8, 3.
- Inglada J, Arias M, Tardy B, Hagolle O, Valero S, Morin D, Dedieu G, Sepulcre G, Bontemps S, Defourny P & Koetz B 2015. Assessment of an operational system for crop type map production using high temporal and spatial resolution satellite optical imagery. *Remote Sensing* 7, 9: 12356-12379.

- Jackson R & Huete A 1991. Interpreting vegetation indexes. *Preventive Veterinary Medicine* 11: 185-200.
- Jenks GF 1967. *International Yearbook of Cartography*. 7th ed.
- Ji CY 1996. Delineating agricultural field boundaries from TM imagery using dyadic wavelet transforms. *ISPRS Journal of Photogrammetry and Remote Sensing*, 51, 6: 268-283.
- Jia K, Liang S, Zhang N, Wei X, Gu X, Zhao X, Yao Y & Xie X 2014. Land cover classification of finer resolution remote sensing data integrating temporal features from time series coarser resolution data. *ISPRS Journal of Photogrammetry and Remote Sensing*, 93: 49-55.
- Jiang Z, Oceanic N, Huete A, Didan K & Miura T 2008. Development of a two-band enhanced vegetation index without a blue band. *Remote Sensing of Environment*, December 2017: 13.
- Jing Y 2011. Assessing Larsi-Integrated Participation Procedure for Urban Adjudication in China. [online], May: 105. Available from:  
[http://www.itc.nl/library/papers\\_2011/msc/la/jing.pdf](http://www.itc.nl/library/papers_2011/msc/la/jing.pdf)
- Johnson B & Xie Z 2011. Unsupervised image segmentation evaluation and refinement using a multi-scale approach. *ISPRS Journal of Photogrammetry and Remote Sensing*, 66, 4: 473-483.
- Johnson DM 2013. A 2010 map estimate of annually tilled cropland within the conterminous United States. *Agricultural Systems*, 114: 95-105.
- Juneja M & Sandhu PS 2009. Performance evaluation of edge detection techniques for images in spatial domain. *International Journal of Computer Theory and Engineering* 1, 5: 614-622.
- Kaganami HG & Bei Z 2009. Region-based segmentation versus edge detection. *IIH-MSP 2009 - 2009 5th International Conference on Intelligent Information Hiding and Multimedia Signal Processing*: 1217-1221.
- Karamura EB, Jogo W, Rietveld A, Ochola D, Staver C, Tinzaara W, Karamura DA, Kubiriba J & Weise S 2013. Effectiveness of agro-ecological intensification practices in managing pests in smallholder banana systems in East and Central Africa. *Acta Horticulturae* 986: 119-126.
- Kavzoglu T & Tonbul H 2017. A comparative study of segmentation quality for multi-resolution segmentation and watershed transform. *IEEE* 2, June.
- Khan MR, De Bie CAJM, Van Keulen H, Smaling EMA & Real R 2010. Disaggregating and mapping crop statistics using hypertemporal remote sensing. *International Journal of Applied Earth Observation and Geoinformation* 12, 1: 36-46.

- Kroon DJ 2009. Numerical optimization of kernel based image derivatives. University of Twente, Enschede, December. Available from: [http://www.k-zone.nl/Kroon\\_DerivativePaper.pdf](http://www.k-zone.nl/Kroon_DerivativePaper.pdf)
- Labadarios D, Mchiza Z, Steyn NP, Gericke G, Maunder E, Davids Y & Parker W 2011. Food security in South Africa: A review of national surveys. *Bulletin of the World Health Organization* [online], 89, 12: 891-899. Available from: <http://www.who.int/bulletin/volumes/89/12/11-089243.pdf>
- Lambert MJ, Waldner F & Defourny P 2016. Cropland mapping over Sahelian and Sudanian agrosystems: A knowledge-based approach using PROBA-V time series at 100-m. *Remote Sensing* 8, 3.
- Lambin EF & Meyfroidt P 2011. Global land use change, economic globalization, and the looming land scarcity. *Proc Natl Acad Sci USA*, 108, 9: 3465-3472.
- Lebourgeois V, Dupuy S, Vintrou É, Ameline M, Butler S & Bégué A 2017. A combined random forest and OBIA classification scheme for mapping smallholder agriculture at different nomenclature levels using multisource data (simulated Sentinel-2 time series, VHRS and DEM). *Remote Sensing* 9, 3: 1-20.
- Lehohla P 2012. *Food security and agriculture 2002 – 2011: In-depth analysis of the General Household Survey data*. [online]. Available from: <http://www.statssa.gov.za/Publications2/Report-03-18-03/Report-03-18-032011.pdf>
- Li D, Zhang G, Wu Z & Yi L 2010. An edge embedded marker-based watershed algorithm for high spatial resolution remote sensing image segmentation. *IEEE Transactions on Image Processing* 19, 10: 2781-2787.
- Li Q, Wang C, Zhang B & Lu L 2015. Object-based crop classification with Landsat-MODIS enhanced time-series data. *Remote Sensing* 7, 12: 16091-16107.
- Liaw A & Wiener M 2002. Classification and regression by random forest. *R News* 2, December: 18-22.
- Lucas R, Rowlands A, Brown A, Keyworth S & Bunting P 2007. Rule-based classification of multi-temporal satellite imagery for habitat and agricultural land cover mapping. *ISPRS Journal of Photogrammetry and Remote Sensing* 62, 3: 165-185.

- Lück W & Van Niekerk A 2016. Evaluation of a rule-based compositing technique for Landsat-5 TM and Landsat-7 ETM+ images. *International Journal of Applied Earth Observation and Geoinformation*, 47: 1-14.
- Lunetta RS, Shao Y, Ediriwickrema J & Lyon JG 2010. Monitoring agricultural cropping patterns across the Laurentian Great Lakes Basin using MODIS-NDVI data. *International Journal of Applied Earth Observation and Geoinformation* [online], 12, 2: 81-88. Available from: <http://dx.doi.org/10.1016/j.jag.2009.11.005>
- Maini R & Aggarwal H 2009. Study and comparison of various image edge detection techniques. *International Journal of Image Processing* 3, 1: 1-11.
- Maisela RJ 2007. Realizing agricultural potential in land reform: The case of Vaalharts irrigation scheme in the Northern Cape Province. Cape Town: University of the Western Cape Press.
- Maselli F & Rembold F 2001. Analysis of GAC NDVI Data for Cropland Identification and Yield Forecasting in Mediterranean African Countries, *Photogrammetric Engineering & Remote Sensing*, May: 593-602.
- Matton N, Canto GS, Waldner F, Valero S, Morin D, Inglada J, Arias M, Bontemps S, Koetz B & Defourny P 2015. An automated method for annual cropland mapping along the season for various globally-distributed agrosystems using high spatial and temporal resolution time series. *Remote Sensing* 7, 10: 13208-13232.
- McNairn H, Ellis J, Van Der Sanden JJ, Hirose T & Brown RJ 2002. Providing crop information using RADARSAT-1 and satellite optical imagery. *International Journal of Remote Sensing* 23, 5: 851-870.
- McNemar Q 1974. Correction to a correction. *Journal of Consulting and Clinical Psychology* 42, 1: 145-146.
- Meer P 2001. Edge Detection with Embedded Confidence. *Computer Engineering* 23, 12: 1-32.
- Meyer HP & Van Niekerk A 2015. Assessing edge and area metrics for image segmentation parameter tuning and evaluation.
- Möller M, Lymburner L & Volk M 2007. The comparison index: A tool for assessing the accuracy of image segmentation. *International Journal of Applied Earth Observation and Geoinformation* 9, 3: 311-321.

- Mueller M, Segl K & Kaufmann H 2004. Edge- and region-based segmentation technique for the extraction of large, man-made objects in high-resolution satellite imagery. *Pattern Recognition* 37, 8: 1619-1628.
- Mulianga B, Bégué A, Clouvel P & Todoroff P 2015. Mapping cropping practices of a sugarcane-based cropping system in Kenya using remote sensing. *Remote Sensing* 7, 11: 14428-14444.
- Muller SJ & Van Niekerk A 2016. Indirect soil salinity detection in irrigated areas using earth observation methods.
- Muthukrishnan R & Radha M 2011. Edge detection techniques for image segmentation. *International Journal of Innovative Research in Computer and Communication Engineering*, 3, 6: 259-267.
- Myburgh G & Van Niekerk A 2013. Effect of feature dimensionality on object-based land cover classification: A comparison of three classifiers. *South African Journal of Geomatics*, 2, 1: 13-27.
- Ortiz A & Oliver G 2006. On the use of the overlapping area matrix for image segmentation evaluation: A survey and new performance measures. *Pattern Recognition Letters* 27, 16: 1916-1926.
- Ozdogan M, Yang Y, Allez G & Cervantes C 2010. Remote sensing of irrigated agriculture: Opportunities and challenges. *Remote Sensing* 2, 9: 2274-2304.
- Peña-Barragán JM, Ngugi MK, Plant RE & Six J 2011. Object-based crop identification using multiple vegetation indices, textural features and crop phenology. *Remote Sensing of Environment*, 115, 6: 1301-1316.
- Peña J, Gutiérrez P, Hervás-Martínez C, Six J, Plant R & López-Granados F 2014. Object-based image classification of summer crops with machine learning methods. *Remote Sensing* [online], 6, 6: 5019-5041. Available from: <http://www.mdpi.com/2072-4292/6/6/5019/>
- Pittman K, Hansen MC, Becker-Reshef I, Potapov PV & Justice CO 2010. Estimating global cropland extent with multi-year MODIS data. *Remote Sensing* 2, 7: 1844-1863.
- Quynh Trang NT, Toan LQ, Huyen Ai TT, Vu Giang N & Viet Hoa P 2016. Object-based vs. pixel-based classification of mangrove forest mapping in Vien An Dong Commune, Ngoc Hien District, Ca Mau Province using VNREDSat-1 images. *Advances in Remote Sensing*, 05, 04: 284-295.



- Ramadevi Y, Sridevi T, Poornima B & Kalyani B 2010. Segmentation and object recognition using edge detection techniques. *International Journal of Computer Science & Information Technology* 2, 6: 153-161.
- Roerdink J & Meijster A 2000. The watershed transform: definitions, algorithms and parallelization strategies. *Fundamenta Informaticae* 41, 1-2: 187-228.
- Roumenina E, Atzberger C, Vassilev V, Dimitrov P, Kamenova I, Banov M, Filchev L & Jeleu G 2015. Single- and multi-date crop identification using PROBA-V 100 and 300 m S1 products on Zlatia Test Site, Bulgaria. *Remote Sensing* 7, 10: 13843-13862.
- Rozenstein O & Karnieli A 2011. Comparison of methods for land-use classification incorporating remote sensing and GIS inputs. *Applied Geography*, 31, 2: 533-544.
- Rydberg A & Borgefors G 1999. Extracting multispectral edges in satellite images over agricultural fields. *Proceedings - International Conference on Image Analysis and Processing, ICIAP 1999*: 786-791.
- Rydberg A & Borgefors G 2001. Integrated method for boundary delineation of agricultural fields in multispectral satellite images. *IEEE Transactions on Geoscience and Remote Sensing* 39, 11: 1678-1680.
- Salman N 2006. Image segmentation based on watershed and edge detection techniques. *The International Arab Journal of Information Technology* 3, 2: 104-110.
- Samaniego L & Schulz K 2009. Supervised classification of agricultural land cover using a modified k-NN technique (MNN) and Landsat remote sensing imagery. *Remote Sensing* 1, 4: 875-895.
- Scharr H 2007. *Optimal filters for extended optical flow. Complex Motion* - [online], 91-103. Available from: <http://www.springerlink.com/index/F561031610812Q7U.pdf>
- Schiewe J 2002. Segmentation of high-resolution remotely sensed data - concepts , applications and problems. *Symposium on Geospatial theory, Processing and Applications, XXXIV*: 6.
- Schultz B, Immitzer M, Formaggio AR, Sanches IDA, Luiz AJB & Atzberger C 2015. Self-guided segmentation and classification of multi-temporal Landsat 8 images for crop type mapping in Southeastern Brazil. *Remote Sensing* 7, 11: 14482-14508.
- Shao Y, Lunetta R., Ediriwickrema J & Iiames J 2010. Mapping cropland and major crop types across the Great Lakes Basin using MODIS-NDVI Data. *Photogrammetric Engineering and Remote Sensing* 75, 1: 73-84.

- Sharma S & Mahajan V 2017. Study and analysis of edge detection techniques in digital images. *IJSRSET* 3, 5: 328-335.
- Shrivakshan GT & Chandrasekar C 2012. A comparison of various edge detection techniques used in image processing. *International Journal of Computer Science Issues (IJCSI)*, 9, 5: 269-276.
- Sinyolo S, Mudhara M & Wale E 2014. The impact of smallholder irrigation on household welfare: The case of Tugela Ferry irrigation scheme in KwaZulu-Natal, South Africa. *Water SA* 40, 1: 145-156.
- Sun Y & He GJ 2008. Segmentation of high-resolution remote sensing image based on marker-based watershed algorithm. *Proceedings - 5th International Conference on Fuzzy Systems and Knowledge Discovery, FSKD 2008* 4: 271-276.
- Thenkabail PS & Wu Z 2012. An automated cropland classification algorithm (ACCA) for Tajikistan by combining landsat, MODIS, and secondary data. *Remote Sensing* 4, 10: 2890-2918.
- Tollefson J 2012. Seven billion and counting. In *NATURE*, 2011 Macmillan Publishers Limited.
- Trimble 2016. *eCognition® Developer 9.2*.
- Turker M & Kok EH 2013. Field-based sub-boundary extraction from remote sensing imagery using perceptual grouping. *ISPRS Journal of Photogrammetry and Remote Sensing*, 79: 106-121.
- Valero S, Morin D, Inglada J, Sepulcre G, Arias M, Hagolle O, Dedieu G, Bontemps S, Defourny P & Koetz B 2016. Production of a dynamic cropland mask by processing remote sensing image series at high temporal and spatial resolutions. *Remote Sensing* 8, 1: 1-21.
- Van Rooyen AF, Ramshaw P, Moyo M, Stirzaker R & Bjornlund H 2017. Theory and application of agricultural innovation platforms for improved irrigation scheme management in Southern Africa. *International Journal of Water Resources Development*, 33, 5: 804-823.
- Veloso A, Mermoz S, Bouvet A, Le Toan T, Planells M, Dejoux JF & Ceschia E 2017. Understanding the temporal behavior of crops using Sentinel-1 and Sentinel-2-like data for agricultural applications. *Remote Sensing of Environment* 199: 415-426.
- Vieira MA, Formaggio AR, Rennó CD, Atzberger C, Aguiar DA & Mello MP 2012. Object-based image analysis and data mining applied to a remotely sensed Landsat time-series to map sugarcane over large areas. *Remote Sensing of Environment*, 123: 553-562.

- Villa P, Stroppiana D, Fontanelli G, Azar R & Brivio PA 2015. In-season mapping of crop type with optical and X-band SAR data: A classification tree approach using synoptic seasonal features. *Remote Sensing* 7, 10: 12859-12886.
- Vintrou E, Desbrosse A, Bégué A, Traoré S, Baron C & Lo Seen D 2012. Crop area mapping in West Africa using landscape stratification of MODIS time series and comparison with existing global land products. *International Journal of Applied Earth Observation and Geoinformation*, 14, 1: 83-93.
- Waldner F & Defourny P 2015. Automated annual cropland mapping using knowledge-based temporal features. *Journal of Photogrammetry and Remote Sensing* 110, December: 1-13.
- Waldner F, Hansen MC, Potapov P V, Löw F, Newby T, Ferreira S & Defourny P 2017. National-scale cropland mapping based on spectral-temporal features and outdated land cover information. *PLoS ONE* 12, 8: 1-25.
- Wardlow BD, Egbert SL & Kastens JH 2007. Analysis of time-series MODIS 250m vegetation index data for crop classification in the U.S. Central Great Plains. *Remote Sensing of Environment* 108, 3: 290-310.
- Watkins B & Van Niekerk A 2019. A comparison of object-based image analysis approaches for field boundary delineation using multi-temporal Sentinel-2 imagery. *Computers and Electronics in Agriculture*, 158, February: 294-302.
- Weidner U 2008. Contribution to the assessment of segmentation quality for remote sensing applications. *International Archives of Photogrammetry, Remote Sensing and Spatial Information Sciences* 37, B7: 479-484.
- Weih RC & Riggan ND 2010. Object-based classification vs. pixel-based classification: Comparative importance of multi-resolution imagery. *The International Archives of the Photogrammetry, Remote Sensing and Spatial Information Sciences* XXXVIII: 1-6.
- Wheeler SA, Zuo A, Bjornlund H, Mdemu MV, Van Rooyen A & Munguambe P 2017. An overview of extension use in irrigated agriculture and case studies in south-eastern Africa. *International Journal of Water Resources Development*, 33, 5: 755-769.
- Williamson I & Ting L 2001. Land administration and cadastral trends – A framework for re-engineering. *Computers, Environment and Urban Systems*, 25: 339-366.

- Wu Z, Thenkabail PS, Mueller R, Zakzeski A, Melton F, Johnson L, Rosevelt C, Dwyer J, Jones J & Verdin JP 2015. Seasonal cultivated and fallow cropland mapping using MODIS based automated cropland classification algorithm. *Remote Sensing*, 7, 1: 1-9.
- Wuest B & Zhang Y 2009. Region based segmentation of QuickBird multispectral imagery through band ratios and fuzzy comparison. *ISPRS Journal of Photogrammetry and Remote Sensing*, 64, 1: 55-64.
- Yan G, Mas JF, Maathuis BHP, Xiangmin Z & Van Dijk PM 2006. Comparison of pixel-based and object-oriented image classification approaches – A case study in a coal fire area, Wuda, Inner Mongolia, China. *International Journal of Remote Sensing* 27: 4039-4055.
- Yan L & Roy DP 2014. Automated crop field extraction from multi-temporal Web Enabled Landsat Data. *Remote Sensing of Environment*, 144: 42-64.
- Yan L & Roy DP 2016. Conterminous United States crop field size quantification from multi-temporal Landsat data. *Remote Sensing of Environment*, 172: 67-86.
- Yang J, He Y & Caspersen J 2017. Region merging using local spectral angle thresholds: A more accurate method for hybrid segmentation of remote sensing images. *Remote Sensing of Environment*, 190: 137-148.
- Zhan Q, Molenaar M, Tempfli K & Shi W 2005. Quality assessment for geo-spatial objects derived from remotely sensed data. *International Journal of Remote Sensing* 26, 14: 2953-2974.
- Zheng B, Myint SW, Thenkabail PS & Aggarwal RM 2015. A support vector machine to identify irrigated crop types using time-series Landsat NDVI data. *International Journal of Applied Earth Observation and Geoinformation*, 34, 1: 103-112.
- Zhou Y, Starkey J & Mansinha L 2004. Segmentation of petrographic images by integrating edge detection and region growing. *Computers and Geosciences* 30, 8: 817-831.
- Ziervogel G, New M, Archer van Garderen E, Midgley G, Taylor A, Hamann R, Stuart-Hill S, Myers J & Warburton M 2014. Climate change impacts and adaptation in South Africa. *Wiley Interdisciplinary Reviews: Climate Change* 5, 5: 605-620.